DOE/PC/30214-T7
(DE84004615)

Energy

FOSSIL

HEAT TRANSFER IN FREEBOARD REGION OF FLUIDIZED BEDS

By
Suleyman Biyikli
Kemal Tuzla
John C. Chen

October 1983

Work Performed Under Contract No. FG22-80PC30214

Lehigh University
Bethlehem, Pennsylvania

Technical Information Center
Office of Scientific and Technical Information
United States Department of Energy

DISCLAIMER

DISCLAIMER

This report has been reproduced directly from the best available copy.

Available from the National Technical Information Service, U. S. Department of Commerce, Springfield, Virginia 22161.

Price: Printed Copy A09
Microfiche A01

Codes are used for pricing all publications. The code is determined by the number of pages in the publication. Information pertaining to the pricing codes can be found in the current issues of the following publications, which are generally available in most libraries: *Energy Research Abstracts (ERA); Government Reports Announcements* and Index (*GRA* and I); *Scientific and Technical Abstract Reports (STAR);* and publication NTIS-PR-360 available from NTIS at the above address.

DOE/PC/30214-T7
(DE84004615)
Distribution Category UC-90e

HEAT TRANSFER IN FREEBOARD REGION OF FLUIDIZED BEDS

by

Suleyman Biyikli
Kemal Tuzla
John C. Chen[+]

Institute of Thermo-Fluid Engineering and Science
Lehigh University
Bethlehem, Pa. 18015

October 1983

[+]Principal Investigator

ACKNOWLEDGEMENT

This work was carried out under the auspices of the U.S. Department of Energy (Grant No. DE-FG22-80PC30214). Technical and project management was provided by the University Program office of the Pittsburgh Energy Technology Center and the Morgantown Energy Technology Center.

TABLE OF CONTENTS

LIST OF FIGURES

Fig. 25a.

Figure 26a Typical capacitance probe signal for glass beads with 275 μm mean diameter, tube is at 19 cm elevation, 0° position. Flow rate is 20 times minimum fluidization.

Figure 26b Probability distribution of voidage for Fig. 26a.

Figure 27a Typical capacitance probe signal for glass beads with 275 μm mean diameter, tube is at 19 cm elevation, 90° position. Flow rate is 20 times minimum fluidization.

Figure 27b Probability distribution of voidage for Fig. 27a.

Figure 28a Typical capacitance probe signal for glass beads with 275 μm mean diameter, tube is at 19 cm elevation, 180° position. Flow rate is 20 times minimum fluidization.

Figure 28b Probability distribution of voidage for Fig. 28a.

Figure 29 Capacitance signal analysis

LIST OF TABLES

NOMENCLATURE

Symbol	Description
A_p	surface area of test tube, m^2
A_S	surface area of a strip, m^2
A_{Dn}	area under a dense phase packet in capacitance signal
A_{Ln}	area under a lean phase packet in capacitance signal
a	constant in equation (28)
B	variable parameter in equation (27)
b	constant in equation (28)
C_1, C_2	constants in equation (32)
C_3, C_3	constants in equation (37)
C_{peL}	effective specific heat of lean phase, J/kg°K
C_{pg}	specific heat of air at constant pressure, J/kg°K
C_{ps}	specific heat of solid particles, J/kg°K
C_{pw}	specific heat of water, J/kg°K
D_T	diameter of test tube, m
d_p	mean particle diameter, μm
d_{pi}	average diameter of successive screens, μm
f_L	fraction of total time lean phase in contact
f_{La}	average fraction of total time lean phase in contact
f_{Lim}	immersed tube fraction of total time lean phase in contact
g	acceleration of gravity, m/s^2

H	freeboard tube elevation, cm
h	local heat transfer coefficient, $w/m^2°C$
H_L	maximum limiting entrainment height, cm
H_{Lt}	maximum limiting entrainment height at entrainment gas velocity, cm
h_{av}	average heat transfer coefficient, $w/m^2°C$
h_{Da}	average dense phase heat transfer coefficient, $w/m^2°C$
h_{La}	average lean phase heat transfer coefficient, $w/m^2°C$
h_g	heat transfer coefficient for gas alone, $w/m^2°C$
h_i	instantaneous heat transfer coefficient, $w/m^2°C$
h_{im}	immerse tube average heat transfer coefficient, $w/m^2°C$
h_m	mean heat transfer coefficient for a packet, $w/m^2°C$
h_n	normalized heat transfer coefficient
h_p	predicted heat transfer coefficient, $w/m^2°C$
h_r	radiative heat transfer coefficient, $w/m^2°C$
k_{eD}	effective dense phase thermal conductivity, $w/m°K$
k_{eL}	effective lean phase thermal conductivity, $w/m°K$
k_g	thermal conductivity of air, $w/m°K$
k_s	thermal conductivity of solid particles, $w/m°K$
M	total number of lean phase contacts to surface in a sample time period
m	number of lean phase contacts to surface in sample time period
N	total number of dense phase contacts to surface in a sample time period
n	number of dense phase contacts to surface in a sample time period
$\dot{m}$	cooling water mass flow rate, kg/s
P	probability distribution of void fraction

Pr	Prandtl number, $C_{peL}\mu_{eL}/k_{eL}$
Q	power input to a strip, w
q	local heat flux, w/m^2
q_D	heat flux during dense phase contact, w/m^2
q_L	heat flux during lean phase contact, w/m^2
Re	Reynolds number $\rho_{eL}U_{sgm}D_T/\mu_{eL}$
T	temperature, °C
T_B	fluidized bed temperature, °C
T_f	film temperature, °C
T_i	cooling water inlet temperature, °C
T_o	cooling water outlet temperature, °C
T_S	tube surface temperature, °C
T_{Sa}	circumferential average tube surface temperature, °C
U_{mf}	minimum fluidization velocity, m/s
U_n	nondimensional gas velocity
U_{sg}	superficial gas velocity, m/s
U_{sgm}	superficial gas velocity based on minimum flow area, m/s
U_t	particle entrainment velocity, m/s
w_i	weight fraction of particles in a specific size range
x	distance from tube surface, μm
x_a	average heat penetration depth, μm
x_n	heat penetration depth for a packet, μm

Greek Symbols

α	void fraction
α_c	void fraction cut-off value for differentiating void between dense phase and lean phase contact with the tube surface

α_D	dense phase void fraction
α_e	effective void fraction in heat penetration depth
α_f	bed void fraction for flow rates close to minimum fluidization
α_L	lean phase void fraction
α_{La}	average lean phase void fraction
α_p	packed bed void fraction
α_{Dim}	immersed tube dense phase void fraction
α_{Lim}	immersed tube lean phase void fraction
ϵ	tube surface emissivity
θ	residence time, s
θ_h	average residence time of dense phase for heat transfer coefficient
θ_p	average residence time of dense phase for heat penetration depth
θ_{Dn}	residence time of a dense phase packet, s
θ_{Ln}	residence time of a lean phase packet, s
θ_{him}	immersed tube residence time of dense phase for heat transfer coefficient, s
μ_{eL}	effective viscosity of lean phase, kg/m·s
μ_f	effective viscosity of fluidized bed, kg/m·s
μ_g	effective viscosity of air, kg/m·s
ρ_g	density of air, kg/m^3
ρ_s	density of solid particles, kg/m^3
σ	Stefan-Boltzmann constant, w/m^2k^4

ABSTRACT

This research involved the study of heat transfer and fluid mechanic characteristics around a horizontal tube in the freeboard region of fluidized beds.

Heat transfer coefficients were experimentally measured for different bed temperatures, particle sizes, gas flow rates, and tube elevations in the freeboard region of air fluidized beds at atmospheric pressure. Local heat transfer coefficients were found to vary significantly with angular position around the tube. Average heat transfer coefficients were found to decrease with increasing freeboard tube elevation and approach the values for gas convection plus radiation for any given gas velocity. For a fixed tube elevation, heat transfer coefficients generally increased with increasing gas velocity and with high particle entrainment they can approach the magnitudes found for immersed tubes. Heat transfer coefficients were also found to increase with increasing bed temperature. It was concluded that this increase is partly due to increase of radiative heat transfer and partly due to change of thermal properties of the fluidizing gas and particles.

To investigate the fluid mechanic behavior of gas and particles around a freeboard tube, transient particle tube contacts were measured with a special capacitance probe in room temperature experiments. The results indicated that the tube surface experiences

alternating dense and lean phase contacts. Quantitative information for local characteristics was obtained from the capacitance signals and used to develop a phenomenological model for prediction of the heat transfer coefficients around freeboard tubes. The packet renewal theory was modified to account for the dense phase heat transfer and a new model was suggested for the lean phase heat transfer. Using only fluid mechanic information, the model predicted heat transfer coefficients with an average deviation of 44.2 percent for the ranges of test conditions covered in this investigation.

Finally, an empirical freeboard heat transfer correlation was developed from functional analysis of the freeboard heat transfer data using nondimensional groups representing gas velocity and tube elevation. This correlation represented all the experimental heat transfer data, from both low temperature and high temperature tests, for particle diameters ranging from 275 to 1400 μm, gas velocities varying from minimum fluidization to terminal velocities, and tube freeboard elevations of 0 to 2.25 m, with an average deviation of 28.8 percent.

1. INTRODUCTION

A promising new technology for utilization of fossil fuels is fluidized bed combustion. Advantages in combustion efficiency, control of SO_2 pollution and reduction in NO_x emissions are anticipated [1]. With such potential benefits, fluidized bed combustion has been considered to be one of the most promising developments, especially for improved coal utilization.

1.1 Heat Transfer in Fluidized Beds

In the majority of designs, the heat of combustion generated in fluidized bed combustors is used to generate steam. The steam in turn can then be used either for process heating or to drive steam turbines for production of electric power. Coolant tubes, carrying the water and steam , are placed within the fluidized bed combustor to transfer the heat obtained from combustion of coal.

In most designs, the heat transfer tubes are located with a portion of the tubes submerged within the fluidized bed and the remaining portion located in the freeboard space above the fluidized bed region of the combustor. Due to the different fluid-dynamic states in the bed region , as compared with freeboard region, the heat transfer around the tubes varies for the two regions. The effective heat transfer coefficients for tubes located

within the fluidized bed region are normally an order of magnitude greater than the heat transfer coefficients of the tubes in the freeboard space. Designers of fluidized bed combustors hope to utilize this different behavior in controlling the operating power level of fluidized bed combustors. A given combustor needs to operate over a wide range of power levels, up to the maximum design output. The ability to "turn down" below design output is desired in order to follow load demand variations for power. Current plans call for turning down the thermal output of a combustor by dropping the fluidized bed level to expose greater portions of the coolant tubes above bed level. The expected decrease in total heat transfer would then permit a lowered combustion rate. The mode of operation depends on the variation of heat transfer coefficient on the surface of the tubes as a function of tube elevation in the freeboard space above the bed.

The rate of heat transfer between a fluidized bed and a submerged tube has been measured by a number of investigators for uniformly sized particles [2-8] and for mixed particle sizes [9]. To the knowledge of this investigator, only limited data are available for circumferentially averaged heat transfer coefficients to tubes in the freeboard region of fluidized beds [10-12],

and there is no detailed information regarding the local heat transfer coefficients around the tubes.

The first published report for freeboard heat transfer produced by George and Grace[10] measured the average heat transfer coefficients around horizontal tubes for several sizes of silica sand. This valuable contribution was limited as a reference in several aspects. Primarily the experimentation was limited to fluidization gas velocities below 1.3 m/s, while fluid bed operations call for fluidization velocities as high as 5.0m/s. The data were restricted to bed temperatures in the range of 120 to 145 °C. Only data for tube-averaged heat transfer coefficients were obtained. The data of references[13-14] indicate a strong variation of the heat transfer coefficient with angular position around submerged tubes. The study reported in reference[10] did not attempt to assess if similar variations of local heat transfer coefficients occur for tubes in the freeboard space.

Wood, Kuwata and Staub[11] measured average heat transfer coefficients for submerged and freeboard horizontal tube banks, for one size of silica sand at room temperature. Byam, Pillai and Roberts[12] measured average heat transfer coefficients in a fluidized bed

combustor operating at 6 atm pressure. Heat transfer in the freeboard was investigated by varying the bed height. They measured average heat transfer coefficients around horizontal tube banks for one size of coal-dolomite particles at a constant fluidizing gas velocity of 1.3 m/s, at bed temperatures of 780-890 °C.

In view of this poor state of knowledge regarding heat transfer to tubes in the freeboard region of fluidized beds, there was a definite need for additional engineering research. Experimental data for the heat transfer coefficients were needed over a range of operating conditions. In addition, fundamental studies of the heat transfer mechanisms were needed in order to develop phenomenological models for correlating the experimental data and for design applications.

1.2 Scope of Present Investigation

The objective of the proposed research program was to improve the state-of-knowledge on heat transfer in freeboard region of fluidized beds. The specific goals were to

(i) Obtain experimental data for local heat transfer coefficients around a horizontal tube in the freeboard region at room temperature.

(ii) Obtain experimental data for circumferentially averaged heat transfer coefficients at elevated bed temperatures.

(iii) Obtain experimental data for transient particle-surface contact around a horizontal tube in the freeboard region, at room temperature.

(iv) Develop a suitable phenomenological model of the heat transfer process, based on the particle-surface contact information.

2. LOW TEMPERATURE EXPERIMENTS

2.1 Experimental Apparatus and Procedure

A rectangular fluidized bed (0.2x0.3 m crossection, 3.0 m height) was designed and fabricated for freeboard experiments at room temperature. Three sides of the bed were constructed from aluminum plates (to decrease the electrostatic charge in the bed) while the fourth side was constructed from glass plates to permit visual observations of the fluidization conditions. The distributor was a sandwich assembly of a perforated steel plate, porous plastic plate and a stainless steel screen. Acrylic plastic doors on the aluminum walls were used for the attachment of heat transfer tubes. A cyclone separator was used to collect and recycle the entrained particles during operation at high fluidization velocities. A flow diagram of the fluidized bed test unit is shown in Figure 1.

A specially instrumented tube was built for the measurement of local heat transfer coefficients. As shown in Figure 2, the test tube was fabricated from a 3.2 cm diameter lexan rod, around which were embedded 8 Inconel foil strips to generate the required heat flux. The power was supplied to each strip separately using individual voltage controls. Thermocouples, located in grooves

beneath the strips, were used to determine rod surface temperatures. During operation the power to the individual strips was adjusted to establish an isothermal temperature of about 40 °C around the tube. In order to calibrate the heat transfer tube, some initial results were obtained with the tube exposed to single phase air convection. Average heat transfer coefficients for single phase air flow were compared with heat transfer coefficients for tubes in cross flow as calculated using standard correlations of references[27,28]. The agreement was within ±6 percent, substantiating the validity of the instrumentation.

Fluidizing air was supplied by a pair of reciprocating compressors; flow rates were measured with annubar sensors (pitot tube rakes) with capability of measuring flow rates of 0.0004 to 0.57 m^3/s. The uncertainty in flow measurements was within ±2.5 percent as specified by the manufacturing company of the annubar sensors. High gas velocities were attained in the fluidized bed, up to 3.5 m/s. Steam was used to humidify the inlet air in order to reduce problems of electrostatic charges in the bed. Without this precaution, electrostatic charges would cause large fluctuations in the readings of electronic instruments which are connected

to the test tubes for data collection.

For each test run, about 10 data samples were recorded and processed to obtain time average information at steady-state conditions. Utilizing measured power input to each heating strip and the respective temperatures of the tube surface and bulk bed, local heat transfer coefficients were calculated employing the following equation;

$$h = \frac{Q}{A_S(T_S - T_B)} \qquad (1)$$

where;

h=local heat transfer coefficient

Q=power input to each strip

A_S=surface area of each strip

T_S= tube surface temperature, local

T_B= bed temperature

Average heat transfer coefficients were calculated by area averaging the local coefficients.

Tests were carried out to determine the variation of heat transfer coefficients with tube elevation in the freeboard region of the fluidized bed. For a selected static bed height, the heat transfer tube was placed at

1.6,19,58, and 225 cm elevations above the static bed. Tube elevation is defined as the height between the static bed upper surface and the centerline of the test tube. The local and average heat transfer coefficients were measured for different particles, air flow rates, and tube elevations. Glass beads with 275 and 850 μm mean diameters, and silica sand with 285 and 465 μm mean diameters were used as fluidizing particles. The weight mean average diameter, as defined in reference [15], was determined from sieve analysis using the relation;

$$d_p = \frac{1}{\sum_i (w/d_p)_i} \qquad (2)$$

Properties of test particles are given in Table 1. Figure 15 shows the variation of cumulative weight fraction with sieve size for all test particles. Entrainment and minimum fluidization velocities were calculated using the mean diameter of the particles. Equations for entrainment and minimum fluidization velocities are given in reference [15].

2.2 Experimental Results

These experiments gave information on (a) circumferential distributions of the local heat transfer coefficients around the horizontal tube, (b) the variation

of average heat transfer coefficients with tube elevation, and (c) effect of static bed height on heat transfer coefficients in the freeboard region. The estimated uncertainty in heat transfer coefficients (see Appendix 1) was ±8 percent due to instrumentation precision and ±2 percent due to air humidification effects, for a total uncertainty of ±10 percent.

a. Local Heat Transfer Coefficients

Local heat transfer coefficients were measured around the circumference of the horizontally placed test tube in the freeboard region of fluidized beds for different test particles.

Experimental results showing the variation of heat transfer coefficient around the tube for a series of tube heights in the freeboard region are plotted in Figures 3 and 4. The test particles were glass beads with 275 μm mean diameter. Local heat transfer coefficients are given at low and high gas velocities. In these polar plots of the local heat transfer coefficient zero degree is defined as the top of the horizontal tube. Figure 3 shows the local heat transfer coefficients for low gas flow rate, corresponding to three times the minimum fluidization velocity. At 1.6 cm elevation the tube is essentially immersed into the bed, while at higher elevations the tube

is exposed to forced convection of air only. At this low gas flow rate, the distinctly reduced heat transfer coefficients for tubes in the freeboard region are quite obvious. Figure 4 shows the heat transfer coefficient at high gas flow rate, corresponding to 40 times the minimum fluidization velocity. At this higher gas flow rate, some particle entrainment occurs into the freeboard region, so that significantly enhanced heat transfer (over air convection) was observed at tube elevations up to 147 cm.

For a given gas flow rate and a given particle size, the local heat transfer coefficient varied with circumferential position around the tube. Maximum heat transfer coefficients tended to occur at the top of the tube. It is seen that the local heat transfer coefficients at all positions around the tube decreased with increasing height in the freeboard region. This trend was consistent for all particles and at all gas flow rates.

At 1.6 cm elevation the tube is essentially immersed into the bed at about three times the minimum fluidization velocity. Local heat transfer coefficients are shown in Figure 5 for this case. After exceeding this gas flow rate, local heat transfer coefficients at the top of the tube decreased slowly, while at the bottom increased with

increasing gas velocity. At the higher gas velocity, the local heat transfer coefficients showed a depression at the sides of the tube. Figure 4 shows this trend at 40 times minimum fluidization velocity. At higher tube elevations, all local heat transfer coefficients increased with increasing gas velocity. While the local heat transfer coefficients at the bottom and top of the tube increased rapidly, the local coefficients showed a slower increase at the sides of the tube with increasing gas flow rates. It is hypothesized that this trend is due to particle motion which results in more particle contact at bottom and top of the tube, and less contact at the sides of the tube. Conceivably, the forward stagnation point(lower surface) is impacted by upward entrained particles, which upon de-entrainment then "rain down" onto the top surface. This process could lead to efficient particle-surface renewal and provide relatively high heat transfer coefficients at the top and bottom portions of the tube. The depressed heat transfer coefficients at the sides of the tube would indicate a gas convective mechanism with relatively small particle-surface transfer. This trend is explained in Chapter 4.3 by using the results of transient bed-surface contact measurements. Lastly, it is seen from Figures 3 and 4 that the heat transfer coefficients are vertically symmetrical about the

axis as expected.

b. Average Heat Transfer Coefficients

Whereas the local heat transfer coefficients are of fundamental interest, design applications require average heat transfer coefficients. In this study, area averaged heat transfer coefficients were calculated from the measured local heat transfer coefficients. The results indicate the effect of freeboard height on average heat transfer coefficient as a function of superficial gas velocity.

Figure 5 shows the average heat transfer coefficients versus nondimensional gas velocity as a function of different test particles for the case when the bottom of the tube was located at the same height as the static bed surface. The heat transfer coefficients, for the case of the tube immersed in the static bed(tube centerline at mid elevation of static bed height), are also shown for two particles for comparison. The immersed tube heat transfer coefficients were found to be in close agreement with heat transfer coefficients for the tube at the static bed surface.

The heat transfer data versus superficial gas velocity for 19 cm tube elevation are shown in Figure 6,

for all particles. At a constant gas velocity, heat transfer coefficients increased with decreasing particle diameters. Similar trends were observed for other elevations tested. This effect of particle size is due to different particle entrainment into the freeboard region. At a constant gas velocity, particle entrainment is higher for smaller diameter particles.

In order to consider the effect of particle diameter it is suggested that nondimensional forms of heat transfer coefficients and gas velocities can be used as shown in Figure 7. The heat transfer coefficients in the freeboard region were normalized by using immersed tube heat transfer coefficients from Figure 5, and single phase heat transfer coefficient calculated for gas convection in cross flow at corresponding gas velocities from a correlation given in references[27,28]. The superficial gas velocities were nondimensionalized by using entrainment and minimum fluidization velocities. Using these dimensionless coordinates, it can be seen that heat transfer data for different test particles form a single band at a given tube elevation. The solid lines, which were determined by eye-approximation, indicate the mean of these bands. It is suggested that these dimensionless parameters may be useful for generalizing heat transfer

data in the freeboard region of fluidized beds, if future accumulation of data agrees with these results. Figure 7 shows that the increase of heat transfer coefficients for a given tube elevation is as much as an order of magnitude with increasing gas velocity in the freeboard region of fluidized beds. For a given tube elevation , heat transfer coefficient increases with increasing gas velocity and approaches the immersed tube value. This approach to immersed tube heat transfer coefficients occurs at different gas velocities for different elevations. At lower elevations, the heat transfer coefficients approach their immersed values at lower gas velocities.

The variations of the heat transfer coefficients along the freeboard height are shown in Figure 8 for different gas velocities. These cross plots were obtained employing the mean values of heat transfer data (solid lines) from Figure 7. The variations of the average heat transfer coefficients with elevation in the freeboard are as much as an order of magnitude, decreasing to gas convection heat transfer with increasing elevation. The decline of the average heat transfer coefficients with increase in elevation was found to be moderated by increasing flow rates. This decrease was sharpest for low

flow rates, reflecting decreased particle entrainment into the freeboard region with lower flow rates.

c. Effect of Static Bed Height on Heat Transfer

The effect of static bed height on the average heat transfer coefficient was studied for some cases. Experiments for different static bed heights were carried out for silica sand (465 μm mean diameter), holding the tube elevation at 19 cm above the static bed, for different static bed heights. The results are shown in Figure 9 for different gas velocities. For a given gas velocity, increasing the static bed depth increases the freeboard heat transfer coefficient for small bed depths. For static bed depths greater than 30 cm, this effect was negligible.

2.3 Comparison with Other Existing Data

To the knowledge of this investigator, very few data are available for heat transfer to tubes in the freeboard region of fluidized beds[10-12]. The available data are for tube bundles and are often complicated by effects of changing static bed heights. In spite of the different operating conditions, the available existing data on average heat transfer coefficients were compared with heat transfer coefficients measured in this study. Table 2 summarizes the test conditions of the various

investigations for data used in this comparison. The comparison is shown in Figure 10 for two different gas velocities over a range of freeboard heights. For a given gas velocity, the heat transfer data of this work agree well with data of Byam etal.[12]. However, the results of Wood et al.[11] and George at al.[10], show higher heat transfer coefficients for the same height and a steeper decline to gas convection coefficients. Only this qualitative comparison is possible, in view of different test conditions.

2.4 Conclusions

The heat transfer characteristics for horizontal tubes in the freeboard region of fluidized beds were investigated experimentally at room temperature. Both local and tube averaged heat transfer coefficients were measured for different operating conditions (gas velocity, particle size, tube elevation). The conclusions drawn from these results may be summarized as follows.

1. It was found that heat transfer coefficients decrease with increasing elevation along the freeboard, and finally approach the coefficient for gas convection heat transfer at a given gas velocity.

2. At a given tube elevation, increasing the gas

velocity increases the heat transfer coefficients and for lower regions of the freeboard the coefficients can approach values corresponding to tubes submerged in the fluidized bed.

3. Heat transfer coefficients in the freeboard region of fluidized beds can be affected by static bed height for a given tube elevation and gas velocity, for shallow beds.

3. HIGH TEMPERATURE EXPERIMENTS

3.1 Experimental Apparatus and Procedure

The high temperature fluidized bed facility is shown in Figure 11. The fluidized bed is an atmospheric pressure fluidized bed with a test section of 46 cm inside diameter and 455 cm height with a 15.3 cm thick refractory lining. The required temperatures for heat transfer experiments are achieved by burning fuel oil in a combustion chamber. The fluidizing air is mixed with hot gases in the combustion chamber to a required temperature and then sent into the fluidized bed. Depending upon the concentration of particles present in the exhaust gases, the gas is directly vented to either the atmosphere or to a quench box, cyclone and through a fan to the atmosphere.

A water cooled heat exchanger was designed, fabricated, and placed into the bed as shown in Figure 12, to measure immersed and freeboard heat transfer coefficients. The heat exchanger was fixed to the bed wall at the top and tightened with steel wires and tie-rods to the bottom of the bed wall to prevent vibration of the heat transfer tube during the experiments. The heat transfer tube was elevated to different freeboard elevations by cutting the inlet and outlet tubes from the top and fixing them again to the bed wall. A detailed

drawing of the heat exchanger system is shown in Figure 13. Cooling water entered from the top and flowed through insulated 1.905 cm diameter stainless steel tubing. The stainless steel tubing and its insulation were located in a 7.6 cm diameter 0.2 cm thick steel tube to prevent damage of the insulation by fluidized particles. A horizontal heat transfer tube which was exposed to the fluidized bed was placed at the bottom of the exchanger system. The inlet and outlet cooling water temperatures were measured by 0.3172 cm diameter thermocouples. There are four thermocouples to monitor the bed temperature, two of which were located 12.5 cm above the heat transfer tube, at 9 and 23 cm distance to the bed wall. These thermocouples were moved together with the heat transfer tube to different elevations in the freeboard. After reaching steady state, the average temperature measured by these two thermocouples was taken as the effective bed temperature. The other two thermocouples were immersed into the static bed and fixed to the bed wall. For steady state conditions the variation of temperature among the four thermocouples was within ±15 °C. For each test run, many samples were recorded and processed to obtain information for steady-state conditions.

The surface temperature of the heat transfer tube was

measured by 0.16 cm diameter Chromel-Alumel type thermocouples which were brazed into semi-circular grooves on the tube surface. Four such thermocouples were equally spaced around the circumference of the tube. The tube was located within the bed and oriented such that the thermocouples indicated the upstream, downstream and side temperatures of the tube surface at the midpoint of the length of the tube. The area-average of the surface temperatures were then used in calculating the heat transfer coefficients. To permit the direct comparison of the heat transfer coefficients, the diameter of the tube was selected to closely match the diameter of the tube used for the room temperature tests. The water flow rate was measured using a rotameter.

Fluidizing air was supplied by a pair of reciprocating compressors, each capable of delivering 850 m^3/hr at 6 bars of pressure. Total air flow rate was measured by a hot wire probe mounted in a Venturi-meter. Gas velocities were corrected considering gas expansion due to high bed temperatures. High gas velocities were reached, up to 5.5 m/s.

The heat transfer flux to the tube was calculated by heat balance from measurements of water flow rate and inlet and outlet water temperatures. To prevent boiling

of water in the tube , the water flow rate was set such that the outlet water temperature was less than 40 °C. The average heat transfer coefficient, based on this heat flux, was then calculated by using Equation(3).

$$h_{av} = \frac{\dot{m}\, C_{pw}(T_o - T_i)}{A_p(T_B - T_{Sa})} \qquad (3)$$

where;

$\dot{m}$= cooling water mass flow rate

C_{pw}= specific heat of cooling water

T_o= outlet temperature of cooling water

T_i= inlet temperature of cooling water

A_p= surface area of the test tube

T_B= temperature of the bed

T_{Sa}= average surface temperature of the tube

The radiation heat transfer coefficient was calculated with;

$$h_r = \sigma\varepsilon(T_B^4 - T_{Sa}^4)/(T_B - T_{Sa}) \qquad (4)$$

where;

$\sigma = 5.67 \times 10^{-8} W/m^2K^4$

ε=tube surface emissivity.

Single phase gas convective heat transfer coefficients

were calculated using convective heat transfer correlations from Hilbert,Knudsen[27,28] for tubes in cross flow, (Equation(5)). Changes of thermal properties with bed temperature were considered by establishing the thermal properties at film temperature. The film temperature was calculated by taking the arithmetic average of tube surface and bed temperatures.

$$\frac{h_g D_T}{k_g} = 0.683 \left(\frac{\rho_g U_{sgm} D_T}{\mu_g}\right)^{0.466} \left(\frac{C_{pg}\mu_g}{k_g}\right)^{1/3} \qquad (5)$$

The tube surface emissivity used in Equation(4), was calculated by using the results of single phase heat transfer experiments. For single phase gas flow, the sum of the radiative and gas convective heat transfer coefficients of Equations(4,5) should be equal to the total heat transfer coefficient obtained by heat balance of Equation(3). This yields a tube surface emissivity as;

$$\varepsilon = \frac{(h_{av}-h_g)(T_B-T_{Sa})}{\sigma(T_B^4-T_{Sa}^4)} \qquad (6)$$

Using the results of the single phase experiments, tube surface emissivity was calculated from Equation(6). The calculated emissivities varied in a narrow range from 0.77

to 0.82. The arithmetic average of the calculated emissivities gave 0.80 which is the oxidized steel emissivity as given in reference[36].

Tests were carried out to determine the variation of average heat transfer coefficients with tube elevation in the freeboard of the high temperature fluidized bed. Tests were carried out at bed temperatures of 300 °C ±5 °C, 500 °C ±7 °C and 750 °C±10 °C. The static bed height was held constant at 36 cm for all the experiments. Heat transfer coefficients were measured for immersed tube (at 15 cm above distributor), and with the tube at 19, 58, and 147 cm freeboard elevations above the static bed. The tube elevation is defined as the height between the static bed upper surface and the centerline of the test tube. The heat transfer coefficients were measured for different test particles and air flow rates. Silica sand with 165 and 1200 μm mean diameters, and limestone with 1400 μm mean diameter were used as fluidizing particles. Size analysis of particles made before and after the experiments indicated the change in mean particle diameters was within ±3 percent. Variation of the cumulative weight fraction with sieve size for all the test particles is given in Figure 15. Properties of test particles are given in Tables 3 and 4. Entrainment and

minimum fluidization velocities were calculated using the mean diameter of the particles. Sphericity of the test particles was approximately unity.

To show the reproducibility of the results, the heat transfer coefficients were measured on two separate days for silica sand with a 465 μm mean diameter when the tube was immersed into static bed. The agreement between the coefficients was within ±4 percent.

3.2 Experimental Results

These experiments provided data on (a) average heat transfer coefficients for gas convection alone, (b) average heat transfer coefficients for immersed tube, (c) the variation of average heat transfer coefficients with tube elevation in the freeboard region, and (d) the effect of bed temperature on heat transfer coefficients. The estimated uncertainty in measured heat transfer coefficients (see Appendix 1) was ±7 percent and this was due to basic limitations in instrumentation precision.

a. Single Phase Heat Transfer Coefficients

Heat transfer coefficients were measured for the horizontally placed test tube for air convection alone at three different steady-state temperatures of 300 °C, 500 °C and 750 °C. Gas velocities up to 5.5 m/s were reached. The

resulting heat transfer coefficients are shown in Figure 16 as a function of gas velocity. Slopes of the curves change slightly at different bed temperatures because the dependence of radiation heat transfer coefficient on gas velocity changed slightly depending on the tube surface temperature, which in turn changed with gas temperature.

These single-phase heat transfer coefficients were used for two purposes. First, these results were used to calculate the tube surface emissivity by Equation(6). This procedure gave an average tube surface emissivity of 0.80. This emissivity was subsequently used to determine the radiative part of heat transfer in fluidized beds, by Equation(4). The second usage of the air heat transfer coefficients was to normalize the freeboard heat transfer data nondimensionally in order to obtain a correlation, as discussed below.

b. Immersed Tube Heat Transfer Coefficients

Average heat transfer coefficients were measured with the test tube located horizontally in the static bed, for different test particles, bed temperatures and gas velocities. The tube was immersed into the static bed at an elevation of 15 cm above the bed distributor. Silica sand with 465 and 1200 μm mean diameters and limestone with 1400 μm mean diameter were used as fluidizing

particles at steady-state bed temperatures of 300 °C, 500 °C and 750 °C. Air flow velocities varied from 0.3 to 5.5 m/s and static bed height was kept constant at a height of 36 cm for all test particles.

Figure 17 plots the average heat transfer coefficients versus gas velocity for different test particles, at steady-state bed temperature of 300 °C. The heat transfer coefficients are higher than corresponding values for ambient temperature experiments. It can be observed that the heat transfer coefficients increase with decreasing particle size for a given gas velocity. For high gas flow rates, heat transfer coefficients are almost independent of gas flow rate. Similar observations can be made when steady-state bed temperatures are 500 °C and 750 °C as shown in Figures 18 and 19. It can be concluded that heat transfer coefficients for an immersed tube increase with increasing bed temperature.

c. Freeboard Heat Transfer Coefficients

Heat transfer coefficients were measured at different tube elevations in the freeboard region of fluidized beds for different bed temperatures, test particles and gas velocities. The test tube was elevated in the freeboard region at heights of 19,58 and 147 cm above the static bed surface. Tube elevation is defined as the height between

the static bed upper surface and the centerline of the test tube. Test particles were silica sand with 465 and 1200 μm mean diameters, and limestone with a 1400 μm mean diameter. Tests were carried out at steady state bed temperatures of 300°C, 500°C and 750°C.

Heat transfer coefficients in the freeboard region were normalized by using immersed tube heat transfer coefficients from Figures 17, 18, 19 and single phase heat transfer coefficients of Figure 16. The superficial gas velocities were nondimensionalized by using entrainment and minimum fluidization velocities. The normalized heat transfer coefficients as a function of nondimensional gas velocity were found to be independent of bed temperature as shown in Figure 20. It can be seen that in these dimensionless coordinates, heat transfer data for different test particles form a band at a given tube elevation. The solid lines indicate the approximate mean of these bands. In these dimensionless coordinates, high temperature heat transfer data agree well with the room temperature data shown in Figure 7. Hence, observations drawn for Figure 7 can also be applied for Figure 20. For a given tube elevation, the heat transfer coefficient increases with increasing gas velocity and approaches the immersed tube value. This approach to the immersed tube

heat transfer coefficients occurs at different gas velocities for different elevations. At lower elevations, the heat transfer coefficients approach their immersed values at lower gas velocities.

Figure 21 shows the variation of the freeboard heat transfer coefficients compared to immersed tube values along the freeboard height for silica sand with 1200 μm mean diameter at different gas velocities. With increasing tube elevation the freeboard heat transfer coefficients decrease and approach values characteristic of gas convection plus radiation heat transfer.

d. Effect of Bed Temperature

An increase of bed temperature increases the radiation heat transfer and changes the physical properties of the fluidizing gas and particles. Total heat transfer coefficients clearly increase with increasing bed temperature. The increase due to a change of thermal properties of the particles and fluidizing gas can be seen by comparing the high temperature heat transfer coefficients without radiation to the corresponding room temperature coefficients. This comparison is given for silica sand with a 465 μm mean diameter for immersed tubes as a function of bed temperature for different gas velocities in Figure 22.

The radiation heat transfer coefficient was calculated by using Equation(4) with a tube surface emissivity of 0.80. The ratio of radiation heat transfer coefficient to total heat transfer coefficient along the freeboard height is shown in Figure 23 for different test particles and bed temperatures at a given gas velocity. Since, for high gas flow rates, the heat transfer coefficients are almost independent of gas velocity at a given bed temperature, the above heat transfer ratio is similar for other gas velocities greater than 1.0 m/s.

For a given elevation and particle size, increasing the bed temperature increases the effect of radiative heat transfer on total heat transfer. The relative contribution of radiation increases with increasing freeboard elevation and approaches a constant fraction of total heat transfer for a given particle size and bed temperature. This increase is due to a decrease of total heat tansfer coefficient with freeboard elevation which approaches gas convection plus radiation. Since, the total heat transfer coefficient decreases with increasing particle size, the percentage contribution of radiation also increases with increasing particle size.

3.3 Comparison with Other Existing Data

The immersed tube heat transfer coefficients are compared with heat transfer data of reference[17] as shown in Figures 17, 18, and 19, at different bed temperatures. The data of reference[17] are for a bundle, of 5 cm diameter stainless steel tubes, in contrast to the single tube of this study. The bed temperatures of reference[17] also do not exactly match the bed temperatures of this study. In spite of these different operating conditions, the data of this work and reference[17] show good agreement. To the knowledge of this investigator, very few data are available for heat transfer to tubes in freeboard region of fluidized beds at high bed temperatures. The data of reference[12] are compared with data of this work for 1200 μm silica sand with 750 °C bed temperature, as shown in Figure 21. The data of reference[12] are for coal-dolomite particles, a tube bundle geometry and for pressurized fluidized beds at 6 atm. In spite of these different operating conditions, the variations of heat transfer coefficient with freeboard elevation show similar trends and are in reasonable agreement.

3.4 Conclusions

The heat transfer characteristics for a horizontal

tube in the freeboard region of a high temperature fluidized bed were investigated experimentally. Heat transfer coefficients were measured for different operating conditions(gas velocity, particle size, tube elevation, bed temperature). The conclusions drawn from these results are summarized as follows.

1. Heat transfer coefficients increase with increasing bed temperature, partly due to an increase of radiation and partly due to a change of effective thermal properties of fluidizing gas and particles.

2. Using the proposed nondimensional coordinates for heat transfer and gas velocity makes the heat transfer data independent of bed temperature and particle size in the freeboard region of fluidized beds.

3. In dimensionless coordinates, the high temperature heat transfer data agree well with the room temperature data. Hence, it is suggested that the heat transfer coefficients can be correlated in the freeboard region of fluidized beds by using these dimensionless coordinates.

4. The relative contribution of radiation heat transfer increases with increasing bed temperature for a

given particle size and freeboard elevation.

5. The decrease of total heat transfer coefficient with increasing particle size and tube elevation leads to an increase in importance of radiation with increasing particle size and tube elevation at a given bed temperature.

6. It was found that the heat transfer coefficients decrease with increasing elevation along the freeboard and finally approach the coefficient for gas forced convection heat transfer at a given gas velocity and bed temperature.

7. At a given tube elevation and bed temperature, increasing the gas velocity increases the heat transfer coefficients. For lower regions of the freeboard the coefficients can approach values corresponding to tubes submerged in the fluidized bed.

8. Comparison of heat transfer data of this work with other limited existing data show good agreement.

4. TRANSIENT BED-SURFACE CONTACT BEHAVIOR

4.1 Experimental Apparatus and Procedure

A capacitance probe was used to measure transient bed-surface contact behavior in fluidized beds at room temperature. Experiments were carried out in the same rectangular fluidized bed which was built for the room temperature heat transfer experiments. Fluidization characteristics at the surface of a horizontal tube were determined by the capacitance probe technique developed at Lehigh[18], using a probe built previously[19]. The test tube shown in Figure 24 consisted of an aluminum solid cylinder with a lexan insert containing the capacitance electrodes, flanked by two aluminum tubes. The electrode leads were connected to a circuit designed to sense capacitance changes of order of a few pf. Details of the circuit are given in reference[19].

The probe output was continously monitored on a digital oscilloscope which captured a transient signal and recorded it on a cassette tape. Several such samples were taken and recorded for each test run. The University's central Cyber computer was used to process the signal.

The capacitance sensed by the probe is proportional to the dielectric constant of the fluidized medium at the

probe electrodes. The dielectric constant in turn depends on the local void fraction. Thus, a capacitance trace versus time can be directly related to the variations in local solids density at the tube surface. The measured capacitance signals were calibrated relative to an upper bound corresponding to the capacitance when the probe is immersed in a loosely packed static bed of particles, and a lower bound corresponding to the capacitance when the probe is fully exposed to air. The intermediate capacitances measured in fluidized conditions were linearly interpolated with respect to these limits.

In order to quantitatively describe dense phase and lean phase fluidization characteristics, Chandran[20] had proposed an arbitrary demarcation between the two phases. The criterion was taken to correspond to an average void fraction 0.80. The suitability of this criterion was examined in the present study by evaluating the measured probability distribution of void fractions.

A typical capacitance probe signal is shown in Figure 25a. To get the probability distribution of void fraction, the signal was digitized and divided into 30 equal intervals between packed-bed and air. The number of data points in each interval is divided by the total number of points to get the probability distribution of

the average void fraction. The probability distribution for the probe signal of Figure 25a is shown in Figure 25b. As shown in this figure, there are two peaks of probability, at void fractions of 0.52 and 0.93. Hence, the signal can be separated into dense phase and lean phase fluidization around an average void fraction of 0.80. The fluidization medium below a 0.80 void fraction is called "dense phase". Above this value it is called "lean phase". In the sample signal, the probability of dense phase contact on the tube surface is higher, hence, the dense phase is dominating.

Some capacitance signals and their probability distributions for the same flow rate but different angular positions around the tube, for 19 cm tube elevation, are shown in Figures 26-28. These figures also confirm that fluidization can be separated into dense and lean phase fluidization around a 0.80 void fraction. The same criterion for the separation can be used for all test particles, tube elevations and gas flow rates. It is seen that at high tube elevations and at the sides of the tube, the lean phase tends to dominate.

Quantitative information on the local fluidization characteristics were obtained by differentiating between a dense phase and a lean phase contact at the tube surface.

Using the notation of Figure 29 and for data obtained over sufficiently long sample times, it was possible to determine the contact residence times of the dense phase at the probe surface. It was also possible to compute the average void fractions of the dense and lean phases. Likewise, the fraction of the total time exposed to each phase could be determined. Average residence times for heat transfer coefficient and heat penetration depth of the dense phase are required for heat transfer model predictions in Chapter 5. The average residence time for the heat transfer coefficient is;

$$\theta_h = \left[\frac{\sum_{n=1}^{N} \theta_{Dn}}{\sum_{n=1}^{N} \sqrt{\theta_{Dn}}} \right]^2 . \qquad (7)$$

The average residence time for heat penetration depth is;

$$\theta_p = \left[\frac{\sum_{n=1}^{N} \theta_{Dn}^{3/2}}{\sum_{n=1}^{N} \theta_{Dn}} \right]^2 \qquad (8)$$

Where N is the total number of occurrences of dense phase contacts, of residence times of θ_{Dn}. The derivation of the above equations are given in Chapter 5, which discuss the heat transfer model development. These quantities

were computed from the capacitance probe signals for each run. The void fraction of the dense phase is calculated from the capacitance signal using the relation;

$$\alpha_D = 1 - \left[\sum_{n=1}^{N} A_{Dn} / \sum_{n=1}^{N} \theta_{Dn}\right] (1-\alpha_p) \quad . \tag{9}$$

The void fraction of the lean phase is calculated using the relation;

$$\alpha_L = 1 - \left[\sum_{m=1}^{M} A_{Lm} / \sum_{m=1}^{M} \theta_{Lm}\right] (1-\alpha_p) \tag{10}$$

The fraction of total time exposed to the lean phase is calculated using the relation;

$$f_L = \sum_{m=1}^{M} \theta_{Lm} / \left[\sum_{n=1}^{N} \theta_{Dn} + \sum_{m=1}^{M} \theta_{Lm}\right] \tag{11}$$

Where N and M are the total number of occurrences of dense and lean phases respectively in a sample time period. Definitions of variables in Equations(7-11) are illustrated in Figure 29.

Tests were carried out to determine the variation of the above fluidization parameters around the circumference

of the tube, at various elevations in the freeboard of the fluidized bed. For a selected static bed height of 36 cm, the capacitance probe was placed at 1.6, 19, 58 and 147 cm elevations above the static bed. Tube elevation is defined as the height between the static bed upper surface and the centerline of the test tube. The local fluidization parameters were measured for different particles, air flow rates, tube elevations and angular positions of 0, 90,180 degrees. Zero degree position is defined as the top of the horizontal tube. Glass beads with 275 and 850 μm mean diameters and silica sand with 465 μm mean diameter were used as fluidizing particles.

To show the reproducibility of the results, fluidization data were measured on two separate days for glass beads with a 850 μm mean diameter with the tube at 1.6 cm elevation and the probe at the zero degreee position. The agreement for void fractions and fraction of time the lean phase was in contact was within ±2 percent. For residence times it was within ±7 percent.

4.2 Experimental Results

As stated earlier, the capacitance probe was used to measure transient bed surface contact behavior. Examples of typical capacitance signals obtained with the horizontal capacitance probe are shown in Figures[25-28].

Analysis of the capacitance probe signals gave information on average residence times of the dense phase for heat transfer coefficient and heat penetration depth, fractional lean phase contact time, and lean and dense phase void fractions. The experiments gave information on (a) local variations of the above fluidization parameters around the immersed tube, (b) variation of the fluidization parameters with tube elevation in the freeboard region.

a. Immersed Tube Fluidization Data

The above fluidization parameters around the circumference of the horizontal test tube were measured when the tube just touches the static bed. At this elevation, the tube is essentially immersed in the fluidized bed. The data for this elevation are called immersed tube data. Tests were carried out for different test particles, gas flow rates, and angular tube positions. Gas velocities up to 3.0 m/s were attained. These fluidization data are shown in Figures[30,32-34], together with Chandran's data[20]. His test tube was immersed in the fluidized bed and his data were for low gas flow rates. At these low gas velocities, the test tube of this study was not completely immersed in the fluidized bed; hence, the data of Chandran[20] can not be

directly compared with the data of this study.

Figure 30 shows the average residence time of the dense phase for heat transfer coefficient, for different test particles and tube angles as a function of nondimensional gas velocity. At minimum fluidization, the tube is not immersed into the bed; hence, the residence time is zero. With increasing gas velocity the residence time increases, passes a maximum value when the tube is immersed into the bed and then decreases, for all the test particles and angular positions. The residence time is found to increase with decreasing particle size for all angular positions and gas velocities. Finally, the zero degree position (top) has the highest and the 90 degree position (side) has the lowest residence times for a given velocity and particle size.

The immersed-tube average residence time of the dense phase for heat penetration depth, as a function of nondimensional gas velocity, is given in Figure 31. Variation of this residence time is similar to the variation of residence time of the dense phase for heat transfer coefficient (Figure 30).

Variation of dense-phase void fraction as a function of dimensionless gas velocity for different test particles

and angular positions is shown in Figure 32. Dense-phase void fraction decreases, passes through a minimum, and then increases again with increasing gas velocity. This behavior is consistent for all test particles and angular positions. Dense phase voidage increases with increasing particle size at all angular positions and gas velocities. The zero degree position was found to have the lowest, and the 90 degree position the highest, void fractions.

Figure 33 shows lean-phase void fraction as a function of nondimensional gas velocity for different test particles and angular positions. Observations similar to that for Figure 32 can be made for Figure 33.

The fraction-of-total-time exposed to the lean phase around the circumference of the test tube for different test particles is shown in Figure 34 as a function of gas velocity. The fraction-of-total-time-the lean phase is in contact decreases, passes through a minimum and then increases with increasing gas velocity. This lean phase contact time increases around the circumference of the tube with increasing particle size for all gas velocities. Zero degrees has the lowest and 90 degrees has the highest fractional total time of lean phase contact for all test particles and gas velocities.

b. Freeboard Fluidization Data

The average residence times of the dense phase for heat transfer coefficient and heat penetration depth (which are discussed in Chapter 5.2), the fraction of total time the lean phase is in contact, and the dense and lean phase void fractions were measured around the circumference of the horizontally placed test tube in the freeboard region of fluidized beds of different test particles. Freeboard fluidization data were normalized with respect to immersed tube data as a function of nondimensional gas velocity at different tube elevations. The data in nondimensional coordinates are shown in Figures (35-39). In these dimensionless coordinates, the change of the fluidization data with particle size and angular position was negligible, and the fluidization data were found to form a single band at a fixed tube elevation. The solid lines represent approximate means of these bands.

Figure 35 shows the variation of normalized average-residence-time of the dense phase for heat transfer coefficient as a function of nondimensional gas velocity. At a given tube elevation, this residence time increases with increasing gas velocity and approaches the immersed tube value. The residence time decreases with increasing

tube elevation. Similar observations can be made for Figure 36, for average-residence-time of dense phase for heat penetration depth.

The normalized dense and lean phase void fractions, and the normalized fractional total time of the lean phase are shown in Figures(37-39) as functions of dimensionless gas velocity. The dense and lean phase void fractions and the fraction-of-total-time the lean phase is in contact increase with increasing freeboard elevation at a given velocity. At a given elevation, they decrease with increasing gas velocity.

4.3 Conclusions

Local, transient bed-surface contact behavior was measured by using a capacitance probe for different test particles, flow rates, tube elevations and tube angles. Analysis of the capacitance signal showed that the tube surface can experience dense and lean phase contacts. An average void fraction of 0.80 can be used as a criterion for the separation of the two phases. The results of transient bed-surface contact experiments are useful as input data for the phenomenological heat transfer model in Chapter 5.

As can be seen in Figure 4, local heat transfer

coefficients at the bottom and top of the tube are higher than the heat transfer coefficients at the sides of the tube. This behavior can be explained by examination of the capacitance probe signals at different angular locations around the tube. Figures 26-28 show the capacitance probe signals and corresponding probability distributions of voidage at different angular positions for a 19 cm tube elevation. As shown in these figures, the sides of the test tube(Figure 27) experience more dilute fluidization than the top and bottom of the tube. Hence, at the sides of the tube, the heat transfer coefficients would be expected to be smaller than the heat transfer coefficients at the top and bottom of the tube.

5. PHENOMENOLOGICAL MODEL

5.1 Formulation

It is apparent from the capacitance probe measurements that the tube surface can experience alternating contact with a dense emulsion phase and a lean void phase. The dense phase is envisaged as a fairly close packed matrix of solid particles(α_D=0.40 to 0.80), and the lean phase is envisaged as a gaseous medium with some entrained particles (α_L=0.80 to 1.00). If the contribution due to radiation is negligible, the heat flux at the tube surface can be written as;

$$q = q_D + q_L$$

where

q_L=heat flux during lean phase contact

q_D=heat flux during dense phase contact

The average predicted heat transfer coefficient (h_p) can be expressed as a weighted average of the dense and the lean phase heat transfer coefficients;

$$h_p = h_{Da}(1-f_{La}) + h_{La}f_{La} \qquad (12)$$

where

f_{La}= average fraction of the total time the lean phase is in contact around the test tube, which was

obtained by area averaging the local fraction-of-total-time the lean phase is in contact, using the experimental results of Chapter 4.

h_{La}= average heat transfer coefficient for the lean phase

h_{Da}=area average heat transfer coefficient for the dense phase

The area-averaged dense and lean phase heat transfer coefficients used in Equation(12) were calculated from two different models, representing the two different types of heat transfer. It is known that dense phase heat transfer occurs by transient conduction while lean phase heat transfer occurs by turbulent convection[20]. Local dense-phase heat transfer coefficients were calculated from the packet renewal model for transient conduction using input fluidization data of Chapter 4. Area averaging the local dense-phase heat transfer coefficients gave the average heat tranfer coefficient to be used in Equation(12). The average lean-phase heat transfer coefficient was calculated from a new lean-phase heat transfer model, using area average lean phase void fraction as input data. Area-average lean-phase void fraction was obtained from the local lean-phase void fractions of Chapter 4. The

following two Sections (5.2 and 5.3) give the details of calculating dense and lean phase heat transfer coefficients.

5.2 Dense Phase Heat Transfer

Dense phase heat transfer in a fluidized bed is a transient process initiated when a packet of dense phase material, or emulsion, comes into contact with a surface of different temperature. The solid particles and the gas are assumed to be at the bulk bed temperature at the outset, and physically one can argue that the first layer of particles and the gas between them will be the first material to be affected by heating or cooling the surface. Ensuing layers of particles begin to participate significantly only when the temperature of the first layer begins to change significantly.

The Mickley-Fairbanks' model[21] (packet theory) for dense phase heat transfer characterized the packet emulsion as a homogenous mixture with an effective thermal conductivity and an effective heat capacity. Many investigators found that the resulting expression overestimated the heat transfer coefficients at short residence times[16,18,20].

Modifications have been suggested by different

workers to improve the basic packet model cited above. Baskakov[37] introduced an empirical, time-dependent contact resistance at the wall/packet interface to achieve a good comparison with data. Yoshida et al.[38] used an approach analogous to the film penetration theory advanced by Toor and Marchello[39] for gas absorbtion into liquids. Their model unified the steady state conduction and unsteady state absorbtion concepts and used a limiting emulsion layer(packet) thickness. The inclusion of a characteristic length that is usually unknown was the limitation of this work. Koppel et al.[40] not only involved the film penetration mechanism of Toor and Marchello to assign a finite thickness to the packet, but also allowed a nonzero surface packet thermal resistance, in the manner of Baskakov[37]. At short residence times, heat penetration depth is within the order of a particle diameter. It is known that within the first particle layer on the surface, void fraction is higher than bulk void fraction of fluidized bed, (Kubie and Broughton[24]). Ozkaynak and Chen[22] proposed that Mickley-Fairbanks' model for dense phase heat transfer can be used with effective thermal properties taking into consideration the voidage changes within the first particle layer. To determine the effective voidage, it was proposed that the packet has the effective void fraction at a distance half

of heat penetration depth away from the wall.

A similar approach is used here. In this study, Mickley-Fairbanks' model[21] was used to calculate the dense phase conductive heat transfer coefficients. The heat transfer coefficients were calculated by using effective thermal properties at effective bed voidages. A heat penetration depth was defined to get effective bed voidage. The effective bed voidage was obtained by averaging the voidage equation of Kubie and Broughton[24] over the heat penetration depth. The derivation of the packet model, heat penetration depth, effective void fraction and thermal properties are given below.

In the well known packet model(Mickley-Fairbanks[25]), it was assumed that the packets are at the bulk bed temperature when they are away from the heat-transfer surface. The governing equation is the one-dimensional transient conduction equation.

$$\frac{\partial^2 T}{\partial x^2} = \frac{(\rho C_p)_{eD}}{k_{eD}} \frac{\partial T}{\partial \theta} \qquad (13)$$

where k_{eD} and $(\rho C_p)_{eD}$ are respectively the thermal conductivity and the volumetric specific heat of the two phase medium that contacts the surface. θ is the residence

time of the dense phase. The boundary conditions are:

$$T(x,0) = T_B$$
$$T(0,\theta) = T_S$$
$$T(\infty,\theta) = T_B$$

The solution is given by Carslaw and Jaeger[23].

$$\frac{T_S - T}{T_S - T_B} = \text{erf} \frac{x}{2\sqrt{\frac{k_{eD}\theta}{(\rho C_p)_{eD}}}} \tag{14}$$

The instantaneous heat transfer coefficient can be obtained as;

$$h_i = \sqrt{\frac{k_{eD}(\rho C_p)_{eD}}{\pi\theta}} \tag{15}$$

The mean heat transfer coefficient over a packet residence time of θ_{Dn} is;

$$h_m = \frac{\int_o^{\theta_{Dn}} h_i d\theta}{\theta_{Dn}}$$

$$h_m = 2\sqrt{\frac{k_{eD}(\rho C_p)_{eD}}{\pi\theta_{Dn}}} \tag{16}$$

The average local heat transfer coefficient can be

calculated for N occurrences of dense phase contact (N packets), each with a residence time of θ_{Dn} as follows;

$$h_D = \frac{\sum_{n=1}^{N} h_m \theta_{Dn}}{\sum_{n=1}^{N} \theta_{Dn}} = 2\sqrt{\frac{k_{eD}(\rho C_p)_{eD}}{\pi}} \quad \frac{\sum_{n=1}^{N} \sqrt{\theta_{Dn}}}{\sum_{n=1}^{N} \theta_{Dn}} \qquad (17)$$

An average residence time of dense phase for heat transfer coefficient can be defined as;

$$\theta_h = \left[\frac{\sum_{n=1}^{N} \theta_{Dn}}{\sum_{n=1}^{N} \sqrt{\theta_{Dn}}}\right]^2 \qquad (18)$$

Subsitution of Equation(18) into Equation(17) yields;

$$h_D = 2\sqrt{\frac{k_{eD}(\rho C_p)_{eD}}{\pi \theta_h}} \qquad (19)$$

which is the average local heat transfer coefficient of the dense phase.

The depth of heat penetration was defined by Ozkaynak and Chen[22] as a depth at which the normalized temperature difference $[(T_S-T)/(T_S-T_B)]$ attains a value of 0.90. The use of Equation(14) yields the heat penetration depth for each dense phase residence time of θ_{Dn}.

$$x_n = 2.32\sqrt{\frac{k_{eD}\theta_{Dn}}{(\rho C_p)_{eD}}} \qquad (20)$$

It is suggested that the heat penetration depth should be averaged over N occurrences of dense phase contact (N packets) each with a residence time of θ_{Dn}.

$$x_a = \frac{\sum_{n=1}^{N} x_n\theta_{Dn}}{\sum_{n=1}^{N} \theta_{Dn}} = 2.32\sqrt{\frac{k_{eD}}{(\rho C_p)_{eD}}}\ \frac{\sum_{n=1}^{N} \theta_{Dn}^{3/2}}{\sum_{n=1}^{N} \theta_{Dn}} \qquad (21)$$

Then, the average residence time of the dense phase for heat penetration depth can be defined as;

$$\theta_p = \left[\frac{\sum_{n=1}^{N} \theta_{Dn}^{3/2}}{\sum_{n=1}^{N} \theta_{Dn}}\right]^2 \qquad (22)$$

Subsituting Equation(22) into Equetion(21) gives the average heat penetration depth as;

$$x_a = 2.32\sqrt{\frac{k_{eD}\theta_p}{(\rho C_p)_{eD}}} \qquad (23)$$

To apply this concept, one needs the variation of local

voidage of packed beds in the vicinity of a constraining wall. This has been investigated by several workers[45-47]. For spherical particles the usual observation is that the voidage variations with distance from the constraining surface take the form of a damped oscillation curve, having a minimum voidage at about one particle radius from the surface. An equation satisfying the above observation was developed by Kubie and Broughton[24] from simple geometrical considerations. The equation agrees well with the experimental data of references[45,47]. Hence, the equation suggested by Kubie and Broughton[24] was selected to predict the variation of void fraction within the first particle layer, as given below;

$$\alpha(x) = 1 - 3(1-\alpha_D)\left[\frac{x}{d_p} - \frac{2}{3}\left(\frac{x}{d_p}\right)^2\right] \quad , \quad \frac{x}{d_p} \leq 1$$

$$\alpha(x) = \alpha_D \quad , \quad \frac{x}{d_p} > 1 \qquad (24)$$

Where x is the distance from the surface and α_D is the dense phase voidage as measured by the capacitance probe in Chapter 4. It is proposed that the effective void fraction(α_e) of the dense phase can be obtained by taking the mean of the Equation(24) from x=0 to $x=x_a$, where x_a is the average heat penetration depth,

$$\alpha_e = \frac{1}{x_a} \int_o^{x_a} \alpha(x)dx \qquad (25)$$

The physical properties should correspond to effective values for the dense phase in the region adjacent to the heat transfer surface. It is proposed that thermal properties of gas and particles should be evaluated at film temperature(T_f), defined as the arithmetic average of tube surface temperature and bed temperature. The effective thermal capacity of fluidized beds is then defined as;

$$(\rho C_p)_{eD} = \rho_s C_{ps}(1-\alpha_e) + \rho_g C_{pg}\alpha_e \qquad (26)$$

Where

ρ_s, C_{ps}=density and specific heat of solid

ρ_g, C_{pg}=density and specific heat of the gas.

There have been several models for the effective thermal conductivity of fluidized beds[48-50]. The method proposed by Bauer and Schlunder[26] was selected by Chandran[20] to be used in the packet renewal model due to its versatility and completeness. In addition to the particle and fluid thermal properties, it accounts for the influence of temperature, pressure, particle shape, size

distribution and porosity on thermal conductivity of the two phase medium. Hence, effective thermal conductivity (k_{eD}) was estimated with the equation proposed by Bauer and Schlunder[26].

$$k_{eD} = k_g[(1 - \sqrt{1-\alpha_e}) + \sqrt{1-\alpha_e}\ (\frac{k_L}{k_g})] \qquad (27)$$

Where k_L is defined as;

$$\frac{k_L}{k_g} = \frac{2}{[1 - B\frac{k_g}{k_s}]} \left[\frac{(1 - \frac{k_g}{k_s})B}{(1-B\frac{k_g}{k_s})^2} \ln(\frac{k_s}{Bk_g}) - (\frac{B+1}{2}) - \frac{B-1}{1-B\frac{k_g}{k_s}} \right]$$

and

$$B = 1.25\ (\frac{1-\alpha_e}{\alpha_e})^{10/9}$$

k_g and k_s are the thermal conductivities of the gas and solid particles respectively. Local dense phase heat transfer coefficients were obtained by using Equations(19,23,25-27) with input fluidization data of ($\theta_h, \theta_p, \alpha_D$) from Chapter 4 for different angular positions, tube elevations, particle sizes and gas flow rates. Area averaging the local coefficients (h_D) gave circumferentially averaged heat transfer coefficients (h_{Da}) which were used in Equation[12] to obtain total

average heat transfer coefficients.

5.3 Lean Phase Heat Transfer

As shown in Chapter 4 from transient bed surface contact results, the tube surface can experience alternating contact with dense phase and lean phase fluidization. Lean phase is a dilute mixture of entrained solid particles in the gas (α_L=0.80 to 1.0). Heat transfer during lean phase contact is hypothesized to occur by turbulent forced convection. It is suggested that average lean phase heat transfer coefficients can be estimated from standard correlations for single phase flow across tubes by using effective physical properties of the lean phase flow. Heat transfer correlations of Hilbert[27], Knudsen and Katz[28] for tubes in a single phase cross flow were modified to predict the average lean phase heat transfer coefficient(h_{La}). Thermal properties for use with Equation(28) were evaluated at the film temperature. As defined above, film temperature is the arithmetic average of the tube surface and the fluidized bed temperatures. The standard heat transfer correlation for single-phase cross flow around a tube is given in references[27,28] as;

$$\frac{h_{La} D_T}{k_{eL}} = a\, Re^{b} Pr^{1/3} \qquad (28)$$

Where

Reynolds number, $Re = \frac{\rho_{eL} U_{sgm} D_T}{\mu_{eL}}$

Prandtl number, $Pr = \frac{C_{peL} \mu_{eL}}{k_{eL}}$

The constants a and b are tabulated below for the ranges of Reynolds numbers in this study.

Re	a	b
4-40	0.911	0.385
40-4000	0.683	0.466

It is proposed that the above heat transfer correlation can be modified by using effective thermal properties of the lean phase in order to predict the lean phase heat transfer coefficients. Effective thermal properties to be used in Equation(28) are suggested below.

D_T= Diameter of heat transfer test tube

U_{sgm}=gas velocity based on minimum flow area around the test tube. Since void fraction is high in lean phase fluidization, the effect of particles on gas velocity is neglected.

k_{eL}=effective thermal conductivity of lean phase

$$C_{peL} = [\rho_s C_{ps}(1-\alpha_{La}) + \rho_g C_{pg}\alpha_{La}]/\rho_{eL} \quad (29)$$

C_{peL}=effective specific heat of lean phase. This expression is obtained by keeping heat capacity constant for a given volume of lean phase fluidization.

$$\rho_{eL} = \rho_s(1-\alpha_{La}) + \rho_g\alpha_{La} \quad (30)$$

ρ_{eL}=effective density of lean phase

μ_{eL}=effective viscosity of lean phase

α_{La}=area-average lean phase voidage

Average lean-phase voidage can be obtained from results of bed-surface contact measurements of Chapter 4, by area averaging the local voidages at different angular positions for different test particles, tube elevations and flow rates. To the knowledge of this investigator, there is no information available for effective thermal conductivity of the lean phase. It is suggested that the effective lean phase thermal conductivity can be obtained from Equation(27) by using an area averaged lean phase voidage.

It is necessary to use an effective viscosity of the lean lean phase in Equation(28). To the knowledge of this

investigator, there is no information available for effective lean phase viscosity but there is some information in references[29-33] for effective viscosity of fluidized beds(μ_f). The effective viscosity of fluidized beds is independent of gas flow rates and particle sizes for mean diameters greater than 100 μm, as given in references[29-33]. An arithmetic average value of 0.47 kg/ms was taken from those references as an effective fluidized bed viscosity(μ_f). Effective viscosities were given for flow rates close to minimum fluidization. It is suggested that weighted averages of the effective fluidized bed and gas viscosities can be used as an estimate for lean phase viscosity(μ_{eL}). Since the heat transfer coefficient in Equation(28) is very insensitive to viscosity changes, the use of the above effective viscosity in Equation(28) will not give high errors in predicted lean phase heat transfer coefficients. For example, for an increase of 2000 percent in effective viscosity, the lean phase heat transfer coefficient will decrease only 33 percent. Hence, the effective lean phase viscosity can be taken as;

$$\mu_{eL} = \mu_g + \frac{1-\alpha_{La}}{1-\alpha_f} (\mu_f - \mu_g) \quad . \tag{31}$$

Where, μ_g is the viscosity of air, and α_f is the fluidized

bed voidage close to minimum fluidization. A value of 0.50 was used for α_f, which is an approximate fluidized bed voidage for flow rates close to minimum fluidization.

Average lean phase heat transfer coefficients($h_{L\ell}$) were calculated by Equation(28) for different test particles, tube elevations and flow rates. They were then used in Equation(12) to give total average heat transfer coefficients.

5.4 Application of Heat Transfer Model

Average heat transfer coefficients around a single horizontal tube in fluidized beds can be predicted by the phenomenological model formulated in Sections 5.1-5.3. This model was assessed with regard to (a) predictions of heat transfer coefficients, using the transient bed-surface contact measurements at room temperature, and (b) increase of heat transfer coefficients with bed temperature due to thermal property changes of fluidizing gas and particles. Note that this model has no adjustable constants.

a. Predictions of Heat Transfer Coefficients

Using the experimentally determined fluidization parameters ($\theta_h, \theta_p, f_L, \alpha_D, \alpha_L$), it was possible to compute average heat transfer coefficients by the proposed

phenomenological model. Average heat transfer coefficients were predicted for different test particles, freeboard tube elevations and gas flow rates at room temperature. Test particles were glass beads with 275 and 650 μm mean diameters and silica sand 465 μm mean diameter. Properties of the particles and gas are given in Table 5. Tube elevations were 1.6,19,58,147 cm above the static bed and gas velocities varied up to 3.0 m/s. The predicted coefficients were compared with respective experimental heat transfer coefficients and the results are shown in Figure 40. It is seen that the model overpredicts for high heat transfer coefficients, which corresponds to immersed tube heat transfer. When the tube is immersed into the fluidized bed, dense phase heat transfer dominates. Hence, the increase in predicted heat transfer coefficients is mostly due to overpredictions of the Mickley-Fairbanks model. Statistical comparisons of the model predictions with the experimental data are given in Table 7. The model predicts the heat transfer coefficients with an average deviation of 44.2 percent. In general, the model successfully predicts the trends exhibited by the experimentally measured average heat transfer coefficients at room temperature.

Model predictions are used to show the variation of

dense phase heat transfer along the freeboard height. Variation of dense phase heat transfer compared to the lean phase along the freeboard height is shown in Figure 41 for glass beads with 275 μm mean diameter at different gas velocities. As can be seen in this figure, at low freeboard elevations when the tube is immersed into the fluidized bed, dense phase heat transfer is an order of magnitude greater than lean phase heat transfer. With increasing freeboard elevation, the contribution of dense phase heat transfer decreases and approaches zero. This approach to zero is different for different gas velocities. The contribution of dense phase heat transfer increases with increasing gas velocity along the freeboard height.

b. Increase of High Temperature Heat Transfer Coefficients

The increase of heat transfer coefficients with increasing bed temperature, due to thermal property changes of fluidizing gas and particles, can be estimated by using the above model. The fluidization data at room temperature were also assumed to be valid at high temperatures. The only unavailable input data for the lean phase part of the model was the effective viscosity of fluidized beds at high temperatures. But as can be seen from the lean phase correlation(Equation(28)), the

correlation is very insensitive to viscosity changes. Hence, it was assumed that we can use room temperature viscosity at high bed temperatures in the lean phase model, Equation(28).

The increases of the heat transfer coefficients with increasing bed temperature (due to thermal property changes of fluidizing particles and gas) were calculated for silica sand with 465 μm mean diameter. Thermal properties of fluidizing gas and solid particles were obtained at film temperatures. Film temperatures were calculated as the arithmetic average of the bed temperature and average tube surface temperature. Average tube surface temperatures were in the range 40-70 °C, 130-150 °C, 180-200 °C at bed temperatures of 300 °C, 500 °C, 750 °C respectively. Thermal properties of fluidizing air and solid particles are given in Table 6.

To show the increase of heat transfer coefficient with bed temperature, high temperature predicted heat transfer coefficients were compared with predicted room temperature heat transfer coefficients for immersed tubes. Figure 42 plots this comparison, indicating very good agreement with the experimental results.

5.5 Conclusions

The mechanism of heat transfer around a horizontal tube in fluidized beds was postulated as dense phase transient conduction and lean phase turbulent convection. At high bed temperatures the effect of radiation becomes significant.

With a knowledge of the fluidization characteristics around horizontal tubes, a general model was developed for average heat transfer coefficient based on combined dense phase and lean phase heat transfer mechanisms. The model was able to successfully predict average heat transfer coefficients for a wide range of test conditions. The trends exhibited by the model predictions were observed to be in general agreement with those found for the experimentally measured average heat transfer coefficients at room temperature, for different gas flow rates, particle sizes and tube elevations.

The increase of heat transfer coefficients at high temperatures due to thermal property changes of fluidizing gas and particles was also explained by using the model.

6. CORRELATION OF DATA

As discussed in previous chapters, it was observed that normalized heat transfer coefficients are only functions of nondimensional gas velocity and freeboard height (distance between static bed upper surface and centerline of the test tube). An attempt was made to nondimensionalize the freeboard height by using transport disengagement height(TDH), defined as the upper limiting freeboard height above which entrainment flux is constant.

Zenz & Weil[41] and Zenz & Othmer[42] gave a simple graphical correlation of TDH. The correlation is based primarily on fluid-cracking catalyst particles and tends to be conservative by high TDH when applied to larger particles, although the authors recommended it for particles up to 400 μm in diameter. Fournel et al.[43] also studied fluid cracking catalyst and obtained a simple correlation for TDH. However, their superficial gas velocities ranged only between 0.11 and 0.22 m/s and extrapolation appears to lead to excessively conservative values. Hence, there appear to be no reliable correlation to predict TDH.

In order to define a general empirical correlation of freeboard heat transfer data, the following procedure was

followed in this investigation: (a) a limiting entrainment height (H_L) was defined and a correlation was obtained for H_L by using the results of the capacitance probe experiments, (b) this H_L was used to nondimensionalize the freeboard height. Regression analysis of the freeboard heat transfer data using the nondimensional freeboard height then gave a nondimensional empirical heat transfer correlation.

a. Limiting Entrainment Height

Limiting entrainment height(H_L) is defined in this study as the freeboard height above the static bed for which the average void fraction around the test tube reaches a value of 0.98 for a given gas velocity. Average void fractions were obtained by area averaging the local void fractions. The local void fractions at different angular positions around the tube were measured by the capacitance probe described in Chapter 4. Local void fractions were measured for different test particles and tube elevations in the freeboard region of fluidized beds at room temperature. As before, freeboard height is defined as the distance between the top of the static bed and the centerline of the test tube. Test particles were glass beads with 275 and 850 μm mean diameters and silica sand with 465 μm mean diameter. Tests were carried out at

freeboard elevations up to 225 cm.

The variation of average void fractions for different test particles along the freeboard height are shown in Figures(43-45). The limiting entrainment height as defined above was obtained from Figures(43-45) for different test particles and plotted in Figure 46 as a function of excess superficial gas velocity (above minimum fluidization velocity). As can be seen from this figure, the limiting entrainment height is a strong function of gas velocity and particle diameter, increasing with increasing gas velocity and with decreasing particle diameter. It was found by Lewis et al.[44] that particle entrainment is independent of bed diameters for bed diameters greater than 7.5 cm and that entrainment is independent of bed depth above a critical value of 11 cm. Hence, the limiting entrainment height can be expected to be independent of static bed depth and bed diameter for the present experiments.

It can be seen from the nondimensional heat transfer data that normalized heat transfer coefficients at room temperature (Figure 7) are slightly higher than the corresponding normalized high temperature coefficients,(Figure 20). This is likely due to a change of density and viscosity of the fluidizing gas at high

temperatures, causing a change in particle entrainment into the freeboard. Hence, it is expected that the limiting entrainment height(H_L) is a function of fluidizing gas density and viscosity. Increasing the gas density and viscosity would be expected to increase the limiting entrainment height. It can also be expected that the limiting entrainment height would decrease with increasing particle density and acceleration of gravity(g). Hence, a general nondimensional correlation of the following form is suggested for the limiting entrainment height.

$$\frac{H_L}{d_p} = C_1 \left[\frac{(U_{sg}-U_{mf})\rho_g \mu_g}{d_p^2(\rho_s-\rho_g)^2 g}\right]^{C_2} \qquad (32)$$

Where C_1 and C_2 are constants to be determined by using least squares curve fitting to Equation(32) by using experimental data. Equation(32) can be written as;

$$\log\left(\frac{H_L}{d_p}\right) = \log C_1 + C_2 \log\left[\frac{(U_{sg}-U_{mf})\rho_g \mu_g}{d_p^2(\rho_s-\rho_g)^2 g}\right] \qquad (33)$$

which is an equation of a straight line in logarithmic coordinates. When the data of Figure 46 were plotted

using the variables of Equation(33) in logarithmic coordinates, all data points did in fact collapse on a straight line, as shown in Figure 47. The equation of the line in Figure 47 is;

$$H_L = 8.32 \times 10^8 \frac{(U_{sg}-U_{mf})\rho_g \mu_g}{d_p(\rho_s-\rho_g)^2 g} \qquad (34)$$

This correlation successfully represents the experimental data for H_L with an average deviation of 6 percent.

b. Empirical Heat Transfer Correlation

Freeboard height(H) was nondimensionalized by using the limiting entrainment height of Equation(34) at entrainment gas velocity (U_t). The limiting entrainment height at terminal entrainment velocity(H_{Lt}) is physically the freeboard height just before entrainment of particles out from the bed. This terminal entrainment height (H_{Lt}) can be obtained from Equation(34), at $U_{sg}=U_t$. Values are given in Table 8 for different particles and bed temperatures. H_{Lt} is almost constant at a given bed temperature. With increasing bed temperature it decreases due to a change of gas density and viscosity. At a bed temperature of 750 °C, the terminal entrainment height decreased 25 percent compared to the height at room

temperature. A nondimensional freeboard height can then be defined as;

$$X = \frac{H}{H_{Lt}} \tag{35}$$

with the limits:

x→ 0 at surface of static bed

x→ 1 at freeboard height where particles would be entrained out from the bed at the limiting terminal velocity

In expectation that freeboard heat transfer data in nondimensional coordinates is a function of nondimensional freeboard height and gas velocity, it seemed reasonable to seek a freeboard heat transfer correlation of the form;

$$h_n = f(X, U_n) \tag{36}$$

where,

$$h_n = \frac{h_{av} - (h_r + h_g)}{h_{im} - (h_r + h_g)}$$

$$U_n = \frac{U_{sg} - U_{mf}}{U_t - U_{mf}}$$

Limiting conditions which must be satisfied are;

(i) h_n approaches 1.0 as X approaches zero

(ii) h_n decreases with increasing X

(iii) h_n increases with increasing U_n

A nondimensional functional relationship which satisfies the conditions is as follows:

$$h_n = \frac{1}{1 + C_3 \left(\frac{X}{U_n}\right)^{C_4}} \tag{37}$$

Where C_3 and C_4 are constants to be determined. Equation(37) can be written as;

$$\log\left(\frac{1}{h_n} - 1\right) = \log C_3 + C_4 \log \left(\frac{X}{U_n}\right) \tag{38}$$

C_3 and C_4 can be found by using a least squares curve fitting to Equation(38) by using experimental heat transfer data. When both low and high temperature heat transfer data are plotted as $(1/h_n - 1)$ versus X/U_n on logarithmic coordinates, all the data points did collapse on a straight line as shown in Figure 48. The resulting equation of the line in Figure 48 which correlates the experimental data points is;

$$h_n = \frac{1}{1 + 23.634 \left(\frac{X}{U_n}\right)^{2.578}} \qquad (39)$$

Statistical comparison of the above equation with the experimental data points is given in Table 9 for different test particles. It is seen that this simple correlation successfully represents all the experimental heat transfer coefficients with an average deviation of 28.8 percent.

The above correlation can be made more simple and compact by subsituting the X and U_n values as given by Equations 35 and 36, to eliminate the calculation of entrainment velocity and corresponding limiting entrainment height. The final form of the correlation is;

$$h_n = \frac{1}{1 + \left[4.1 \times 10^{-9} \frac{H\, d_p (\rho_s - \rho_g)^2 g}{(U_{sg} - U_{mf}) \rho_g \mu_g}\right]^{2.578}} \qquad (40)$$

The above correlation can predict the freeboard heat transfer coefficients for a horizontal tube in the freeboard region of fluidized beds at given elevations and gas velocities. Immersed tube heat transfer coefficients are required as an input for the correlation, which can be obtained from the existing heat transfer data or from correlations for immersed horizontal tubes, some of which

are given in references[2-9].

7. SUMMARY AND CONCLUSIONS

The objective of the research program was to improve the state-of-knowledge on heat transfer for horizontal tubes in the freeboard region of fluidized beds. To satisfy the objective, the study (i) measured local and average heat transfer coefficients at ambient bed temperature, (ii) obtained circumferentially averaged heat transfer coefficients at high bed temperatures, (iii) experimentally measured bed-tube contact dynamics, (iv) developed an empirical heat transfer correlation for horizontal tubes in the freeboard region of fluidized beds, and (v) developed a phenomenological model for horizontal tube heat transfer based on bed-tube contact dynamics. The following major results and conclusions were obtained from this study.

1. Both local and average heat transfer coefficients were obtained experimentally as a function of different operating conditions (particle size, gas flow rate, static bed depth and tube elevation) in the freeboard region at room temperature. Test particles were glass beads and silica sand with mean diameters ranging from 275 to 850 μm. Gas velocities were attained up to 3.0 m/s and freeboard tube elevations ranged up to 225 cm above the static bed. The results showed that heat transfer

coefficients decrease with increasing tube elevation, finally approaching the values for gas convection for any gas velocity. For example, for glass beads with 275 μm mean diameter and at 1.5 m/s gas velocity, average heat transfer coefficients decreased from 275 W/m^2C at 1.6 cm elevation to 27 W/m^2C at 147 cm elevation.

2. Average heat transfer coefficients were measured around a horizontal tube at high bed temperatures for different particles and tube elevations as a function of gas velocity in the freeboard region of fluidized beds. Bed temperature was varied up to 750 °C. Test particles were silica sand and limestone with mean diameters ranging from 465 to 1400 μm. Tube elevation was varied up to 147 cm and gas velocity varied up to 5.5 m/s. It was observed that heat transfer coefficients increase with bed temperature, and it was shown that this increase is partly due to radiative heat transfer and partly due to a change of the thermal properties of the fluidizing gas and particles.

3. Transient bed-surface contact behavior around a horizontal tube was measured experimentally by a capacitance probe, at room temperature. The results indicated that the tube surface experiences alternating dense and lean phase contacts. Dense phase is envisaged

as closely packed particles (voidage in the range of 0.40 to 0.80) and lean phase is regarded as a gaseous medium with some entrained particles (voidage in the range of 0.80 to 1.00). Quantitative information from these contact measurements were used as an input to a phenomenological heat transfer model which accounts for both the dense phase and lean phase heat transfer. It is proposed that dense phase heat transfer occurs by transient conduction and lean phase heat transfer by turbulent convection. The packet renewal theory was modified to account for the dense phase heat transfer and a new model was suggested for the lean phase heat transfer. Using only the fluid mechanic information on the bed-tube contacts, the model predicted heat transfer coefficients with an average deviation of 44.2 percent from the experimental data, for the test conditions covered in this study.

4. A separate empirical, freeboard-heat-transfer correlation was developed. This correlation represented all the experimental heat transfer data from both low temperature and high temperature tests, for particle diameters ranging from 275 to 1400 μm, gas velocities varying from minimum fluidization to terminal velocities, and tube freeboard elevations of 1.6 cm to 225 cm with an

average deviation of 28.8 percent. The final form of the correlation is

$$h_n = \frac{1}{1 + \left[4.1 \times 10^{-9} \frac{H\, d_p (\rho_s - \rho_g)^2 g}{(U_{sg} - U_{mf}) \rho_g \mu_g}\right]^{2.578}}$$

Designation	Size Range (μm)	Mean Size d_p (μm)	U_{mf} (m/s)	U_t (m/s)
Glass beads	200-300	275	0.0615	2.15
Glass beads	680-1100	850	0.434	6.66
Silica sand	115-350	285	0.065	2.24
Silica sand	250-700	465	0.173	3.65

Table 1 Properties of the test particles

Reference	Particles	Mean Particle Size (μm)	Heat Transfer Tube	Static Bed Height (m)	Bed Temperature (°C)	Bed Pressure (atm)
George and Grace (1979)	Silica sand	102,470,890	Tube Bundle	0.22-0.75	120-145	1
Byam et al. (1980)	Coal-Dolomite	1100	Tube Bundle	1.2-1.5	780-890	6
Wood, et al. (1981)	Silica sand	930	Tube Bundle	0.15-0.70	Room Temperature	1
This Work	Glass beads Silica sand	275, 850 285, 465	Single Tube	0.36	Room Temperature	1

Table 2 Test conditions of various investigators

T_B °C	Silica Sand d_p=465μm	Silica Sand d_p=1200 μm	Limestone d_p=1400 μm
25	3.65	9.04	10.97
300	3.94	10.01	11.70
500	4.02	10.20	12.00
750	4.08	10.50	12.25

Table 3 Entrainment velocities of test particles in m/s.

T_B °C	Silica Sand d_p=465 μm	Silica Sand d_p=1200 μm	Limestone d_p=1400 μm
25	0.173	0.680	0.790
300	0.110	0.560	0.710
500	0.090	0.540	0.690
750	0.081	0.480	0.630

Table 4 Minimum fluidization velocities of test particles in m/s.

	ρ, kg/m^3	C_p, J/kg °K	k, w/m °K
Glass	2480	753	0.89
Air	1.223	1004	0.026
Silica	2526	735	1.17
Limestone	2548	837	1.20

Table 5 Thermophysical properties of test particles at room temperatures

T_B °C	300	500	750	
T_{Sa} °C	40-70	130-150	180-200	
T_f °C	177.5	320	470	
ρ, kg/m^3	2526	2526	2526	Silica (34)
C_{ps}, J/kgK	961	1047	1256	
k_s, w/m K	1.36	1.56	1.81	
ρ, kg/m^3	0.798	0.592	0.448	Air (35)
C_{pg}, J/kgK	1038	1054	1097	
k_g, w/m K	0.037	0.046	0.057	
μ_g, kg/ms	2.48×10^{-5}	3.17×10^{-5}	3.6×10^{-5}	

Table 6 Thermophysical properties of test particles at high bed temperatures

Particles	Average Deviation ,%	Standard Deviation,%
Silica sand, 465 µm	49.8	51.4
Glass beads, 275 µm	29.3	35.3
Glass beads, 850 µm	53.5	58.0
Overall Deviation,%	44.2	48.2

Table 7 Comparison of phenomenological heat transfer model with the experimental data

Particles	T_B=25 °C	T_B= 300 °C	T_B= 500 °C	T_B= 750 °C
Glass beads 275 µm	224 cm	-	-	-
Glass beads 850 µm	220 cm	-	-	-
Silica sand 285 µm	225 cm	-	-	-
Silica sand 465 µm	225 cm	197 cm	185 cm	174 cm
Silica sand 1200 µm	218 um	196 cm	183 cm	172 cm
Limestone 1400 µm	219 cm	194 cm	182 cm	173 cm

Table 8 Limiting entrainment height at entrainment velocity for different test particles and bed temperatures

Particles	Average Deviation (%)	Standard Deviation (%)
Limestone, 1400 μm	24.6	27.7
Glass beads, 275 μm	27.0	39.4
Silica sand, 465 μm	24.2	28.4
Glass beads, 850 μm	42.0	51.8
Silica sand, 1200μm	39.0	47.3
Silica sand, 285 μm	16.2	23.8
Overall Deviation (%)	28.8	36.4

Table 9 Comparison of the empirical correlation with the experimental data

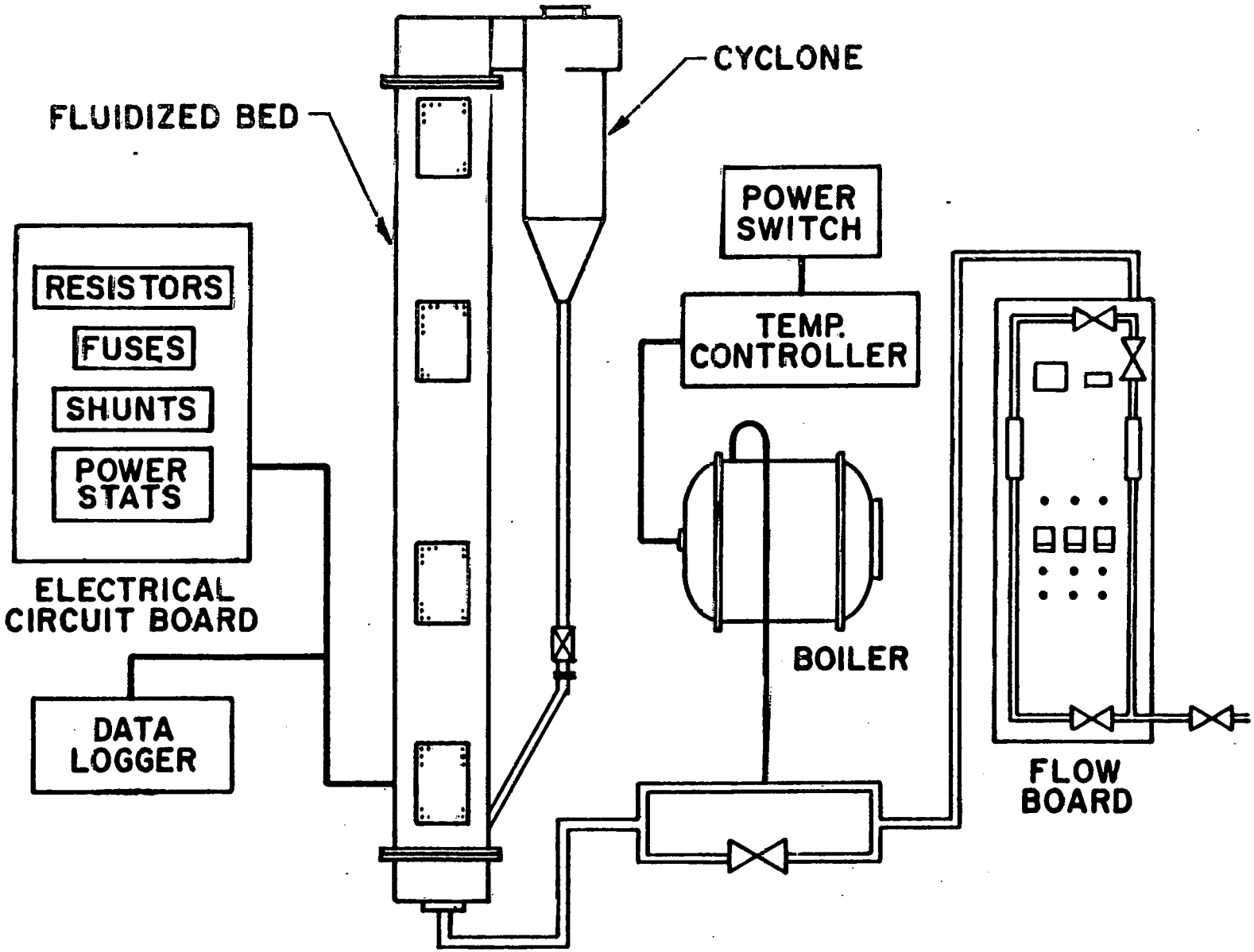

Figure 1 Flow diagram for the fluidized bed test unit

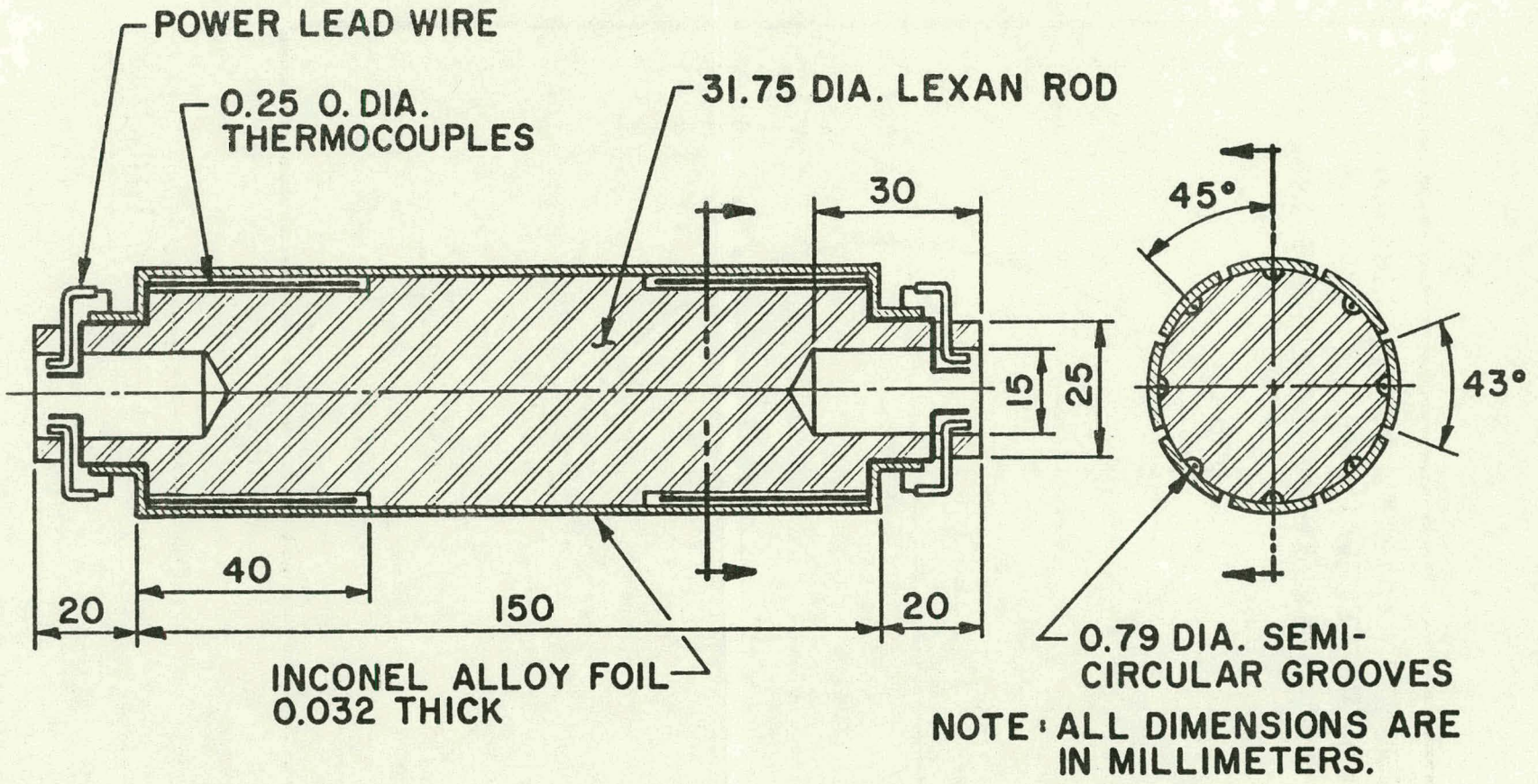

Figure 2 Test tube of local heat transfer coefficients

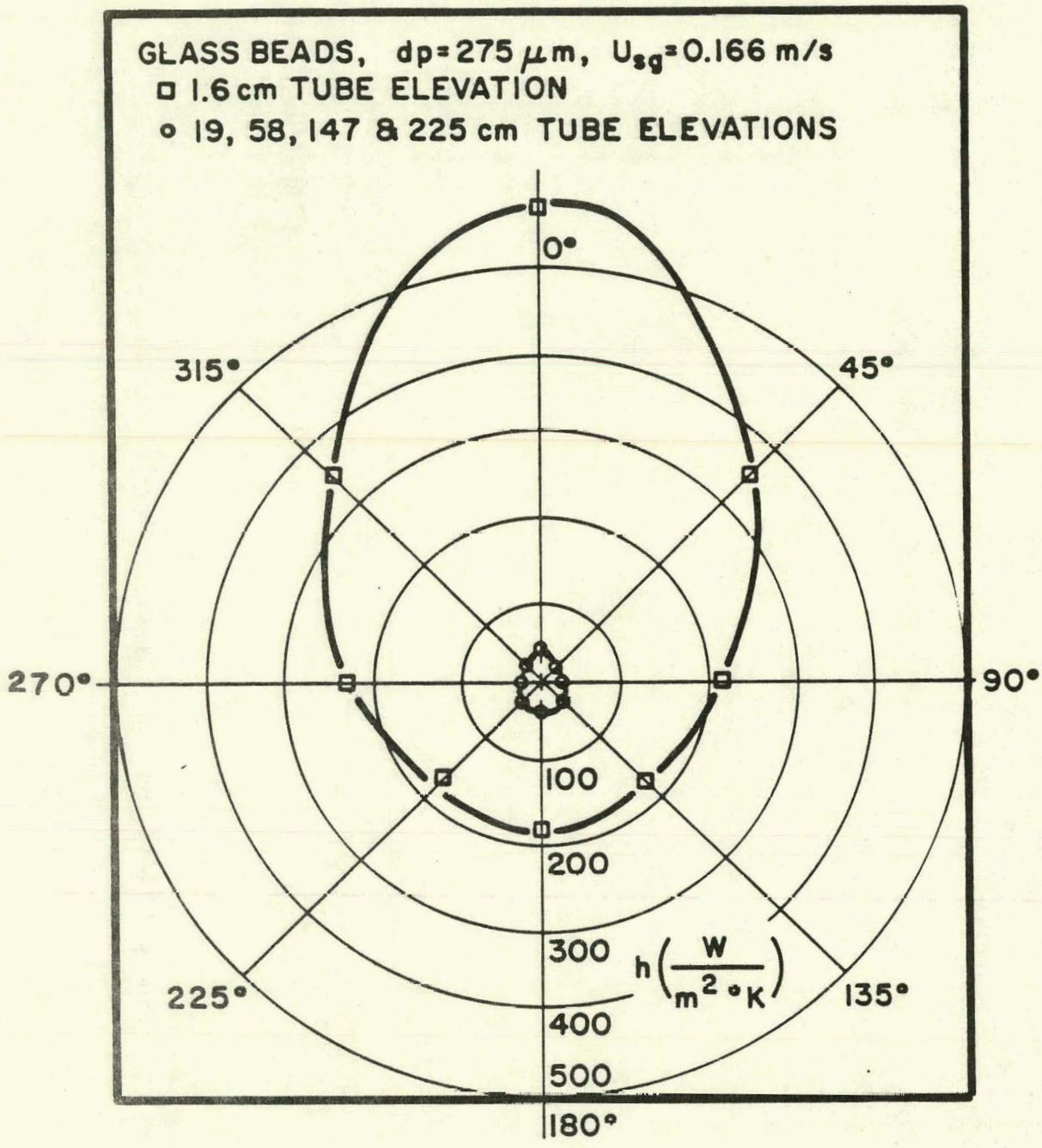

Figure 3 Local heat transfer coefficient around the tube in freeboard region for three times minimum fluidization velocity

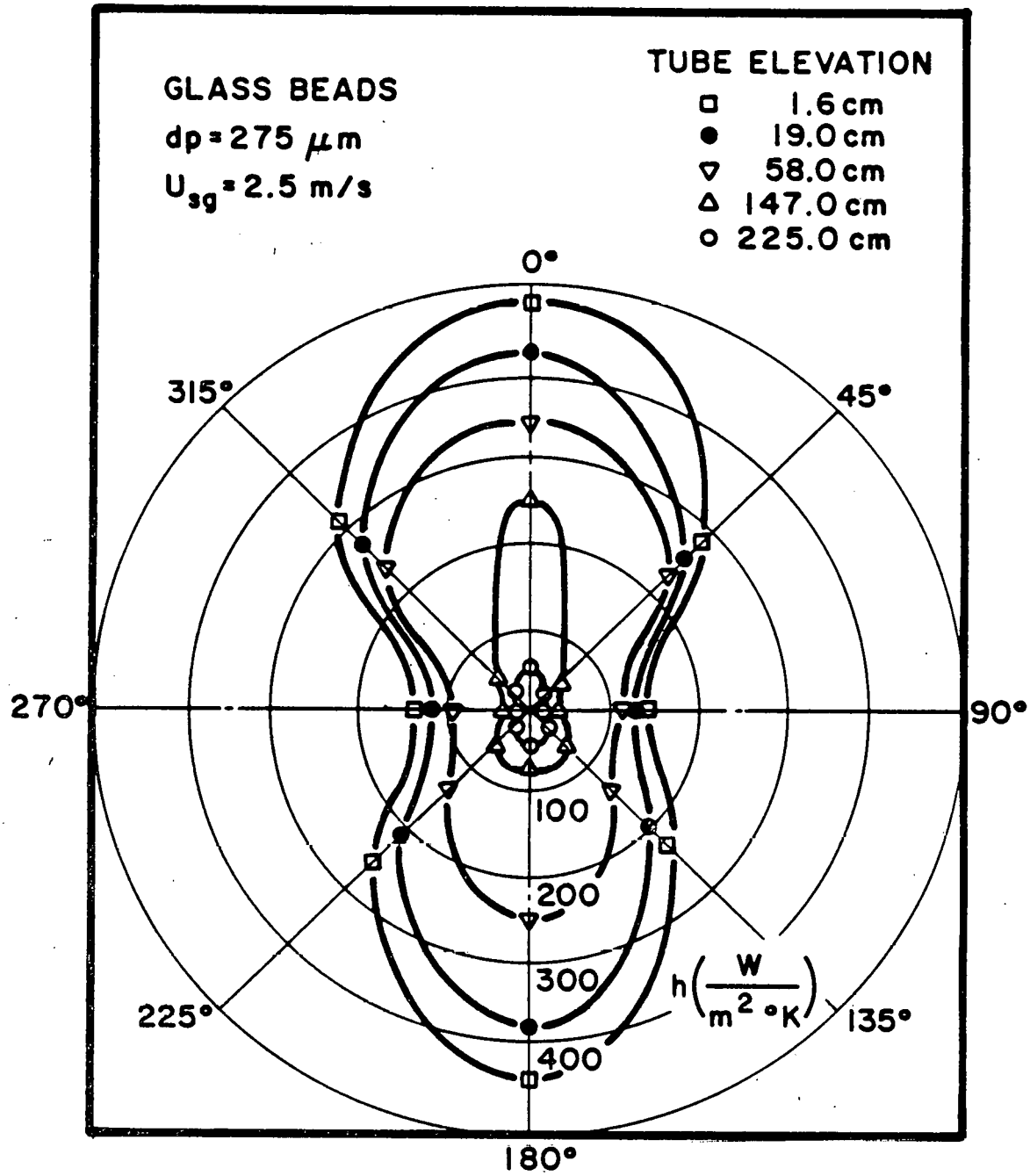

Figure 4 Local heat transfer coefficient around the tube in freeboard region for 40 times minimum fluidization velocity

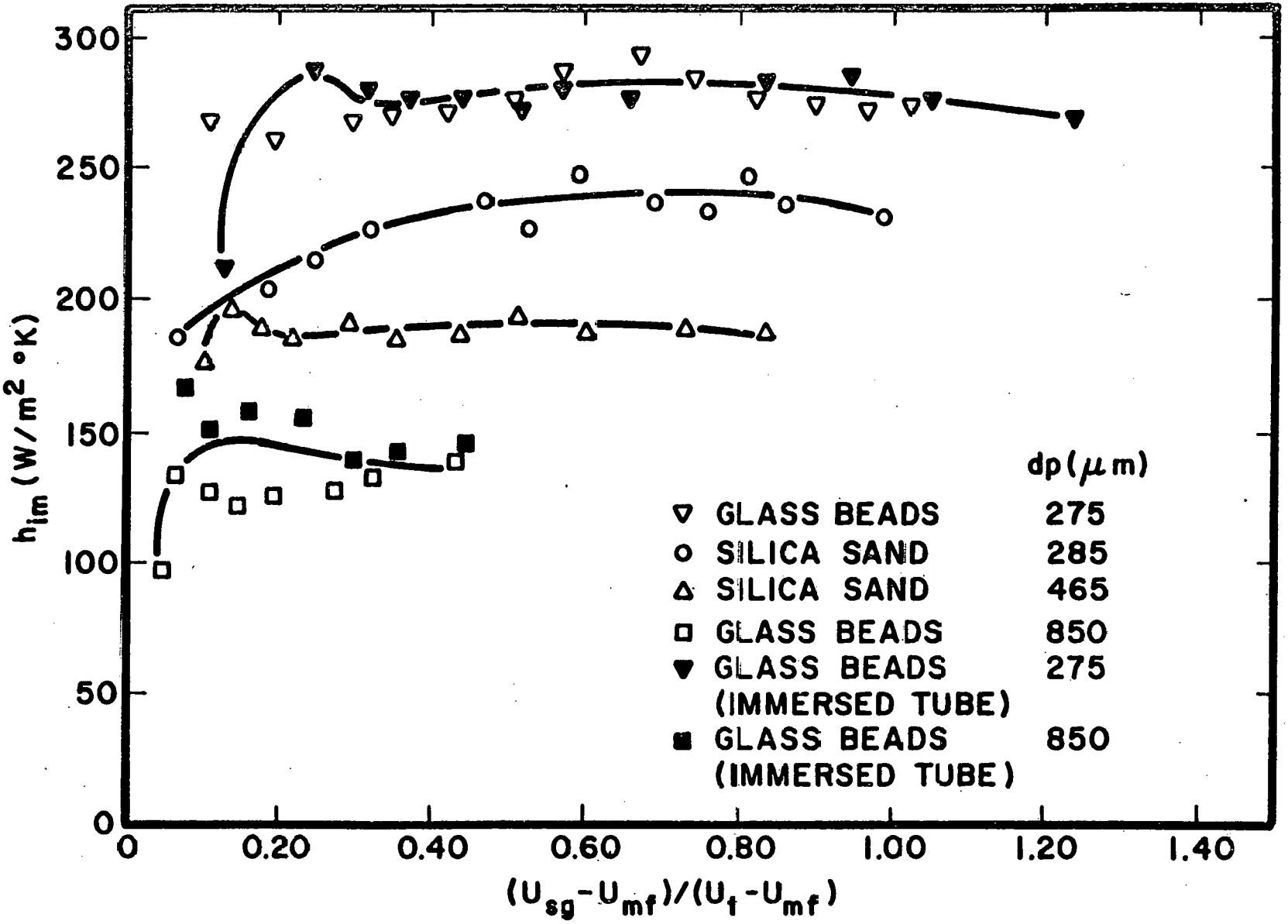

Figure 5 Average heat transfer coefficients at static bed surface and immersed tubes

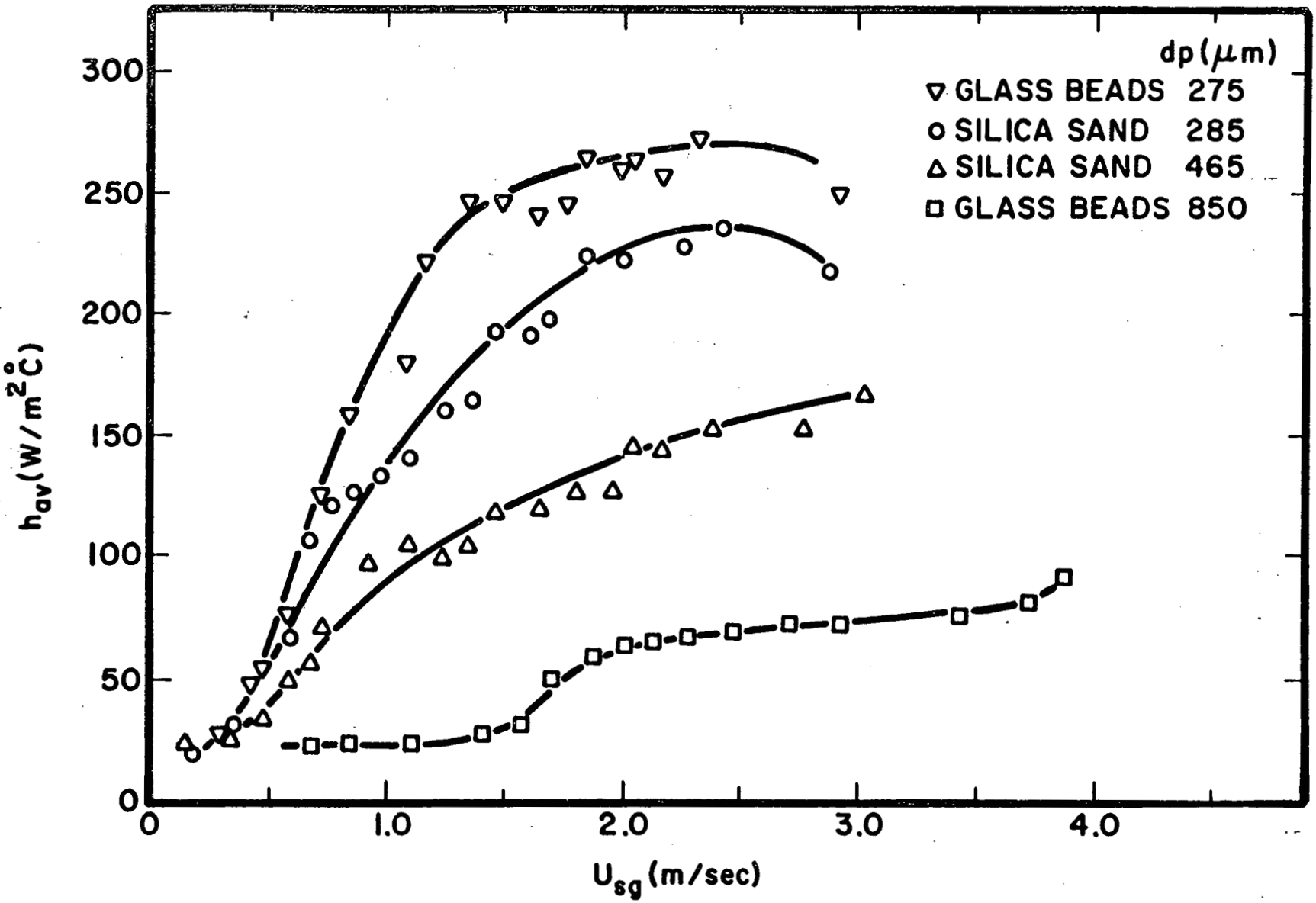

Figure 6 Average heat transfer coefficients for tubes at 19 cm elevation

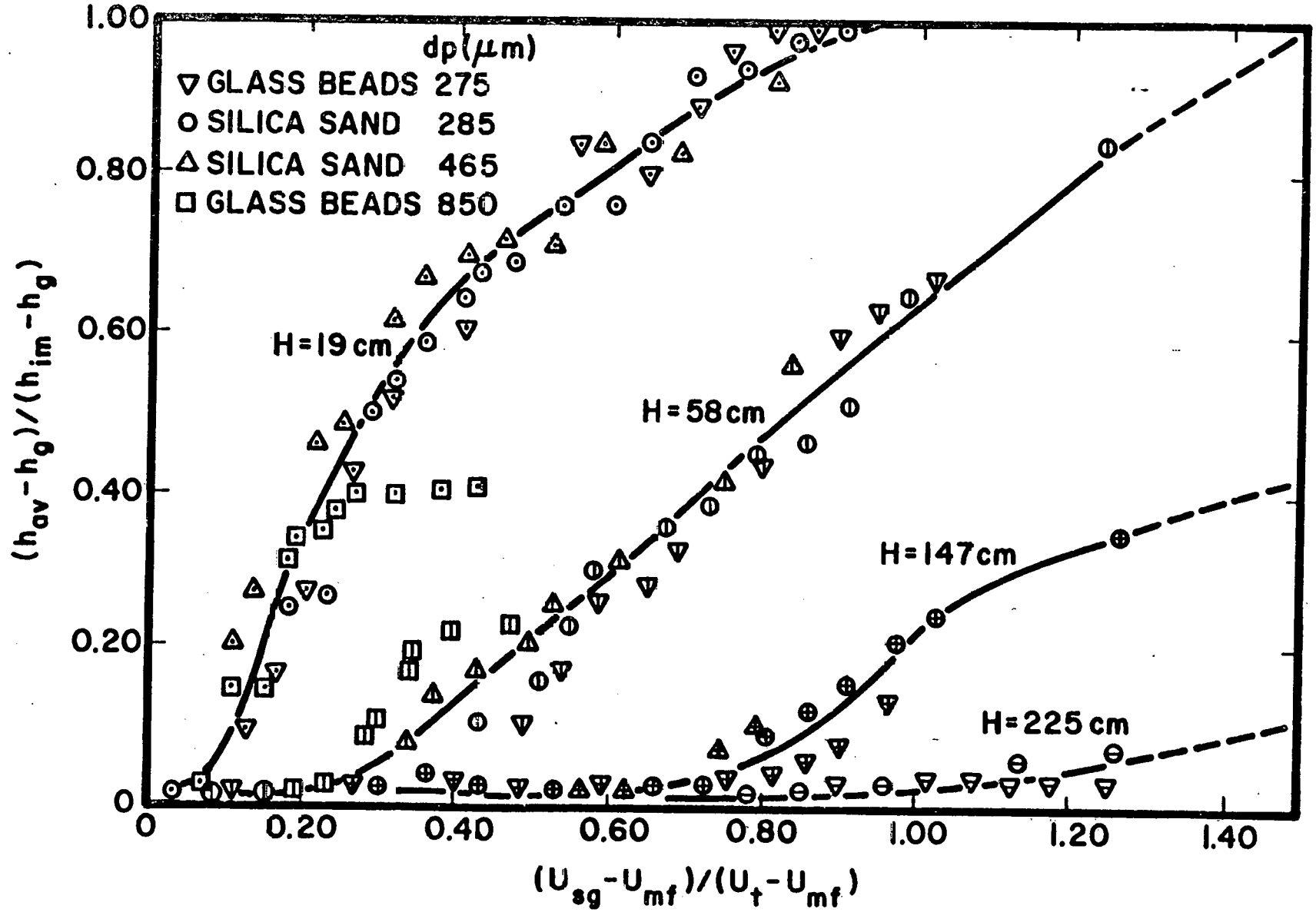

Figure 7 Average heat transfer coefficients as a function of gas velocity in freeboard region for different test particles

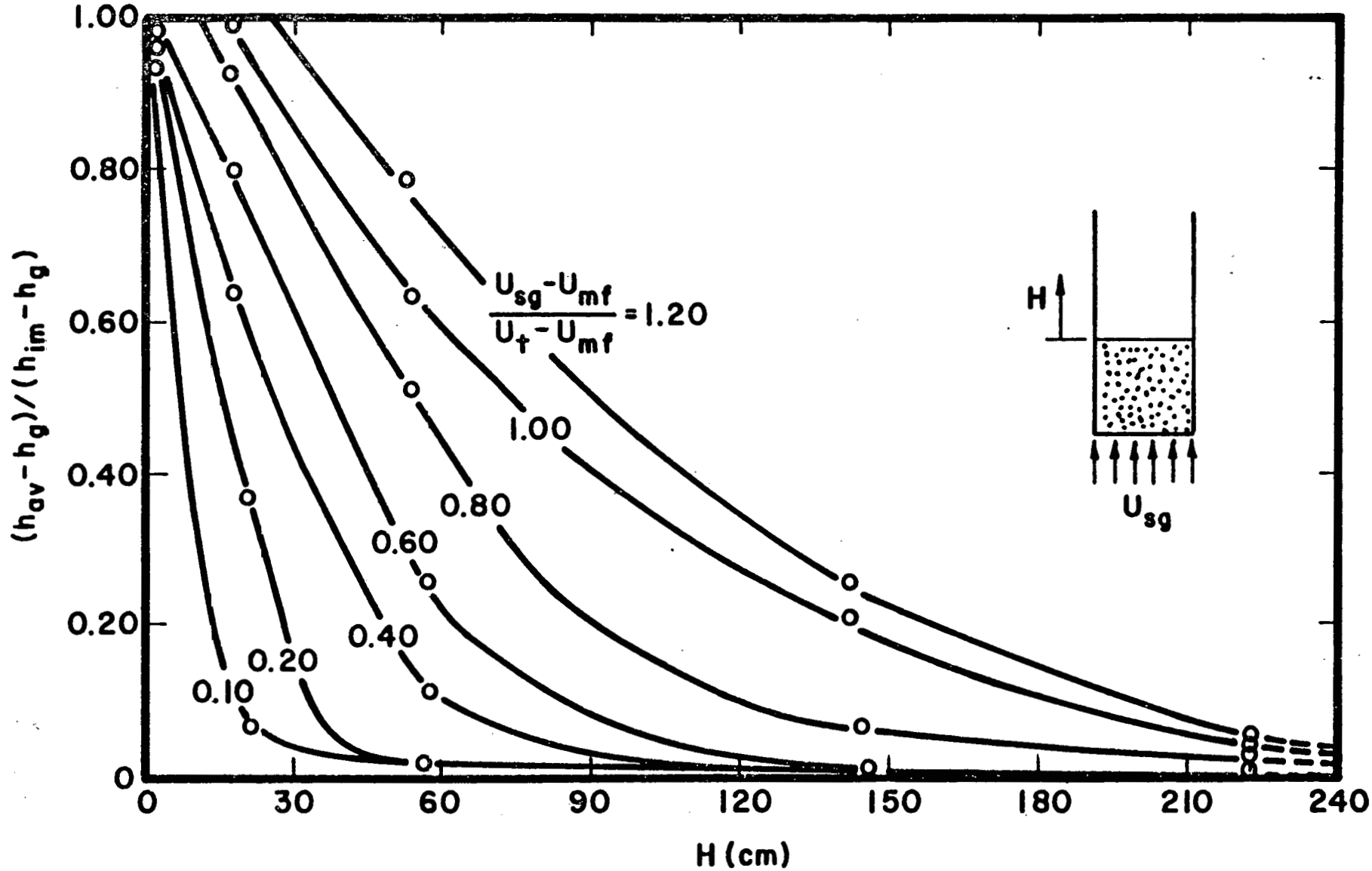

Figure 8 Variation of normalized heat transfer coefficient along the freeboard for different gas velocities

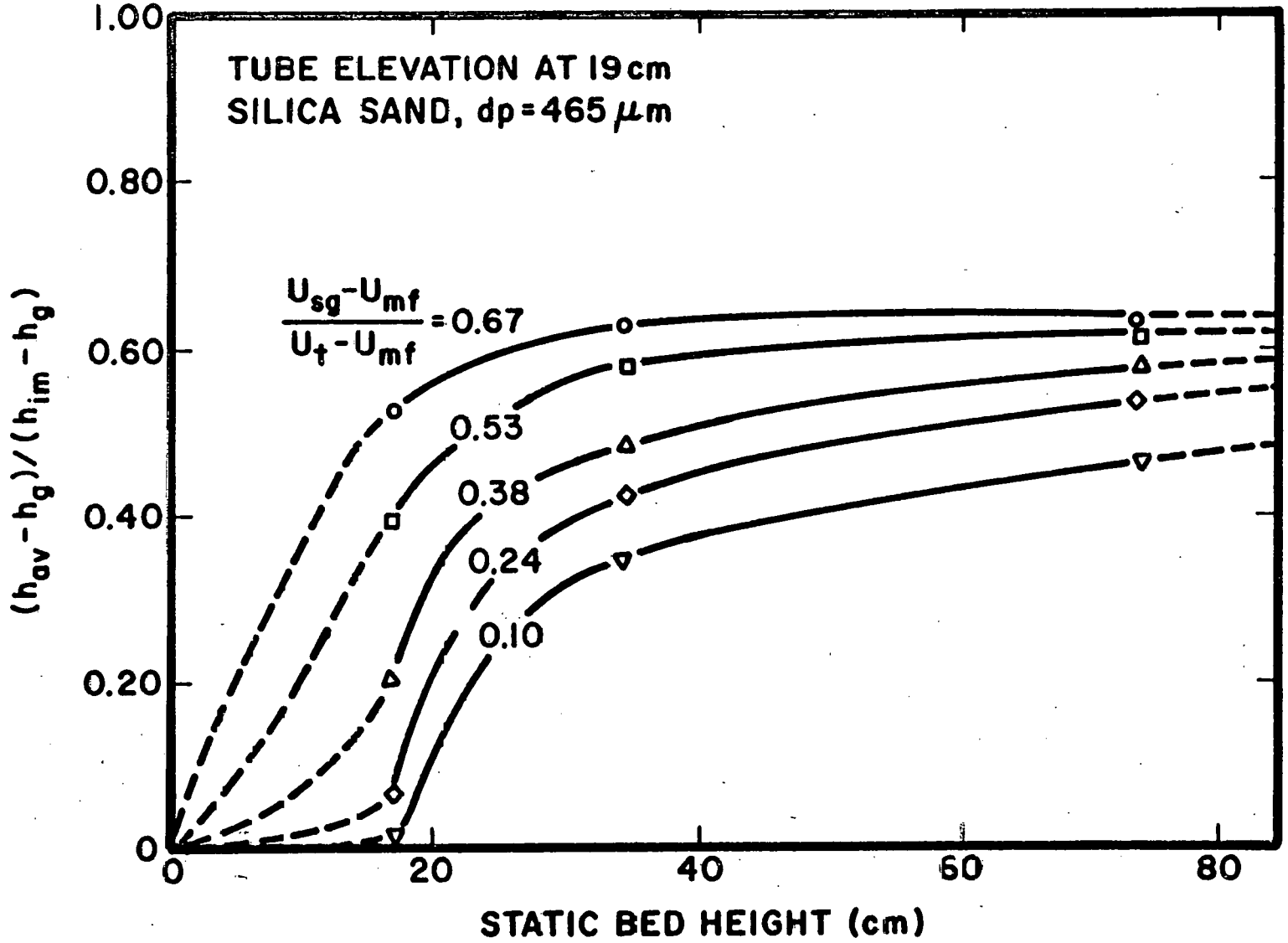

Figure 9 Effect of static bed height on heat transfer coefficients

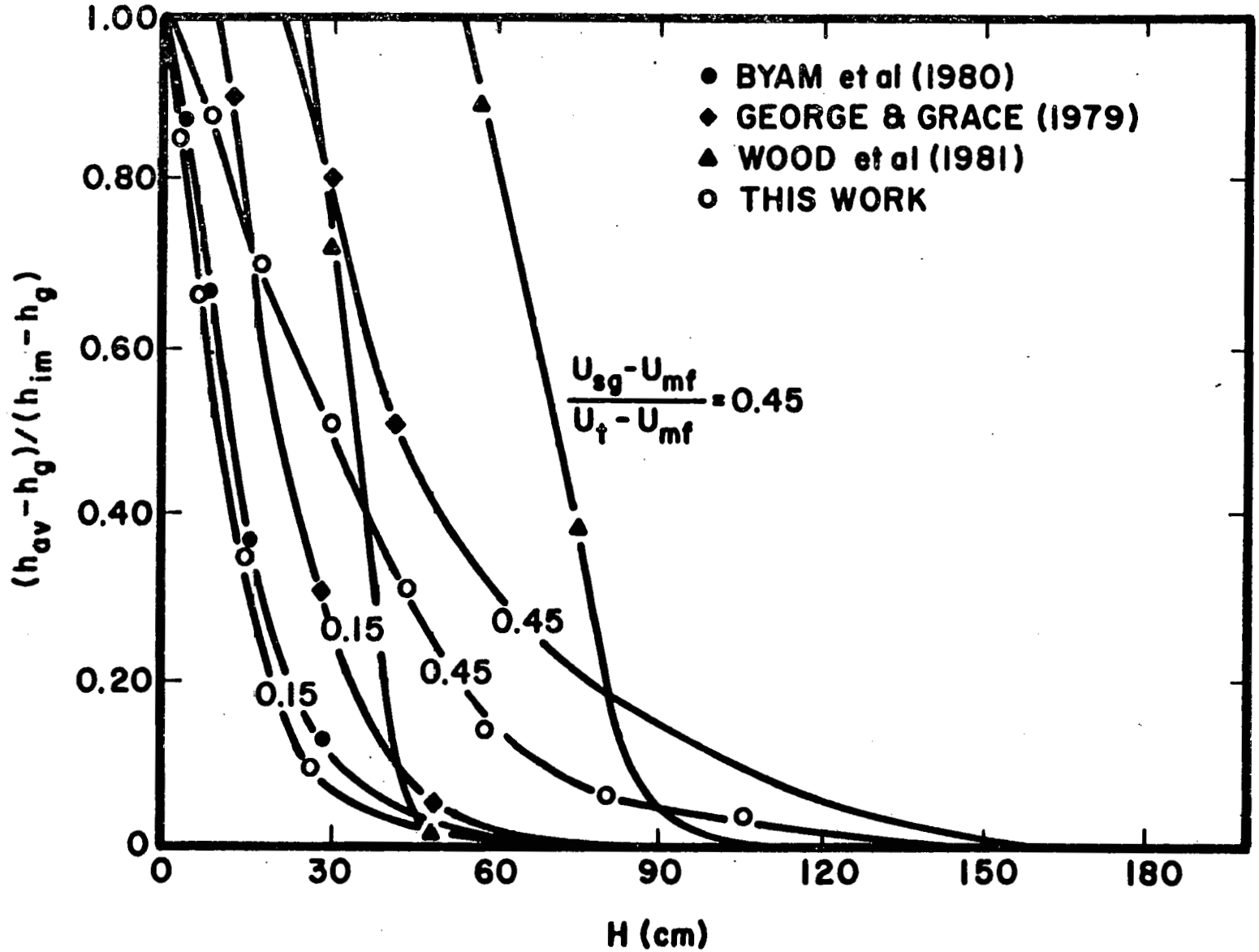

Figure 10 Comparison of heat transfer coefficients in the freeboard region of fluidized beds

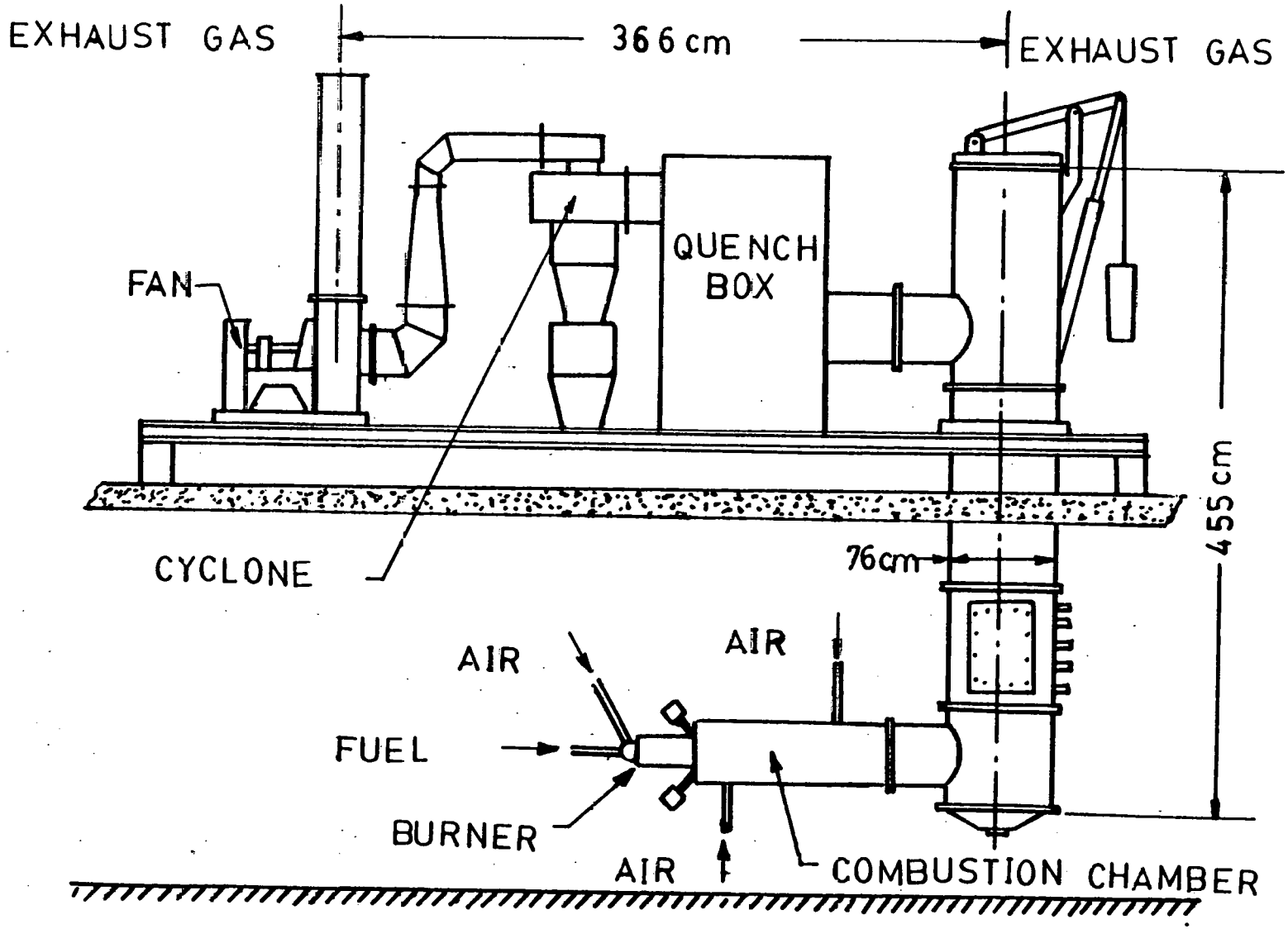

Figure 11 High temperature fluidized bed

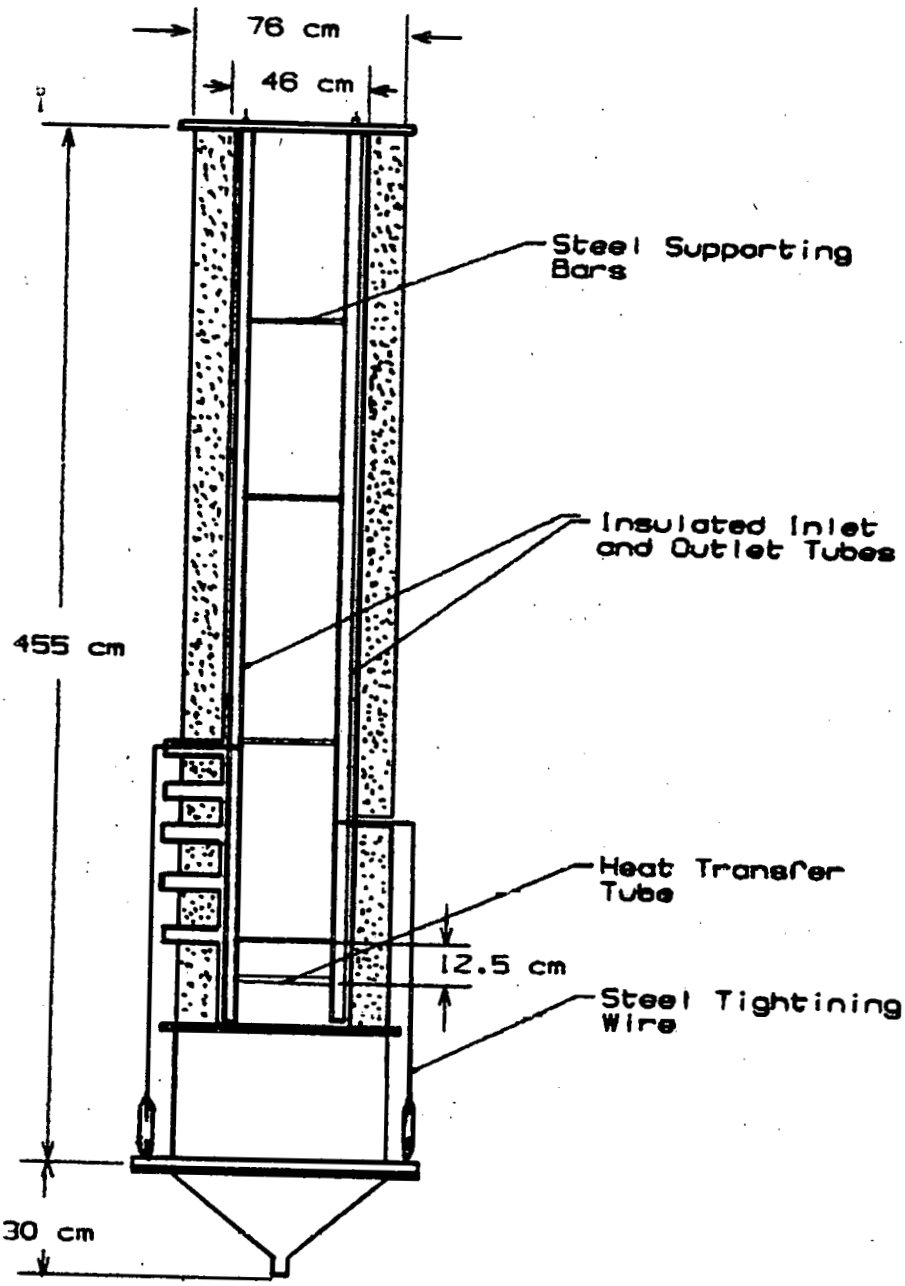

Fig. 12 High temperature fluidized bed and heat transfer test tube

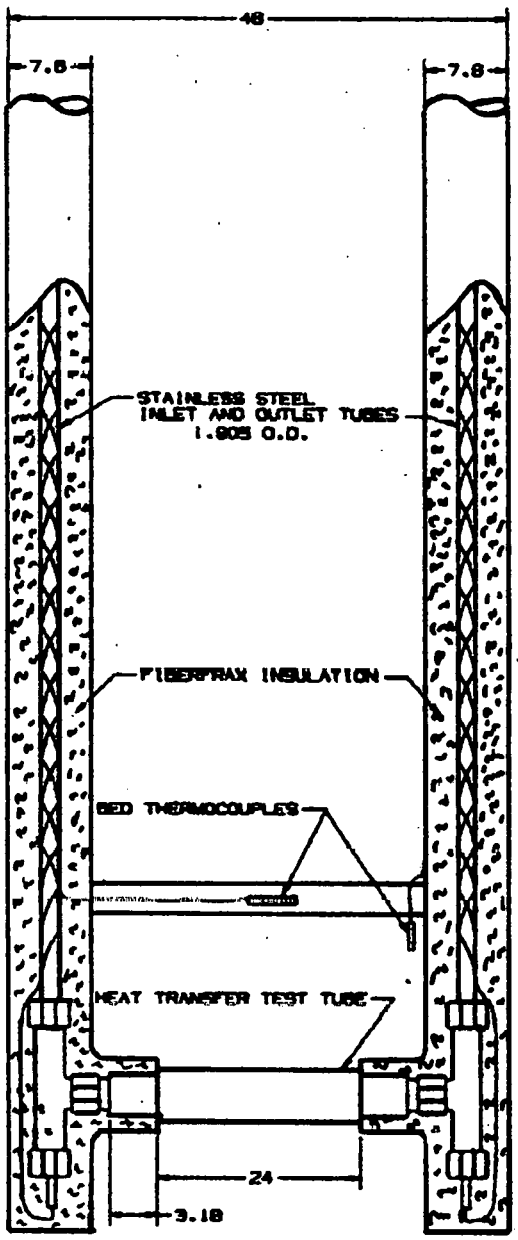

Fig. 13 Instrumented heat transfer test tube for high temperature fluidized bed

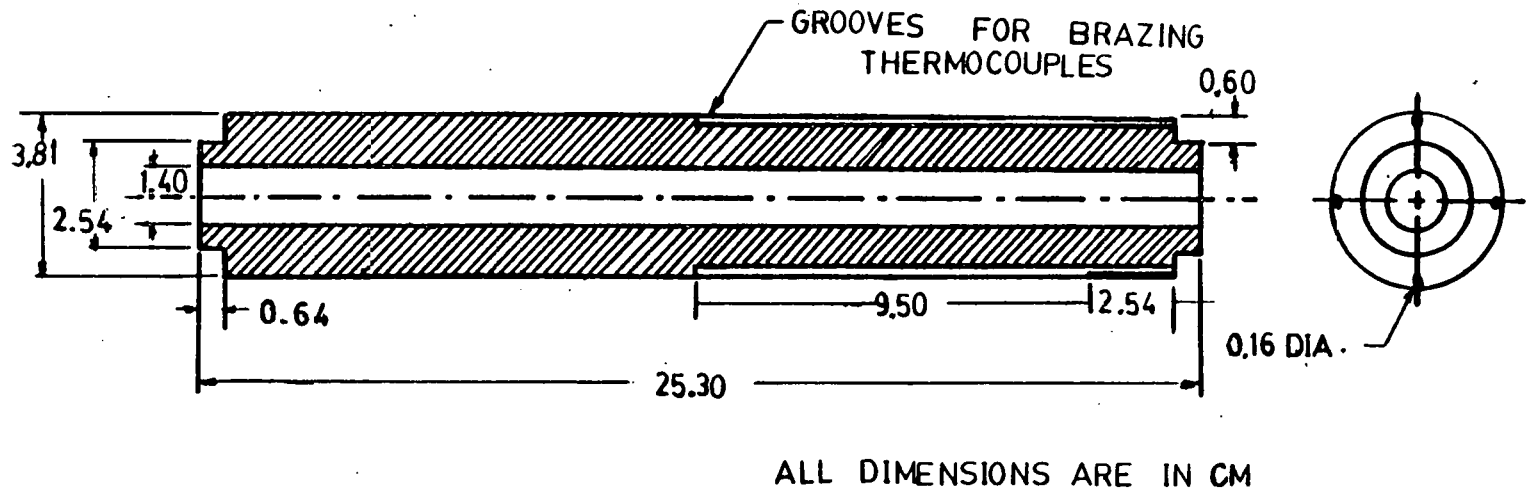

Fig. 14 Heat transfer tube test section for high temperature fluidized bed

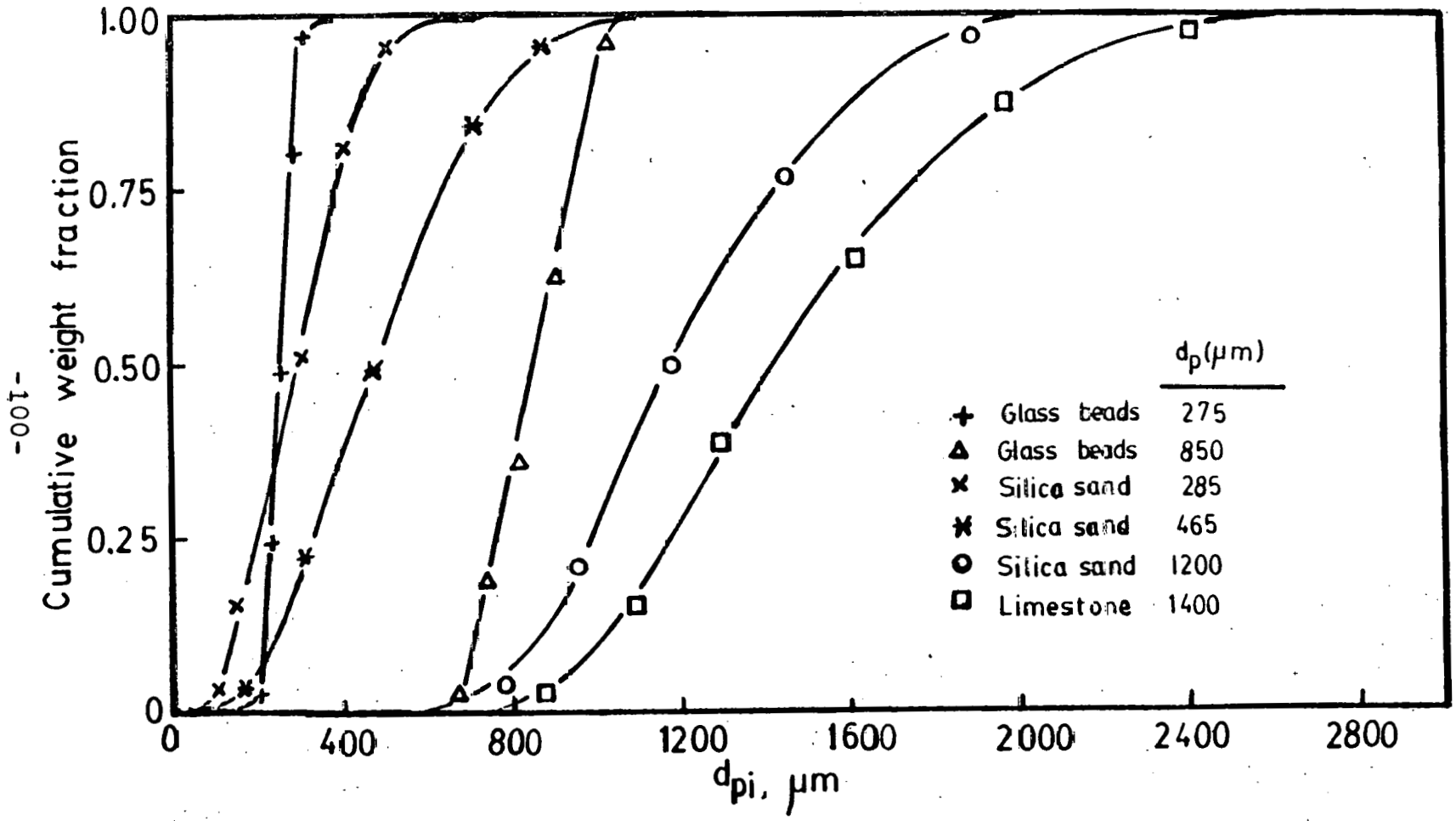

Fig. 15 Variation of cumulative weight fraction with sieve size for all the test particles

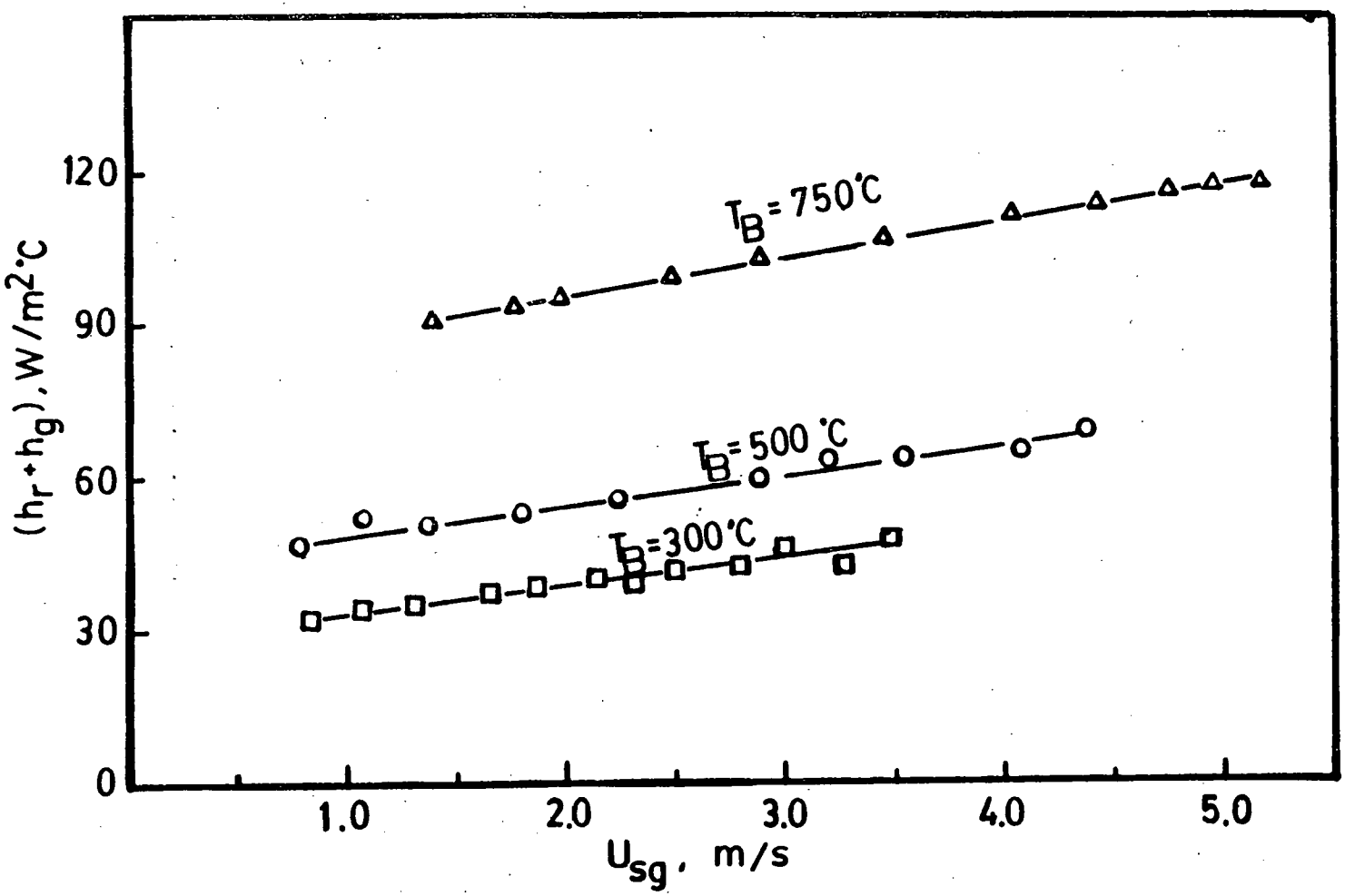

Fig. 16 Heat transfer coefficient for gas alone at high bed temperatures

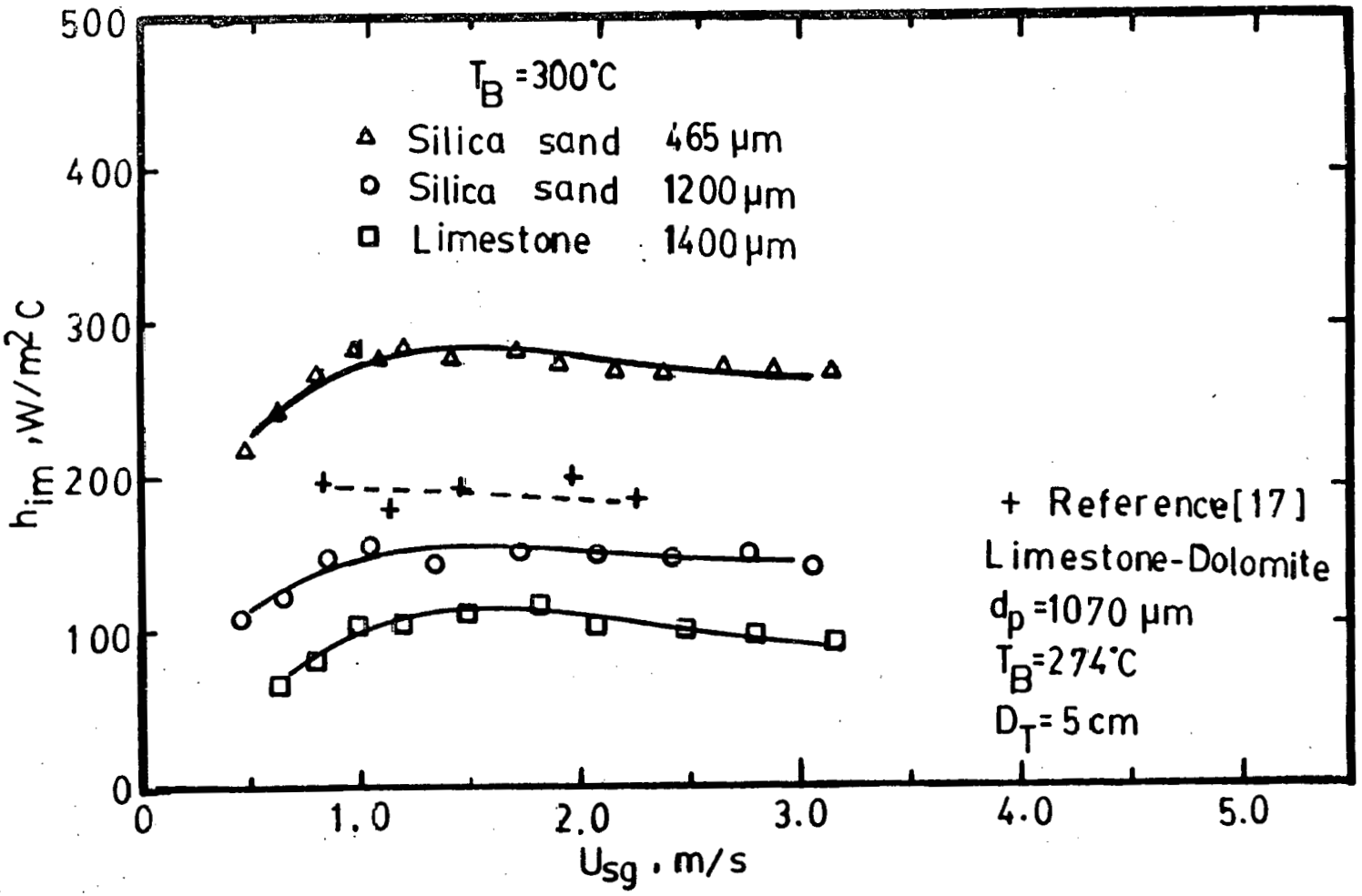

Fig. 17 Immersed tube heat transfer coefficients at high bed temperature of 300 °C for different test particles

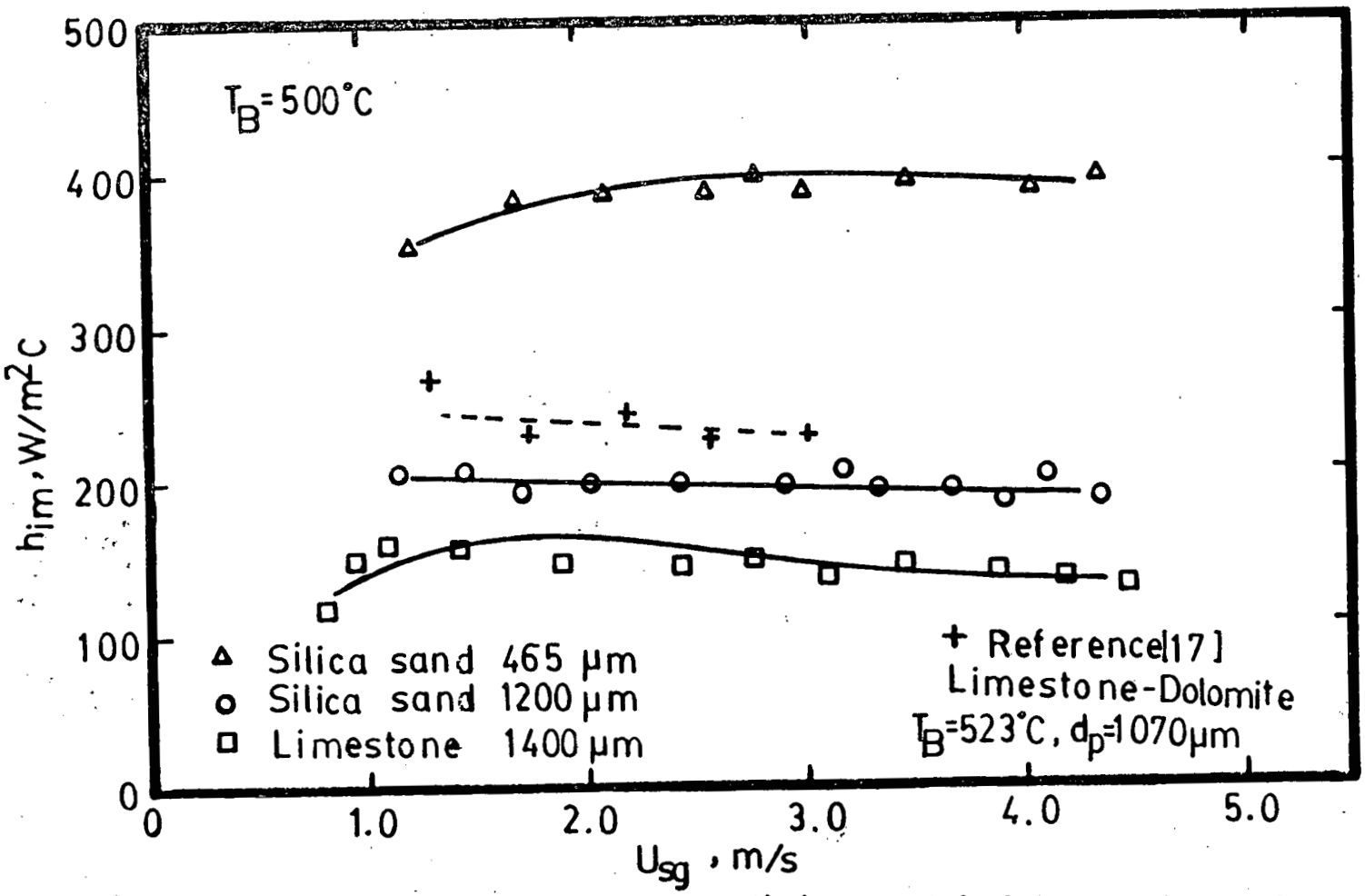

Fig. 18 Immersed tube heat transfer coefficients at bed temperature of 500°C for different test particles

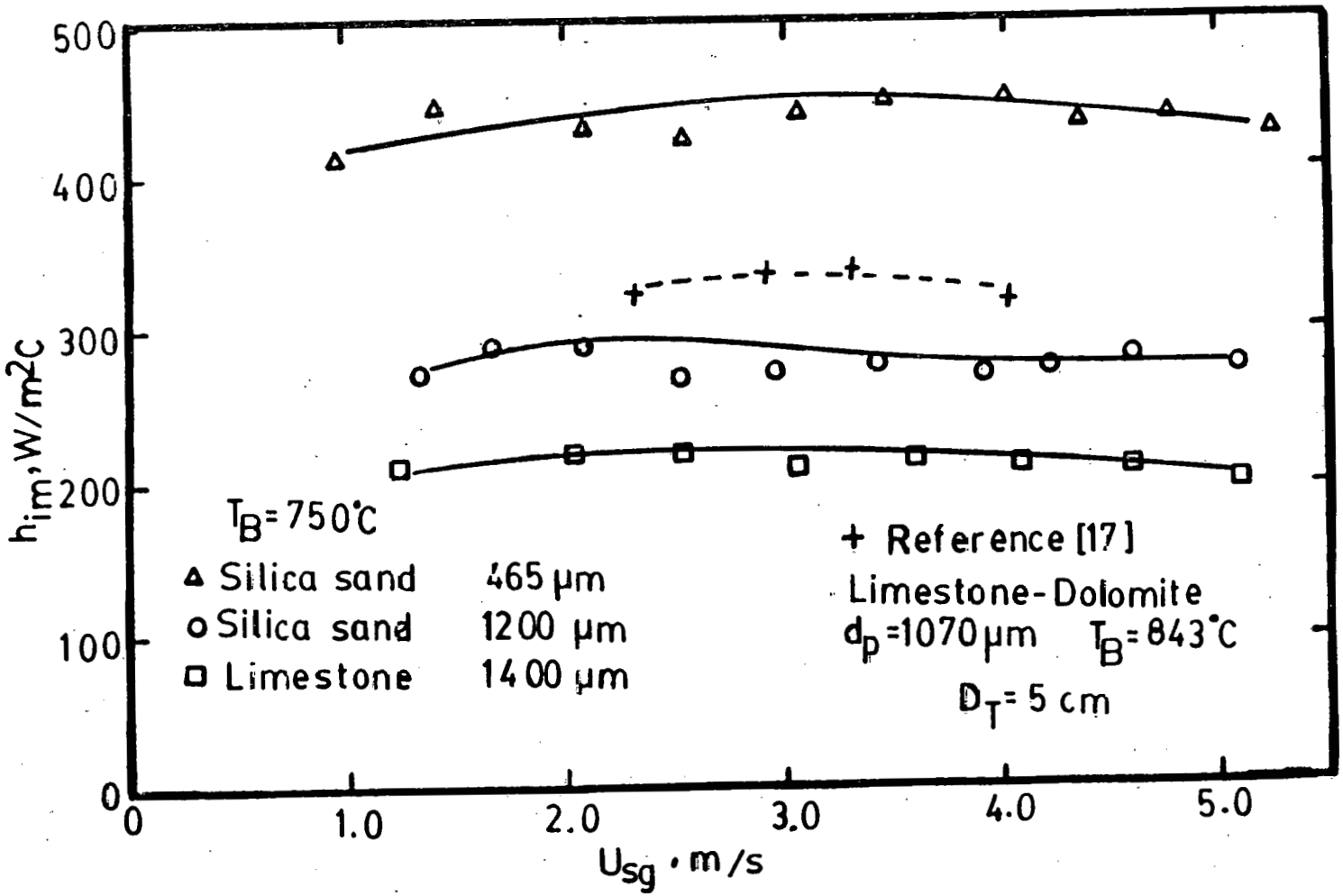

Fig. 19 Immersed tube heat transfer coefficients at bed temperature of 750°C for different test particles

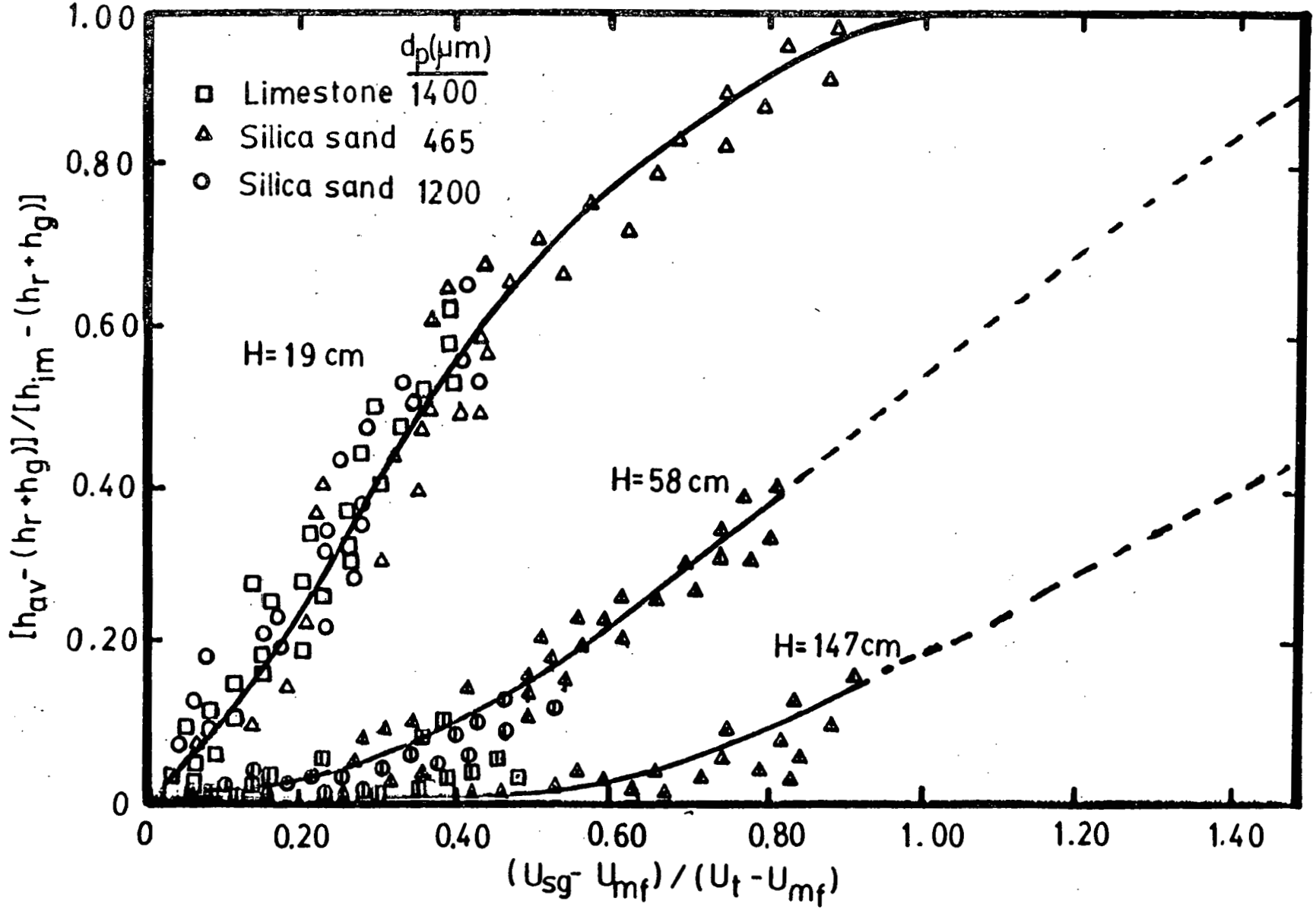

Fig. 20 Normalized heat transfer coefficients as a function of nondimensional gas velocity for different tube elevations

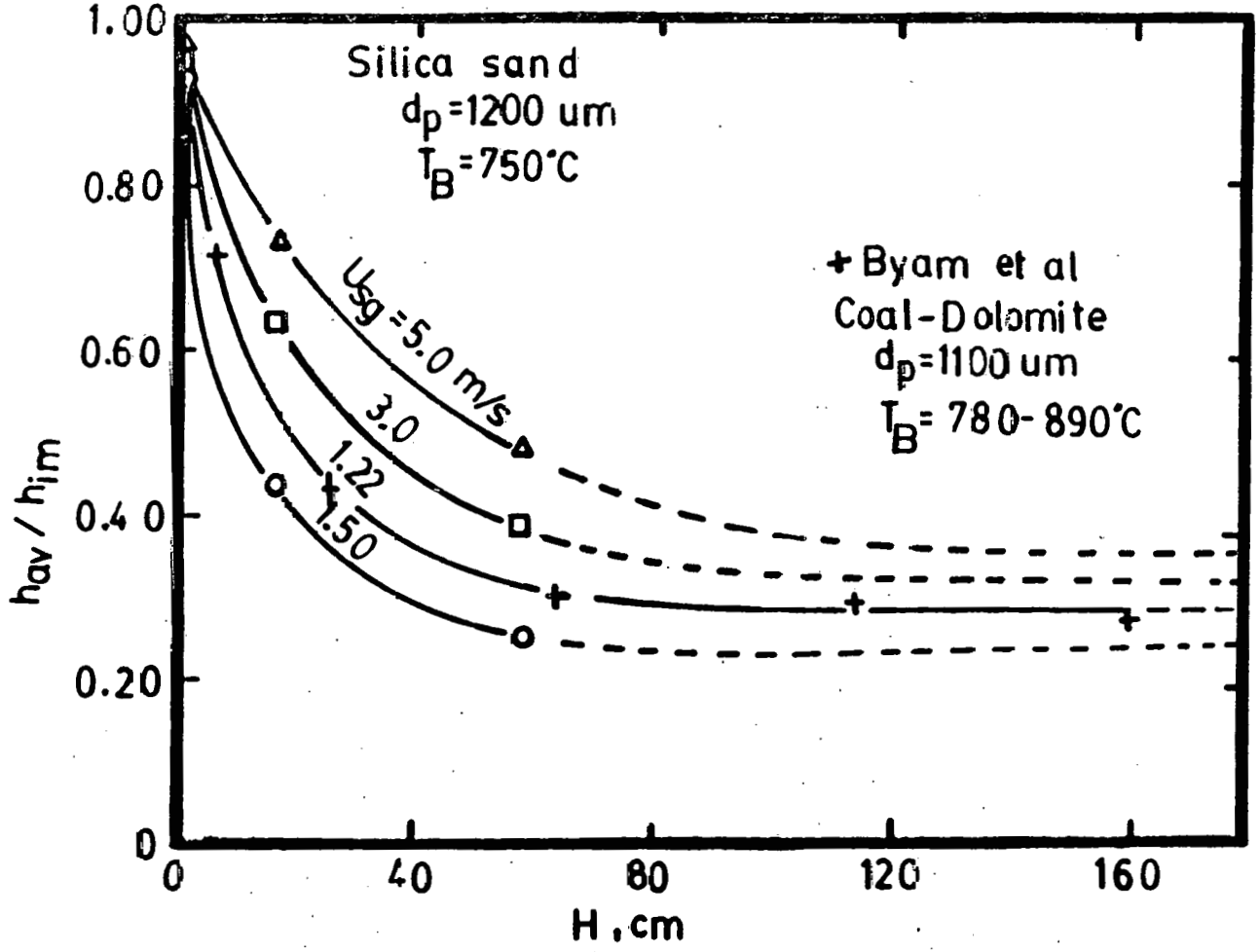

Fig. 21 Variation of heat transfer coefficients along the freeboard height and comparison with other existing data

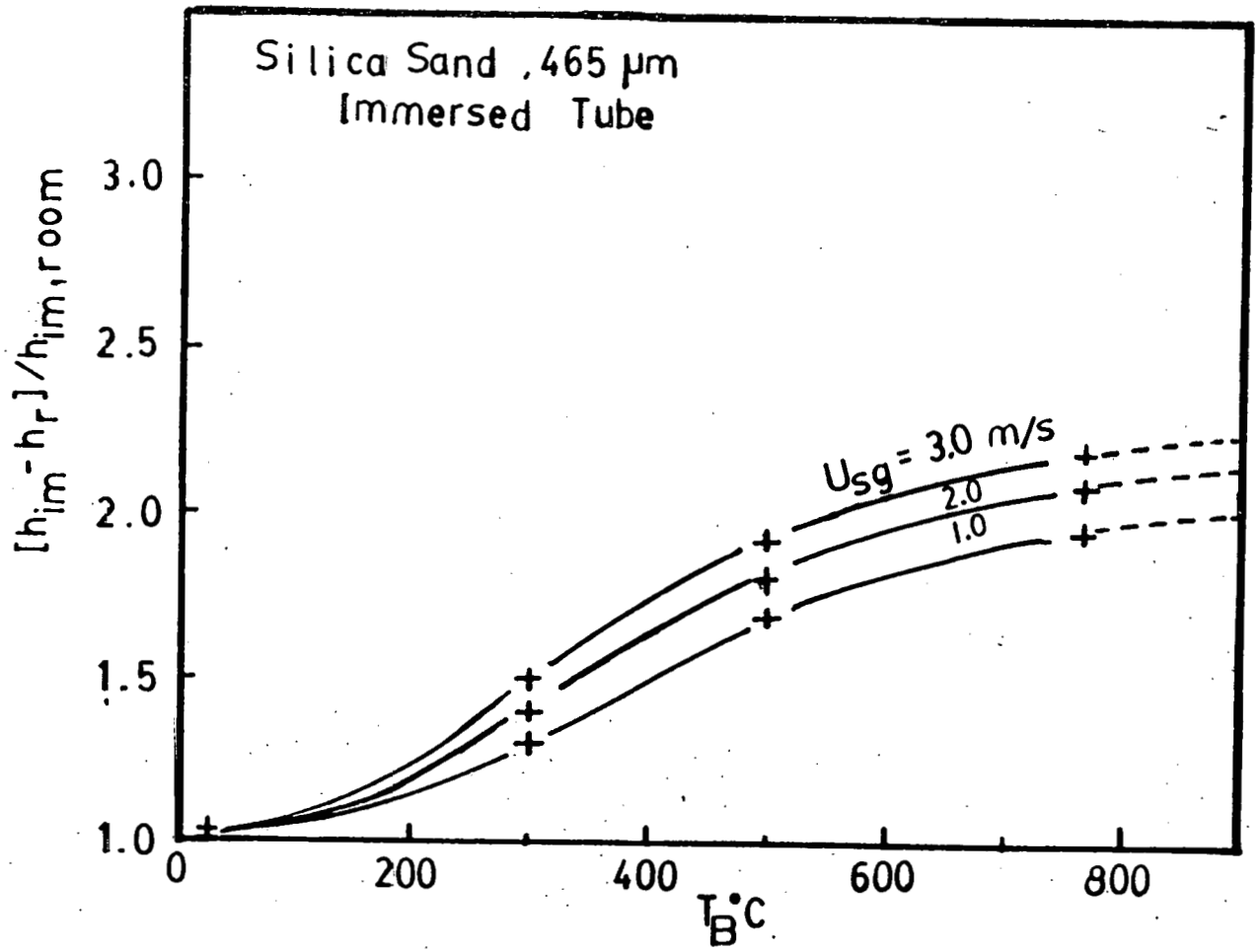

Figure 22 Increase of heat transfer due to thermal property changes of fluidizing gas and particles

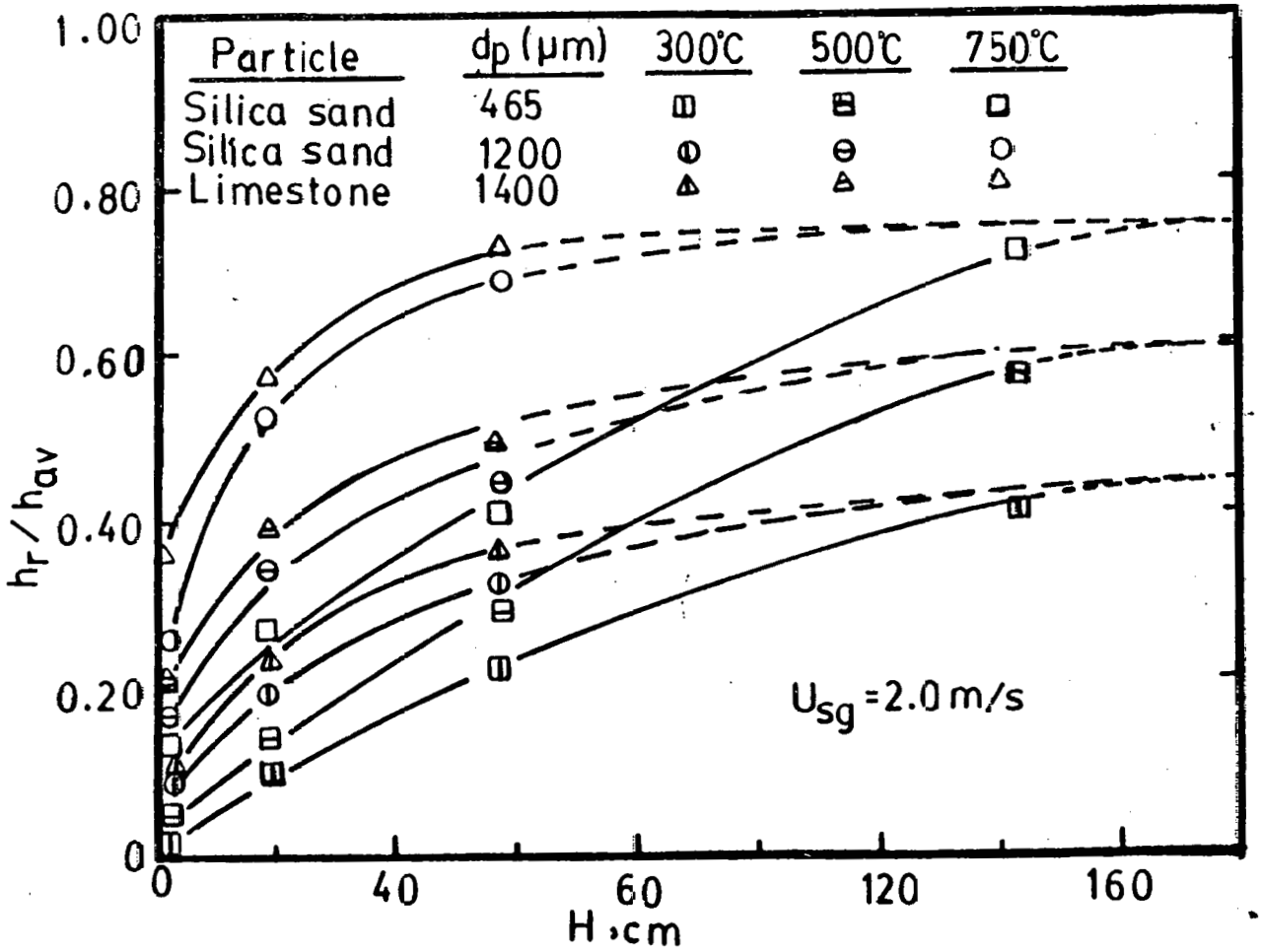

Fig. 23 Effect of radiative heat transfer on total heat transfer along the freeboard height for different test particles and bed temperatures

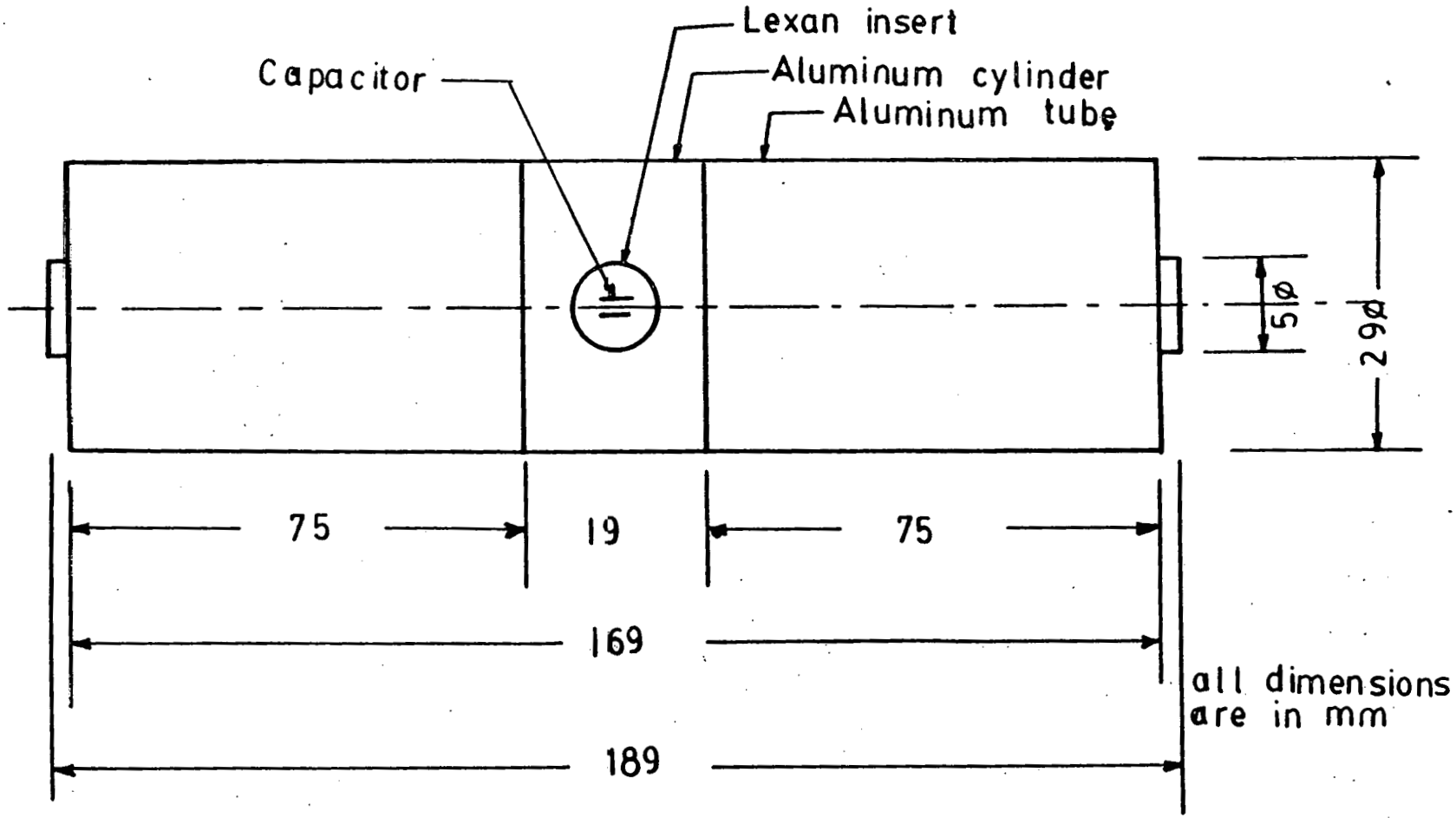

Figure 24 Capacitance test probe for local measurements at room temperature

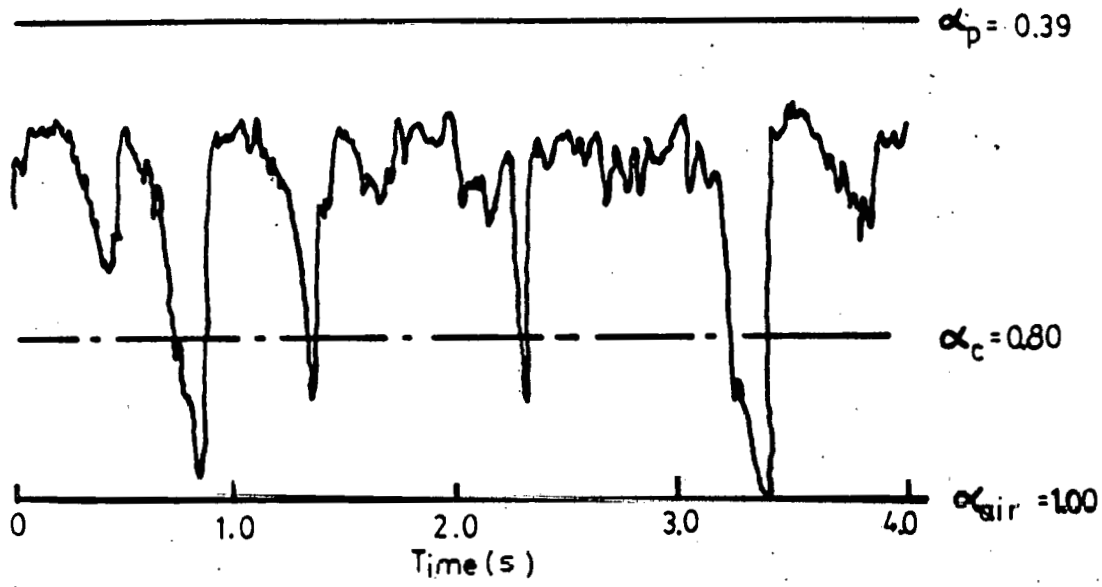

Figure 25a Typical capacitance probe signal for glass beads with 275 μm mean diameter, tube is at 1.6 cm elevation, 0° position. Flow rate is 20 times minimum fluidization.

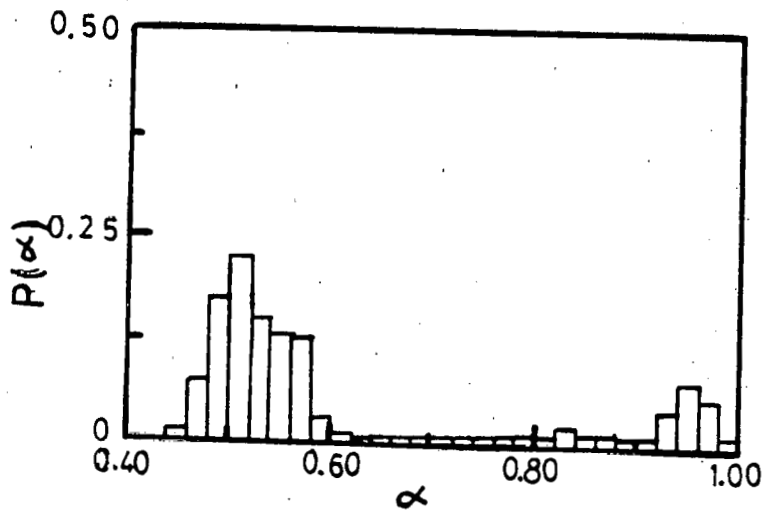

Fig. 25b Probability distribution of voidage for Fig. 25a.

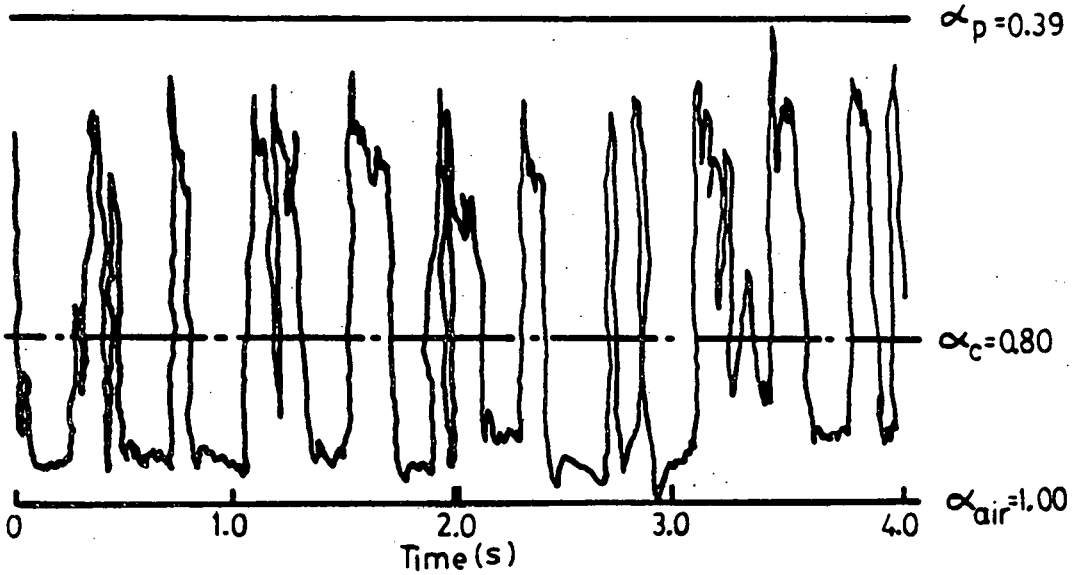

Fig. 26a Typical capacitance probe signal for glass beads with 275 μm mean diameter, tube is at 19 cm elevation, 0° position. Flow rate is 20 times minimum fluidization.

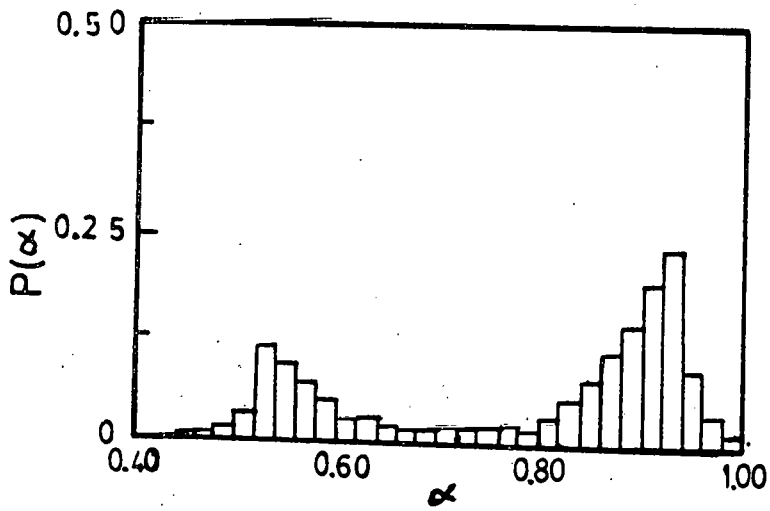

Fig. 26b Probability distribution of voidage for Fig. 26a.

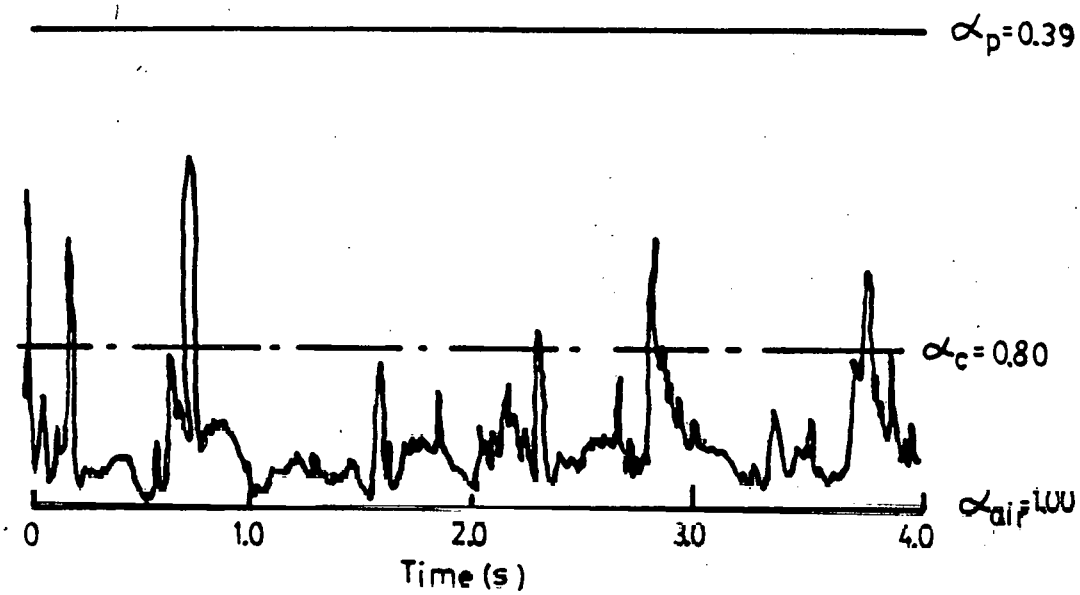

Fig. 27a Typical capacitance probe signal for glass beads with 275 μm mean diameter, tube is at 19 cm elevation , 90° position. Flow rate is 20 times minimum fluidization.

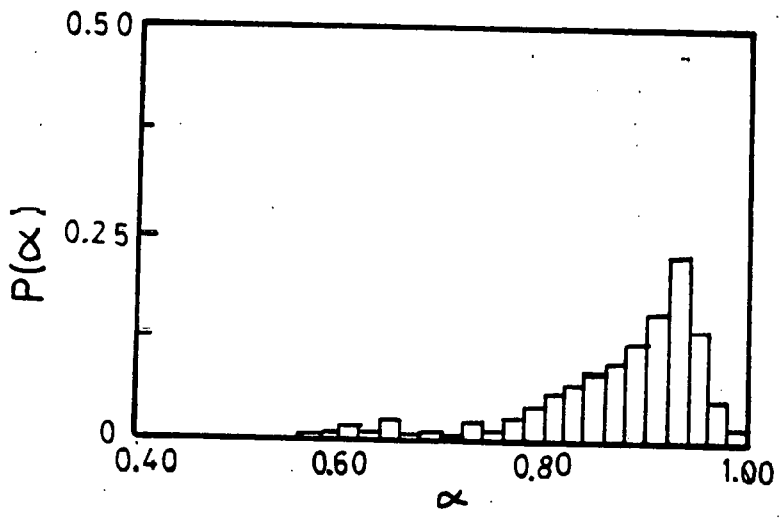

Fig. 27b Probability distribution of voidage for Fig. 27a.

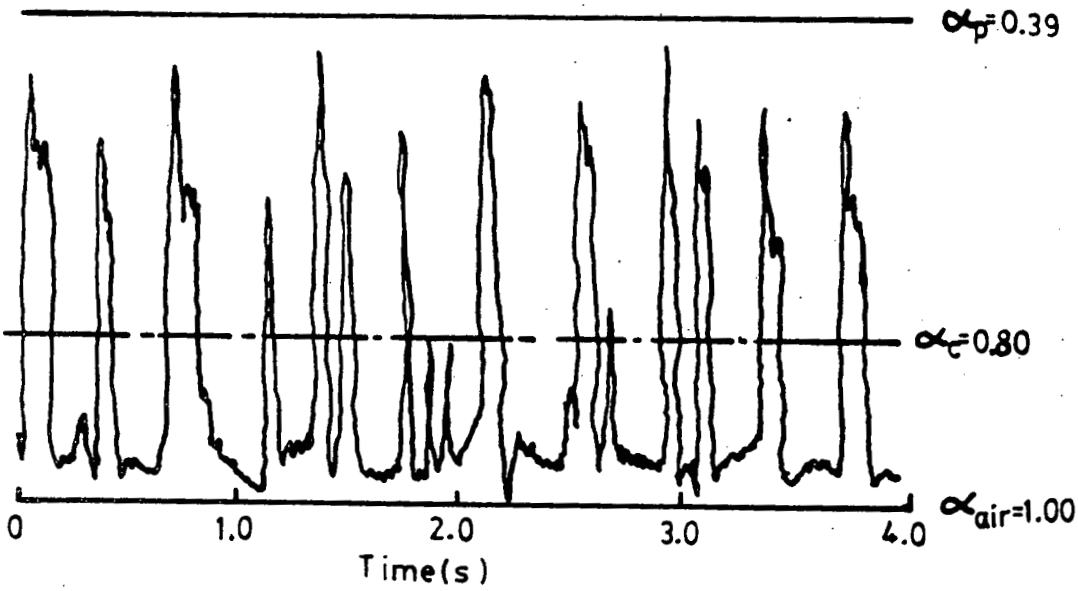

Fig. 28a Typical capacitance probe signal for glass beads with 275μm mean diameter, tube is at 19 cm elevation, 180° positiom. Flow rate is 20 times minimum fluidization.

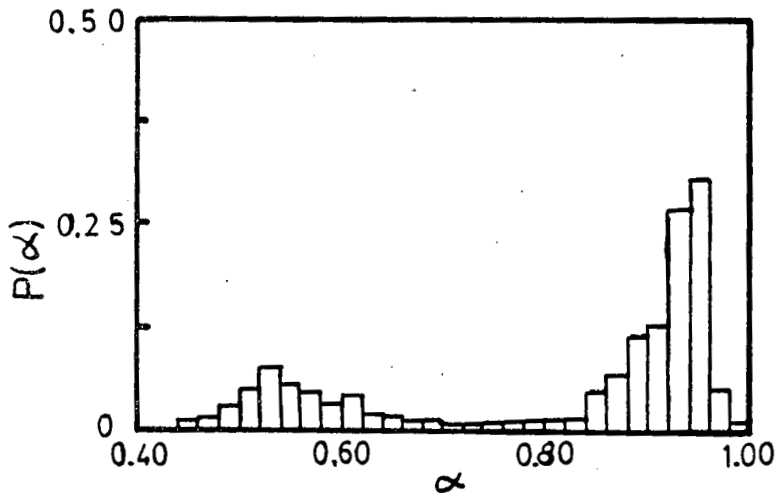

Fig. 28b Probability distribution of voidage for Fig. 28a.

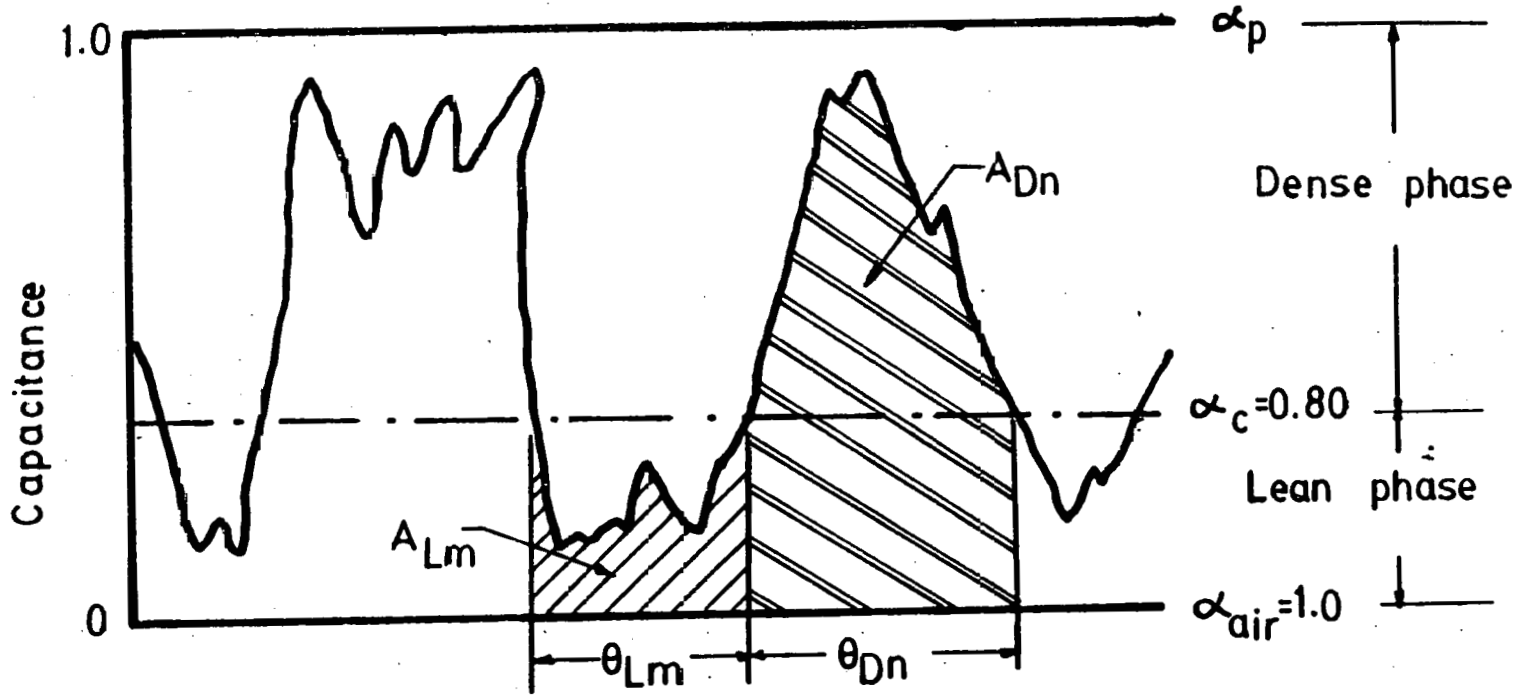

Fig. 29 Capacitance signal analysis

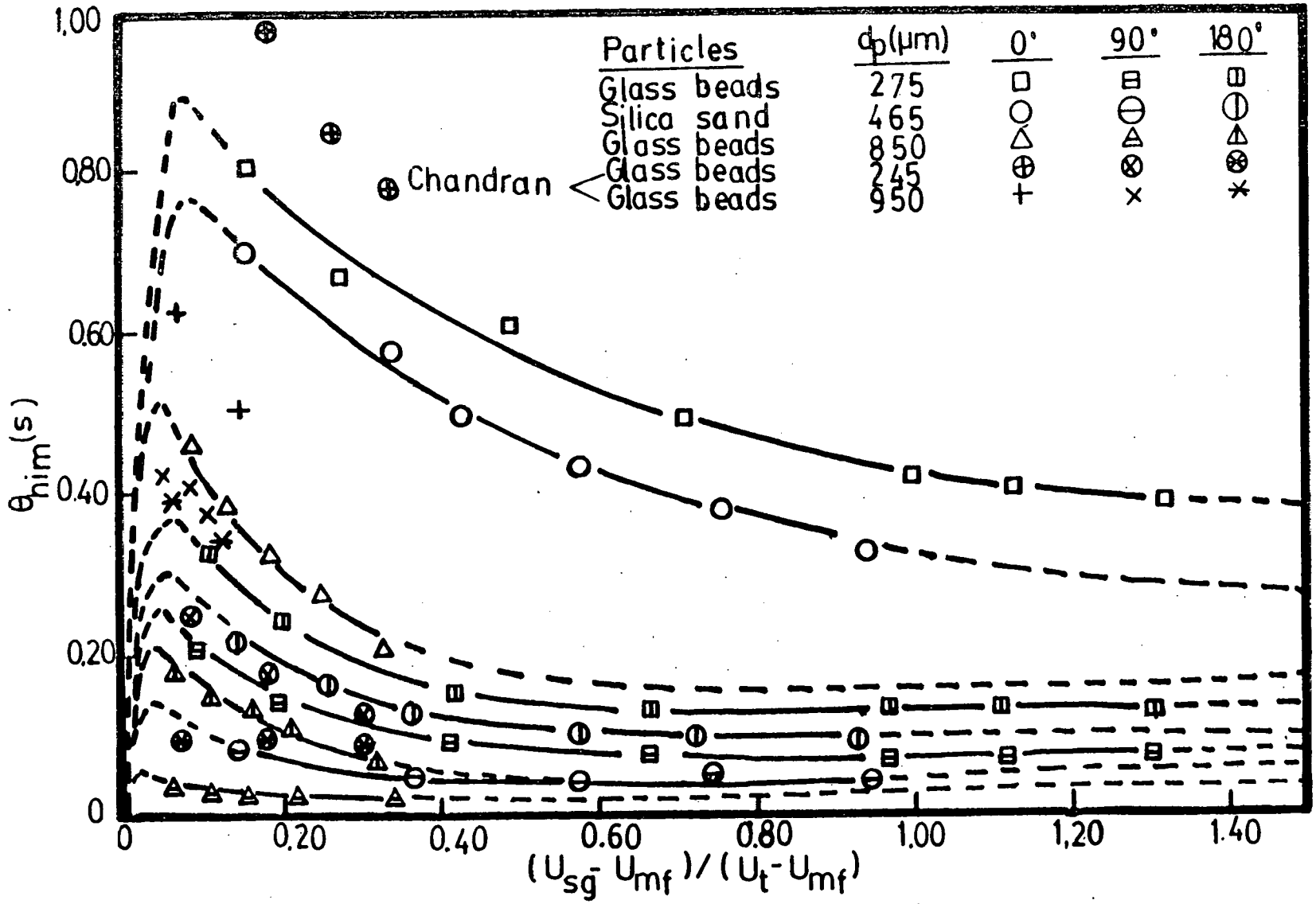

Fig. 30 Immersed tube average residence time of dense phase for heat tansfer coefficient as a function of nondimensional gas velocity

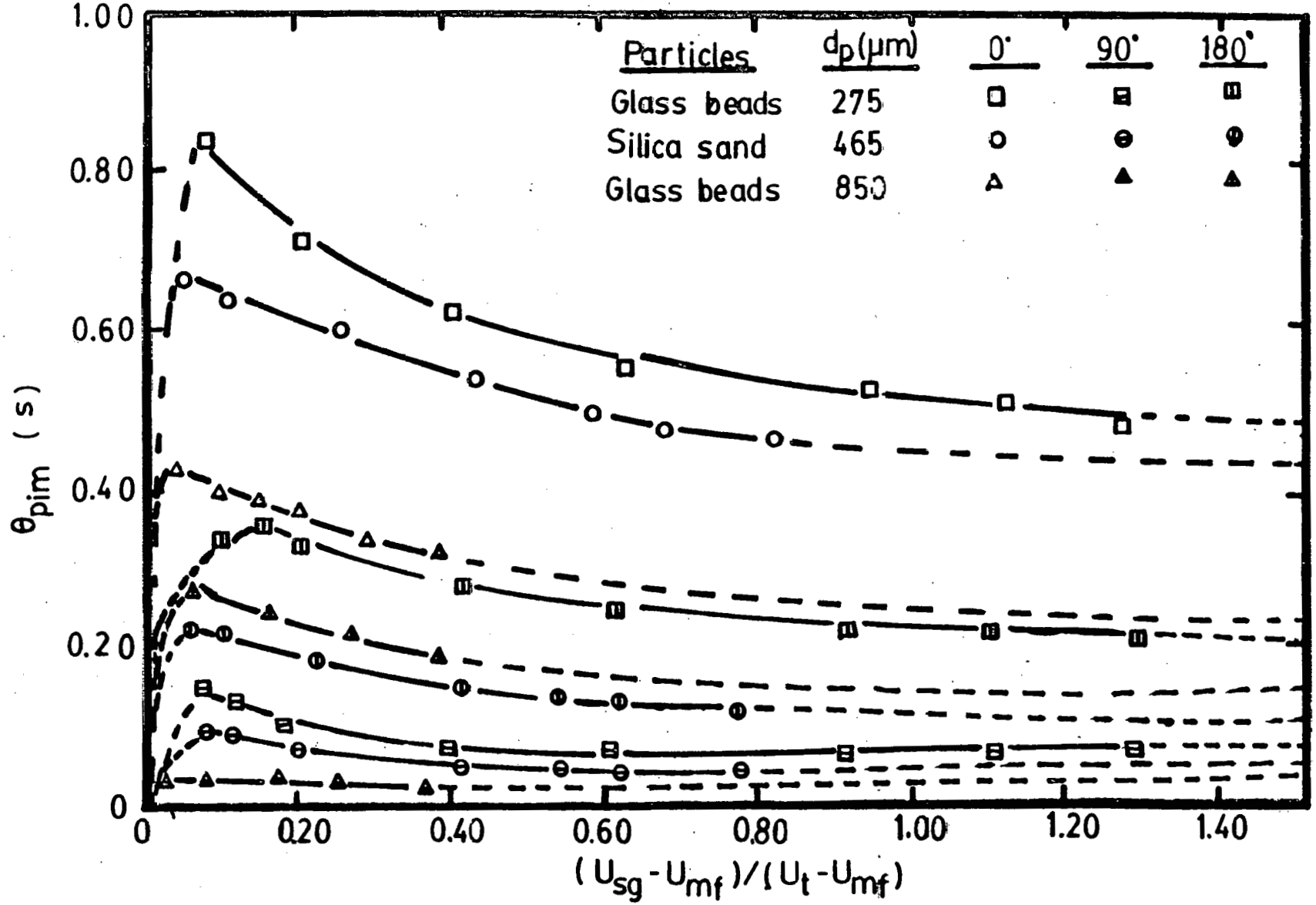

Fig. 31 Immersed tube average residence time of dense phase for heat penetration depth as a function of nondimensional gas velocity

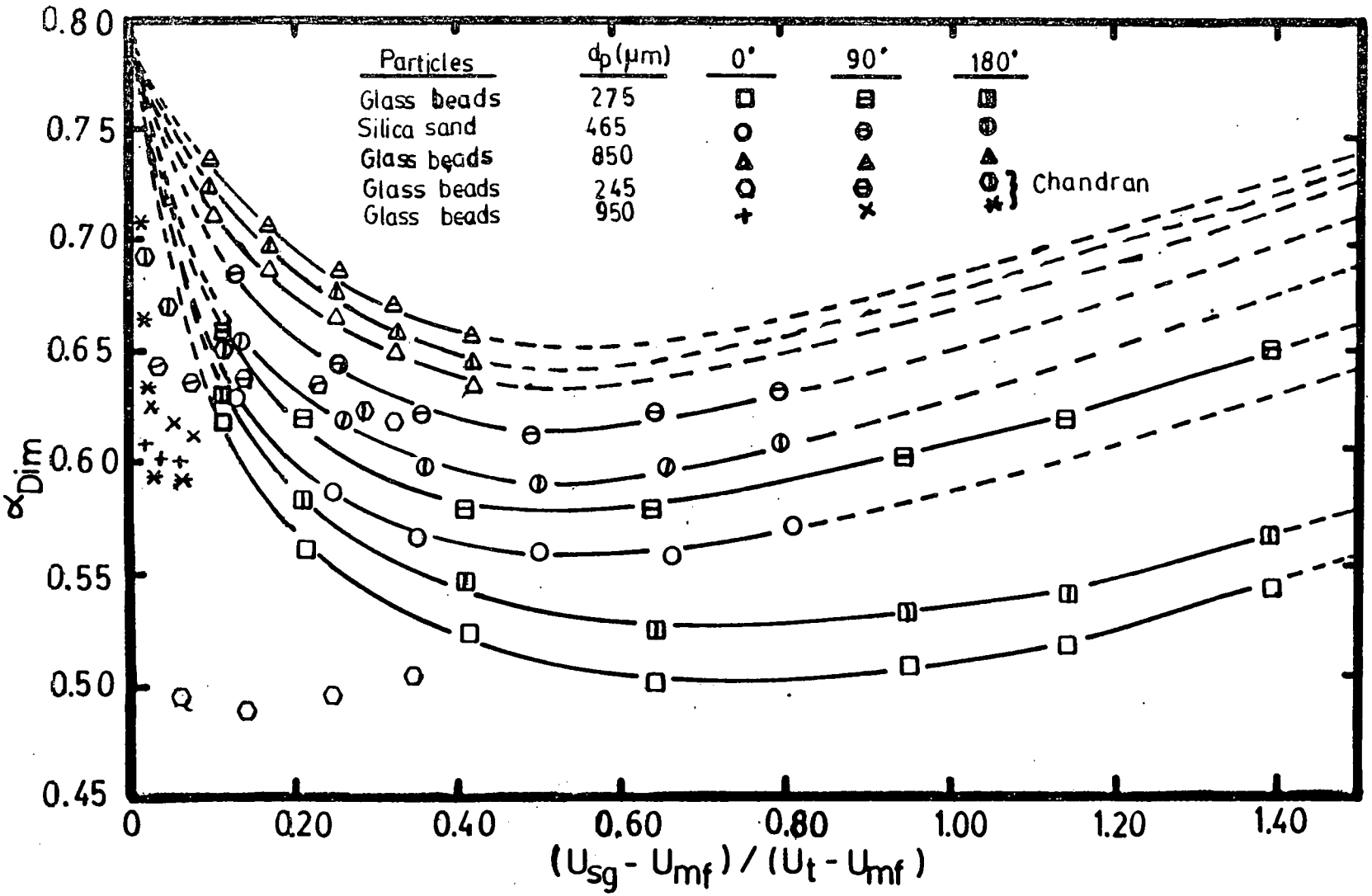

Fig. 32 Immersed tube dense phase void fraction as a function of nondimensional gas velocity for different test particles and angular positions

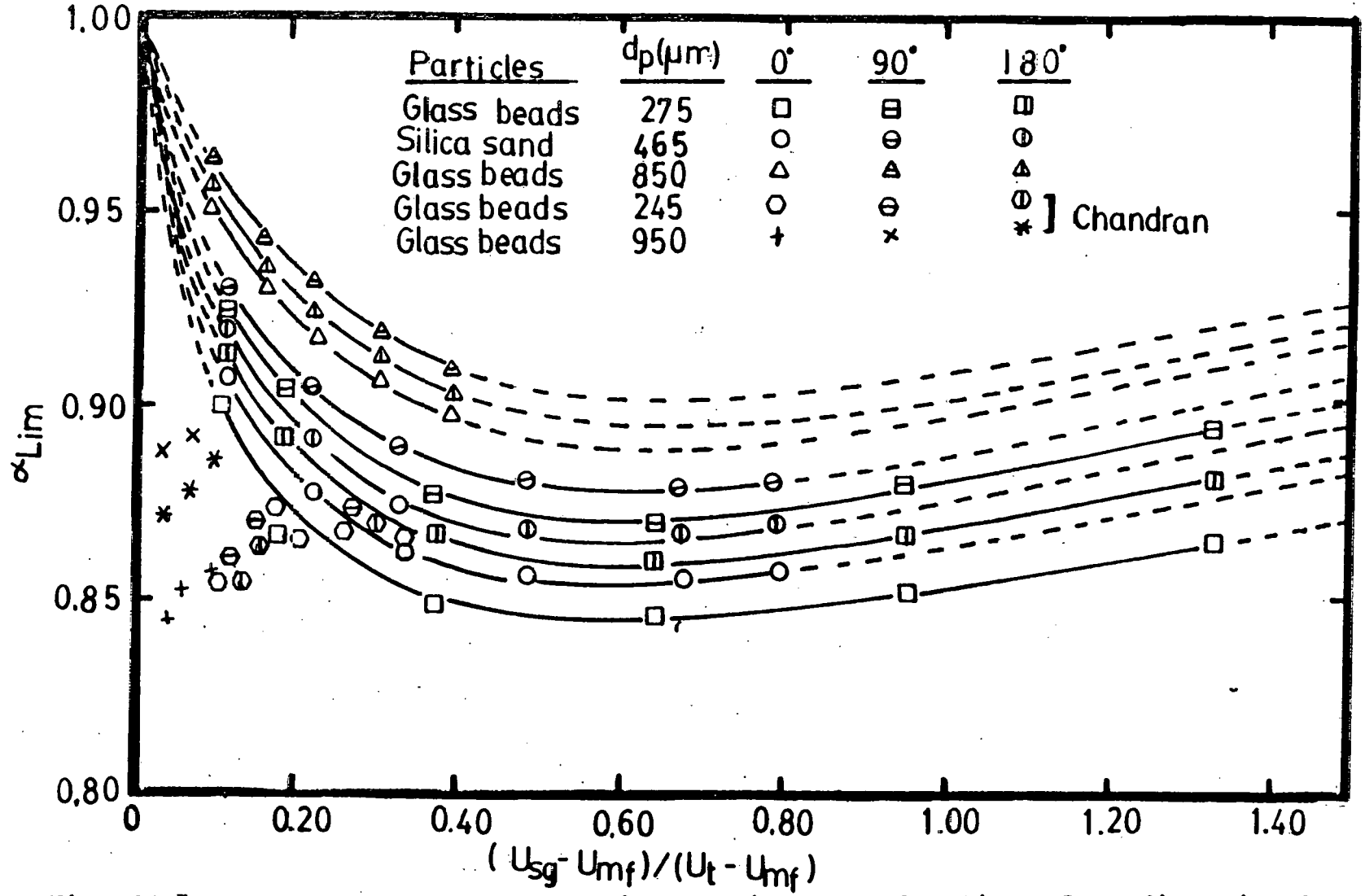

Fig. 33 Immersed tube lean phase void fraction as a function of nondimensional gas velocity for different test particles and angular positions

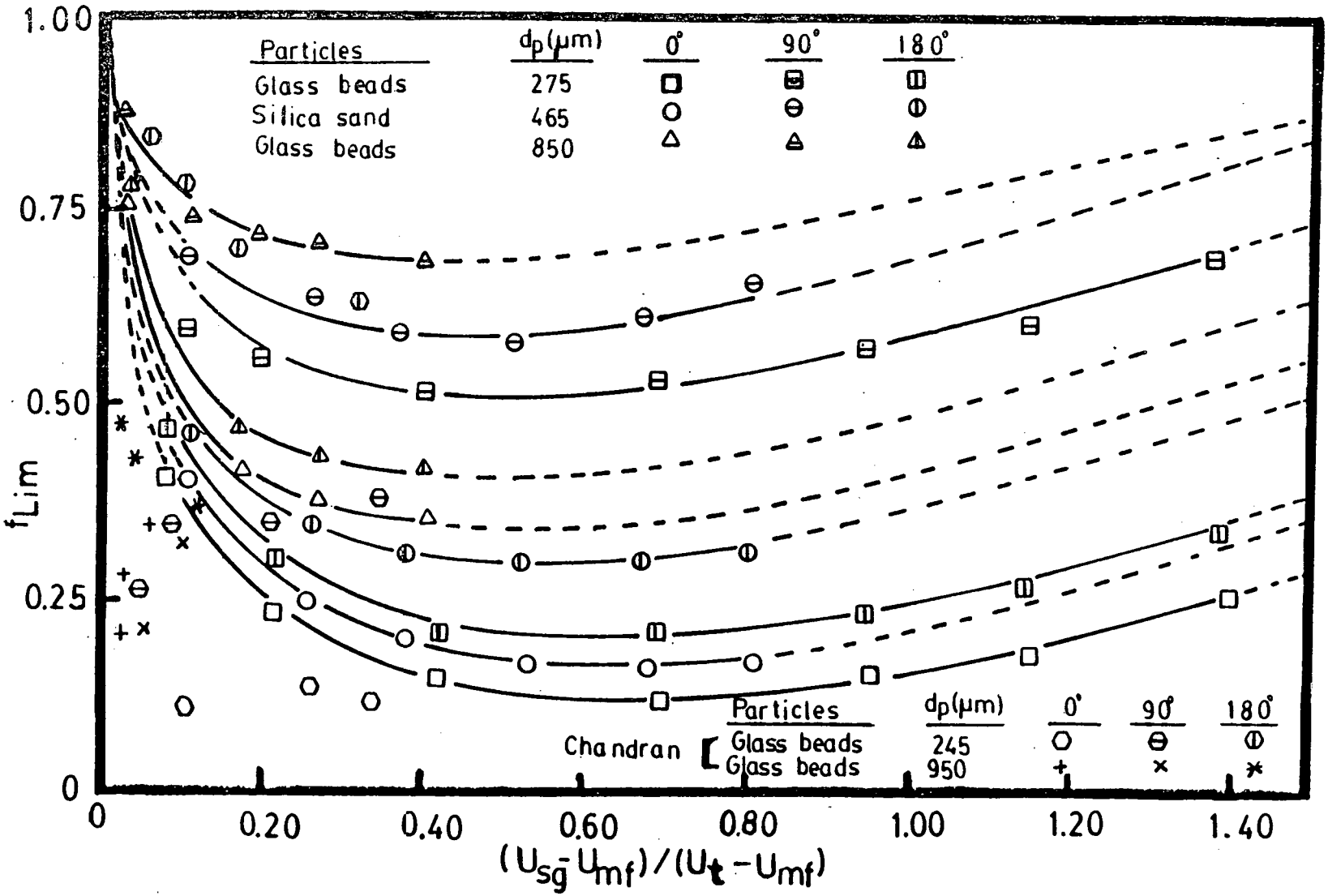

Fig. 34 Immersed tube fraction of total time of lean phase as a function of nondimensional gas velocity for different test particles and angular positions

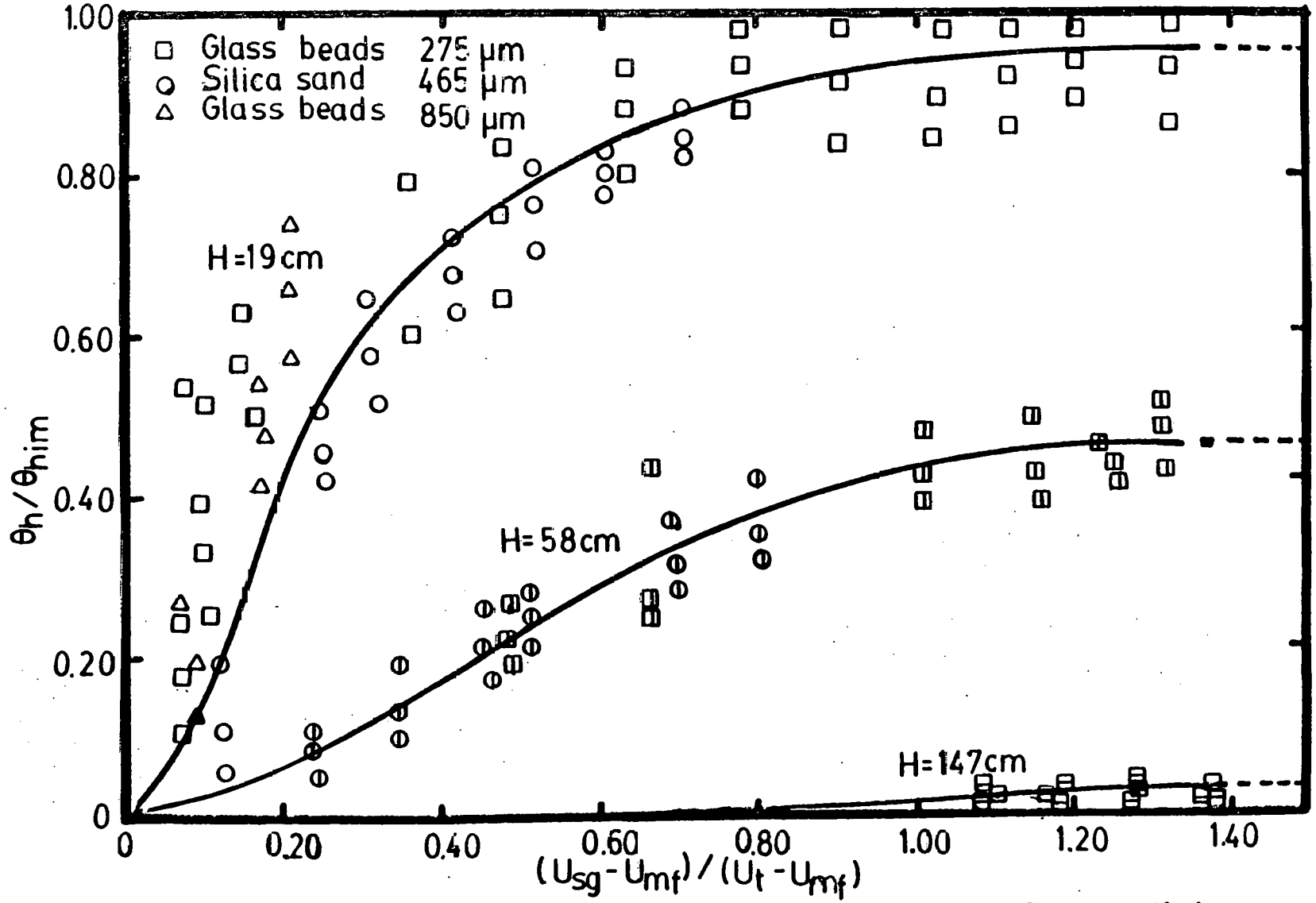

Fig. 35 Normalized residence time of dense phase for heat transfer coefficient as a function of nondimensional gas velocity

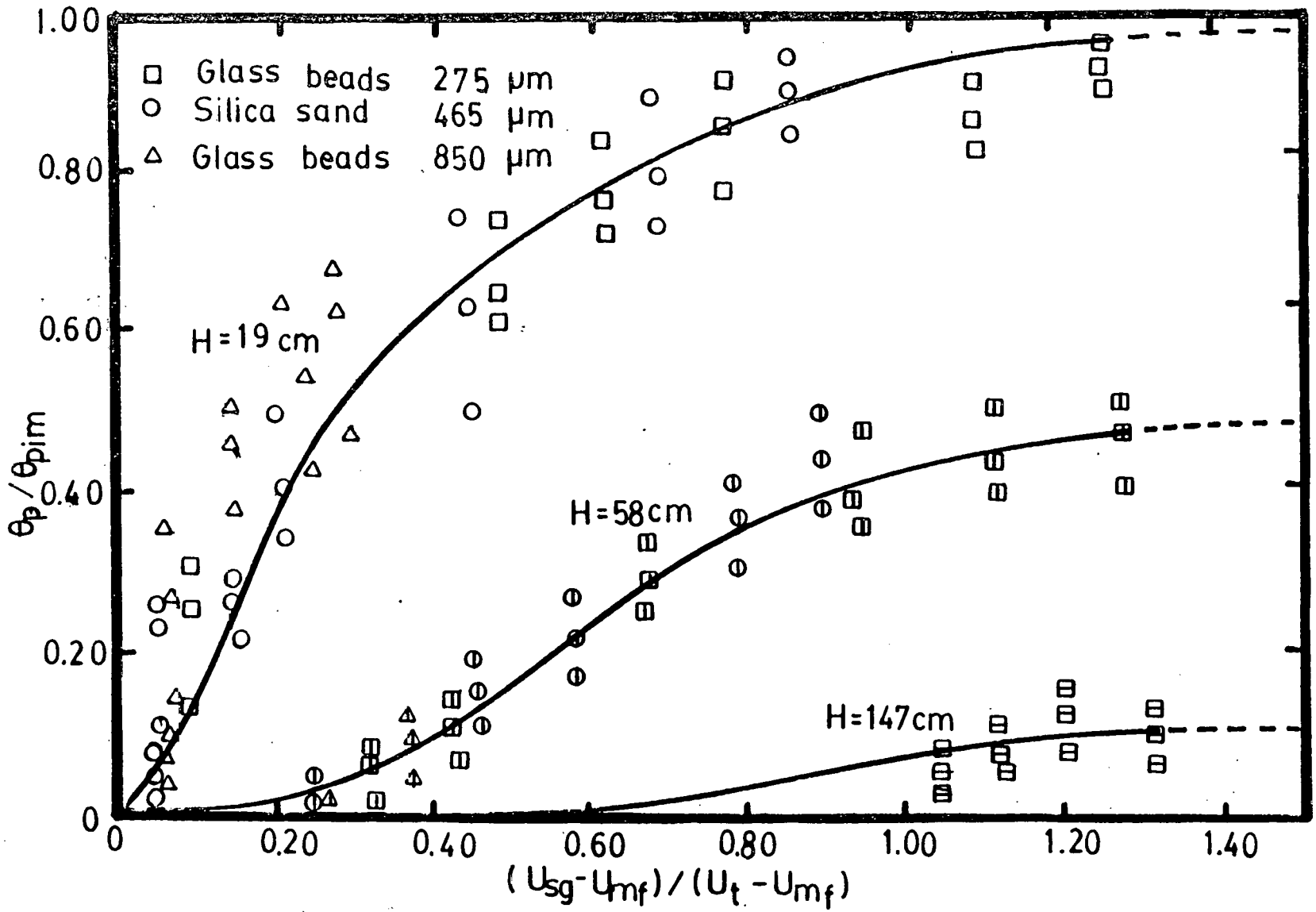

Fig. 36 Normalized residence time of dense phase for heat penetration depth as a function of nondimensional gas velocity

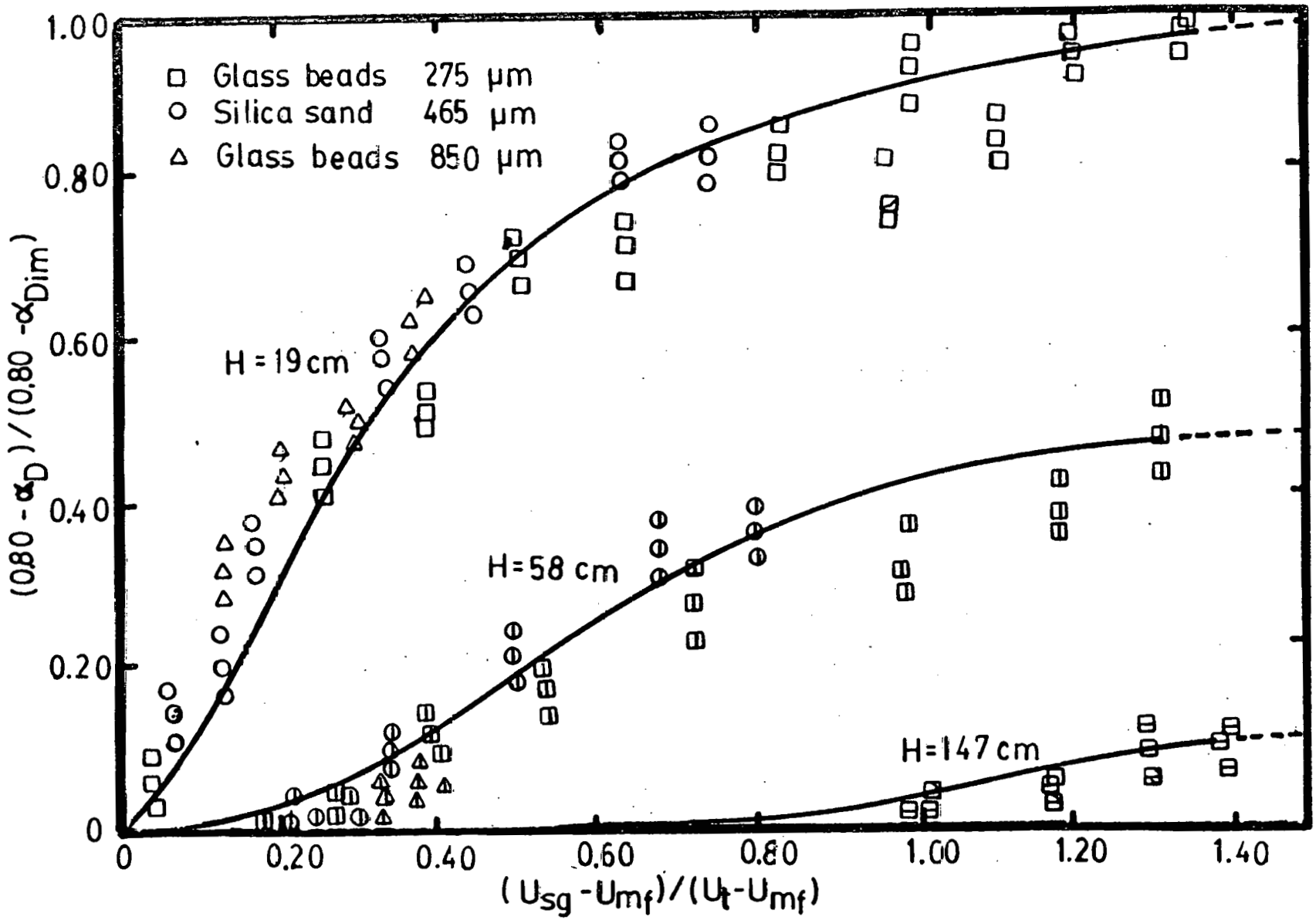

Fig. 37 Normalized dense phase void fraction as a function of nondimensional gas gas velocity for different tube elevations

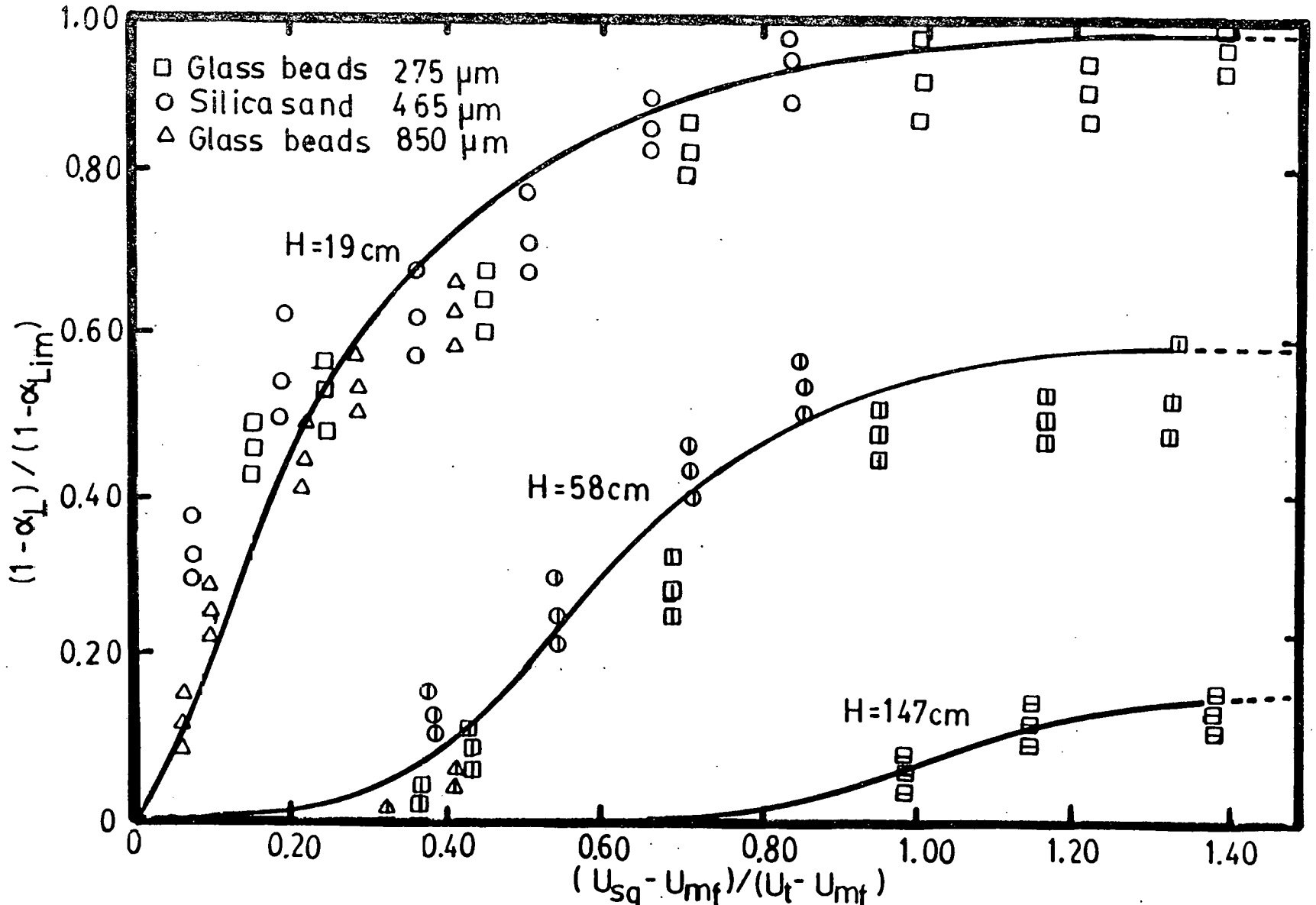

Fig. 38 Normalized lean phase void fraction as a function of nondimensional gas velocity for different tube elevations

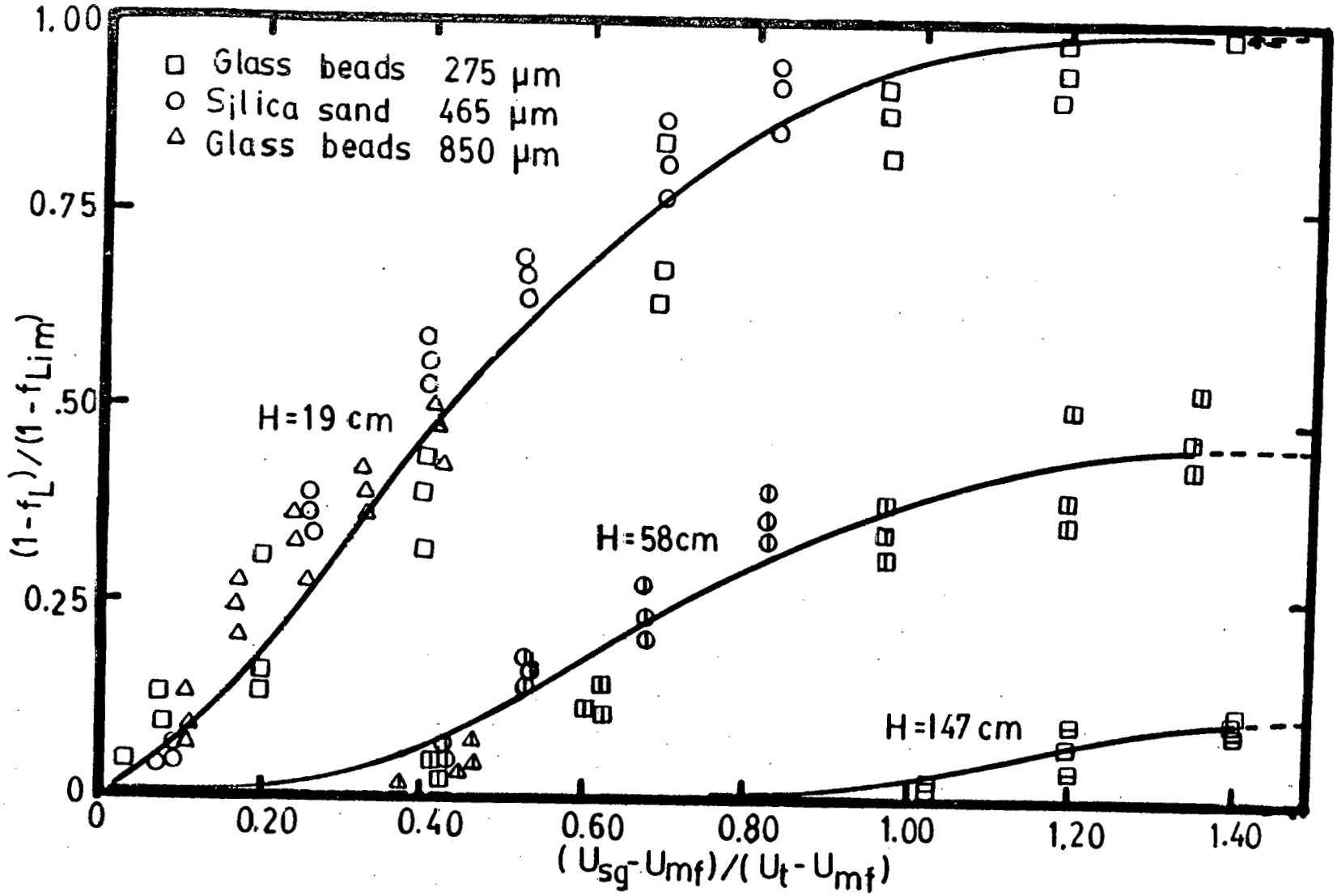

Fig. 39 Normalized fraction of time lean phase in contact as a function of nondimensional gas velocity

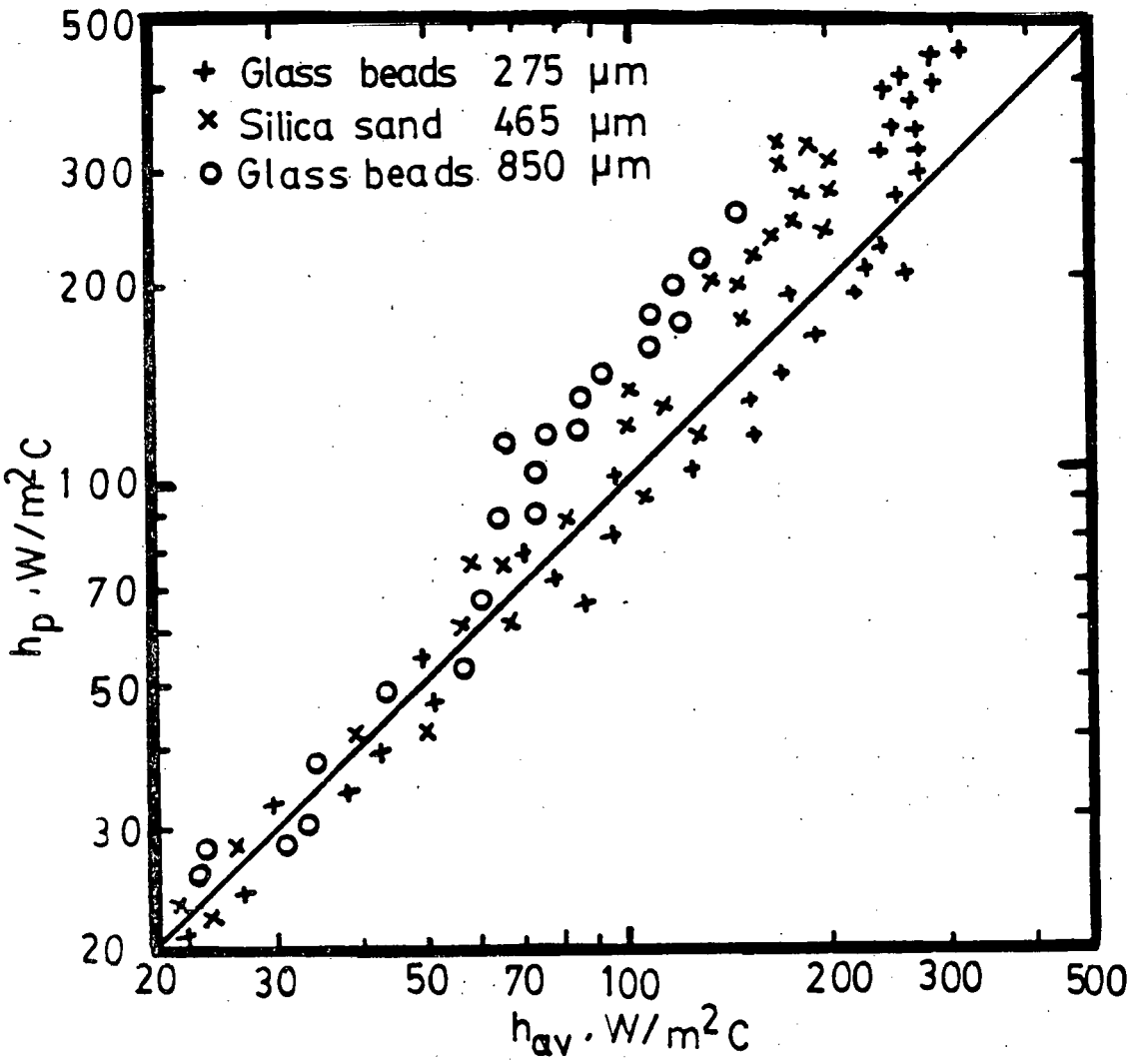

Fig. 40 Comparison of experimental heat transfer coefficients (h_{av}) with heat transfer coefficients of phenomenological model(h_p)

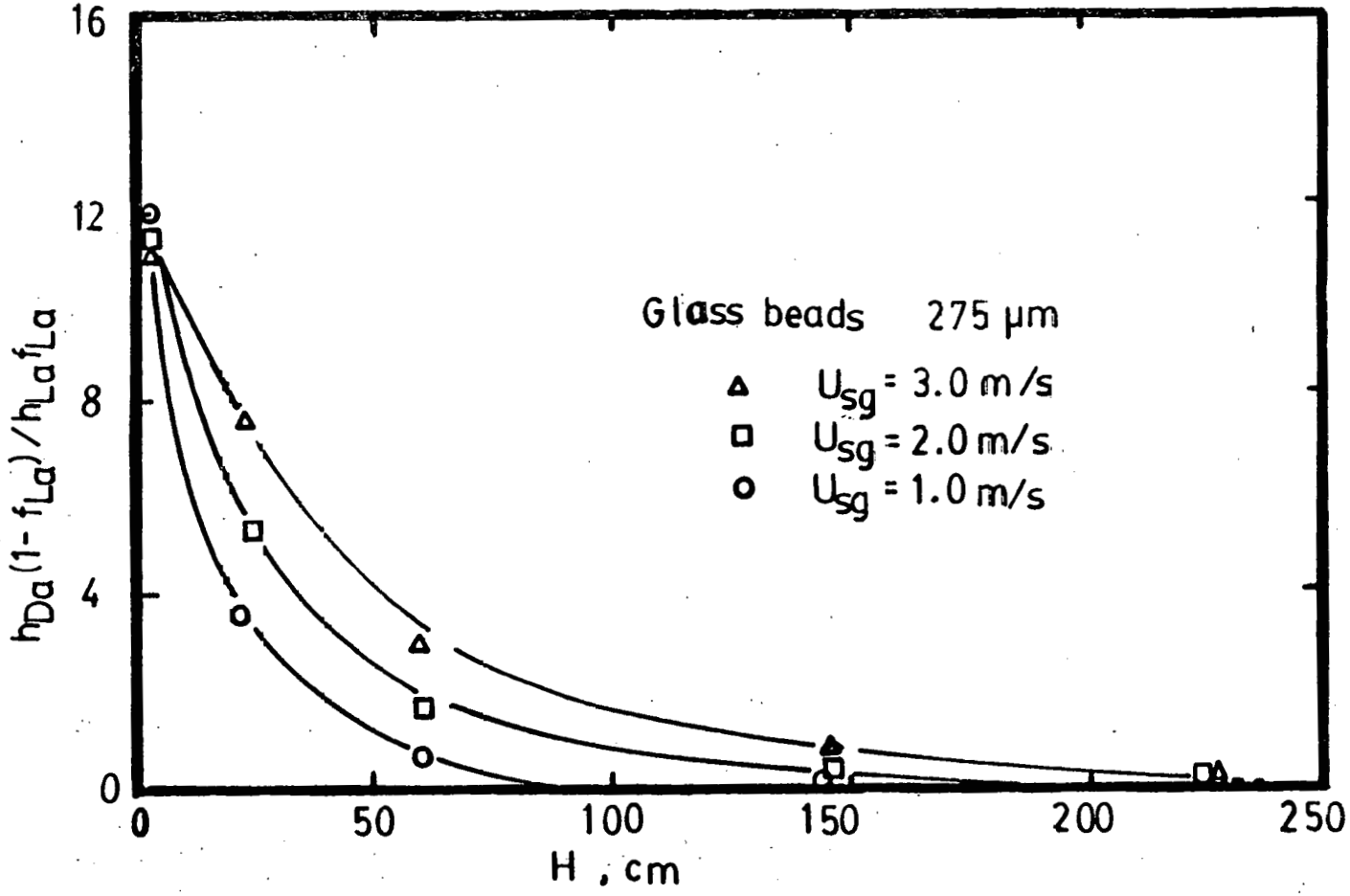

Fig. 41 Variation of dense phase heat transfer compared to lean phase heat transfer along the freeboard height

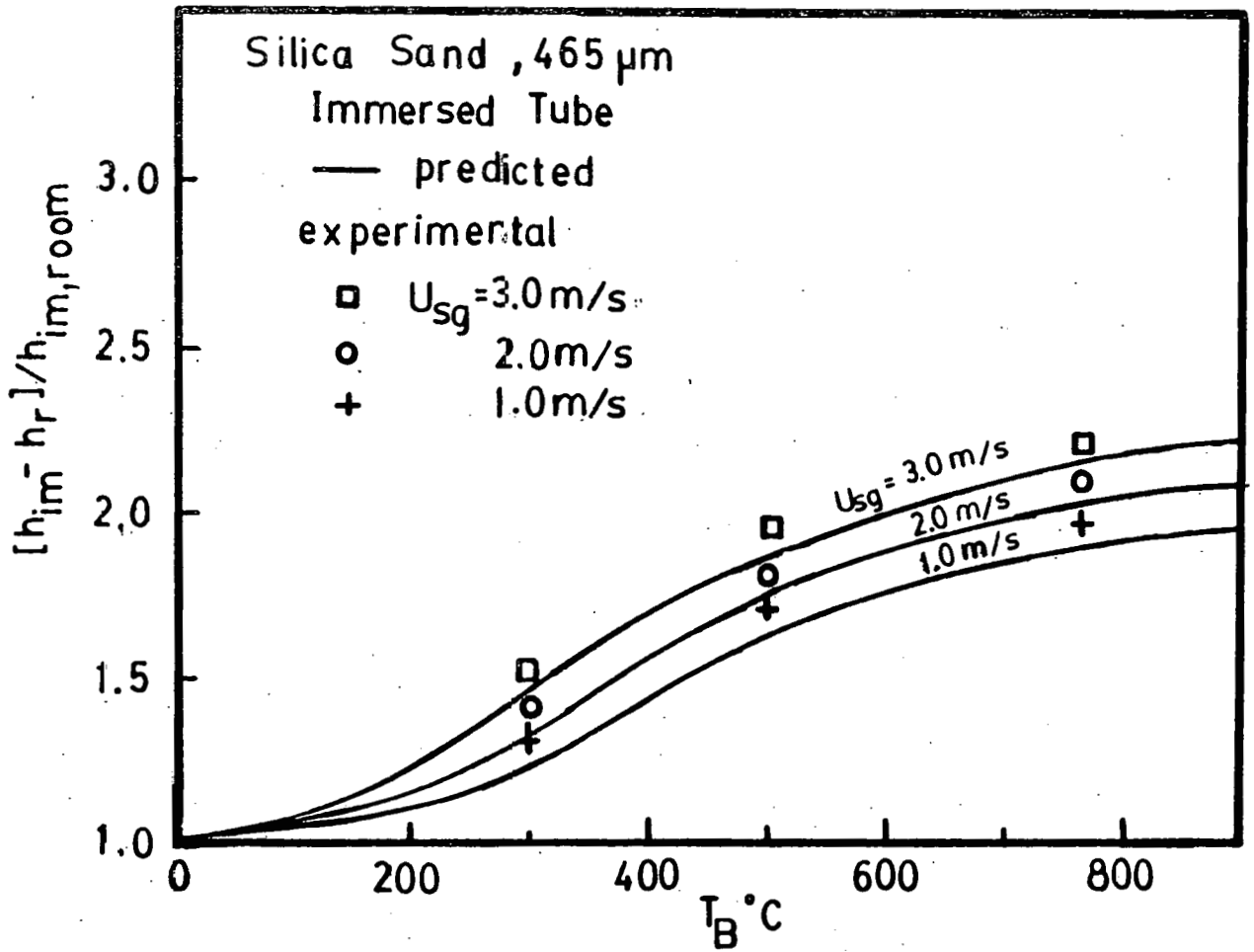

Fig. 42 Increase of high temperature heat transfer coefficients with bed temperature due to thermal property changes of fluidizing gas and particles

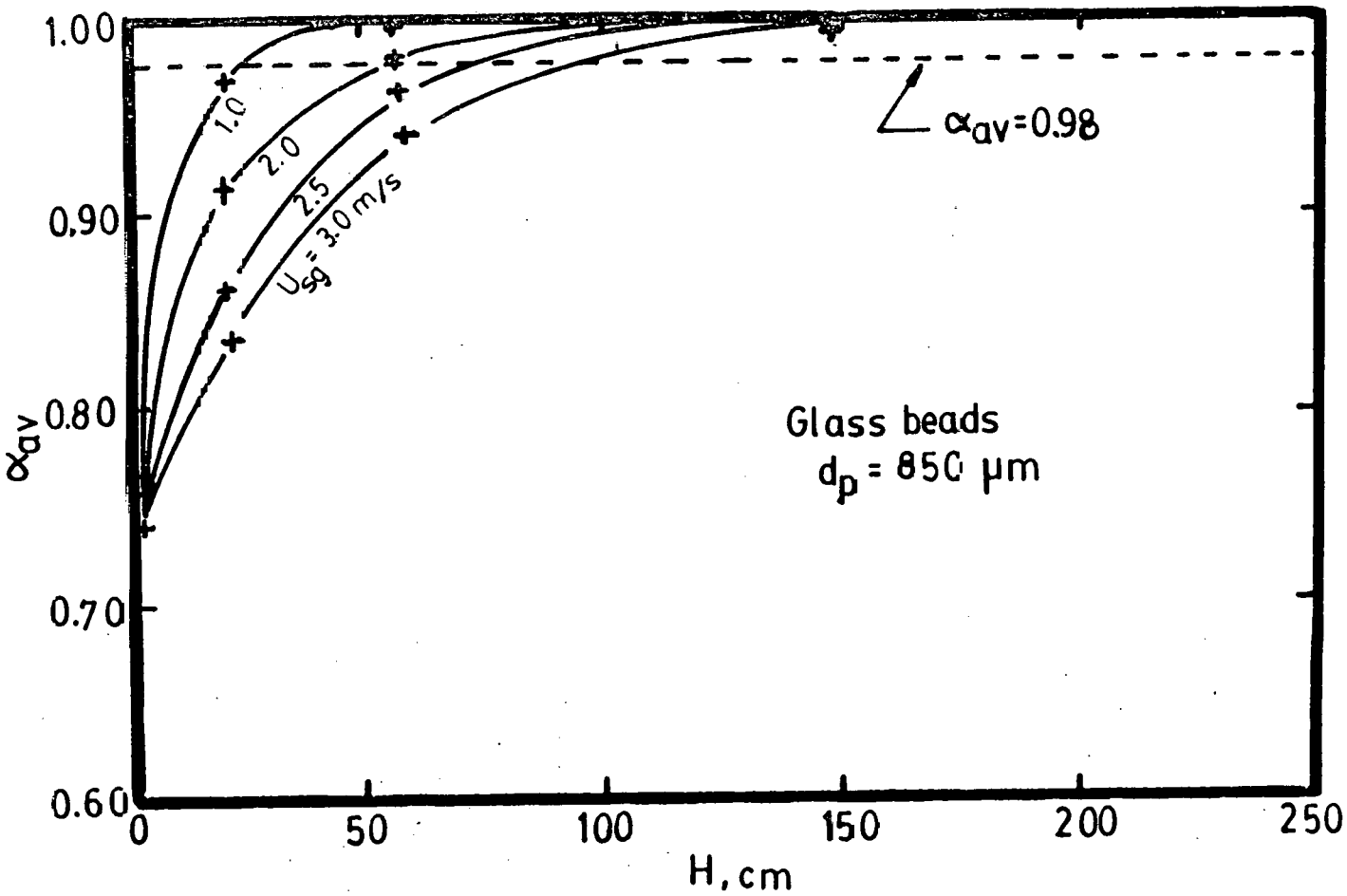

Fig. 43 Variation of average void fraction for glass beads with 850 μm mean diameter along the freeboard height

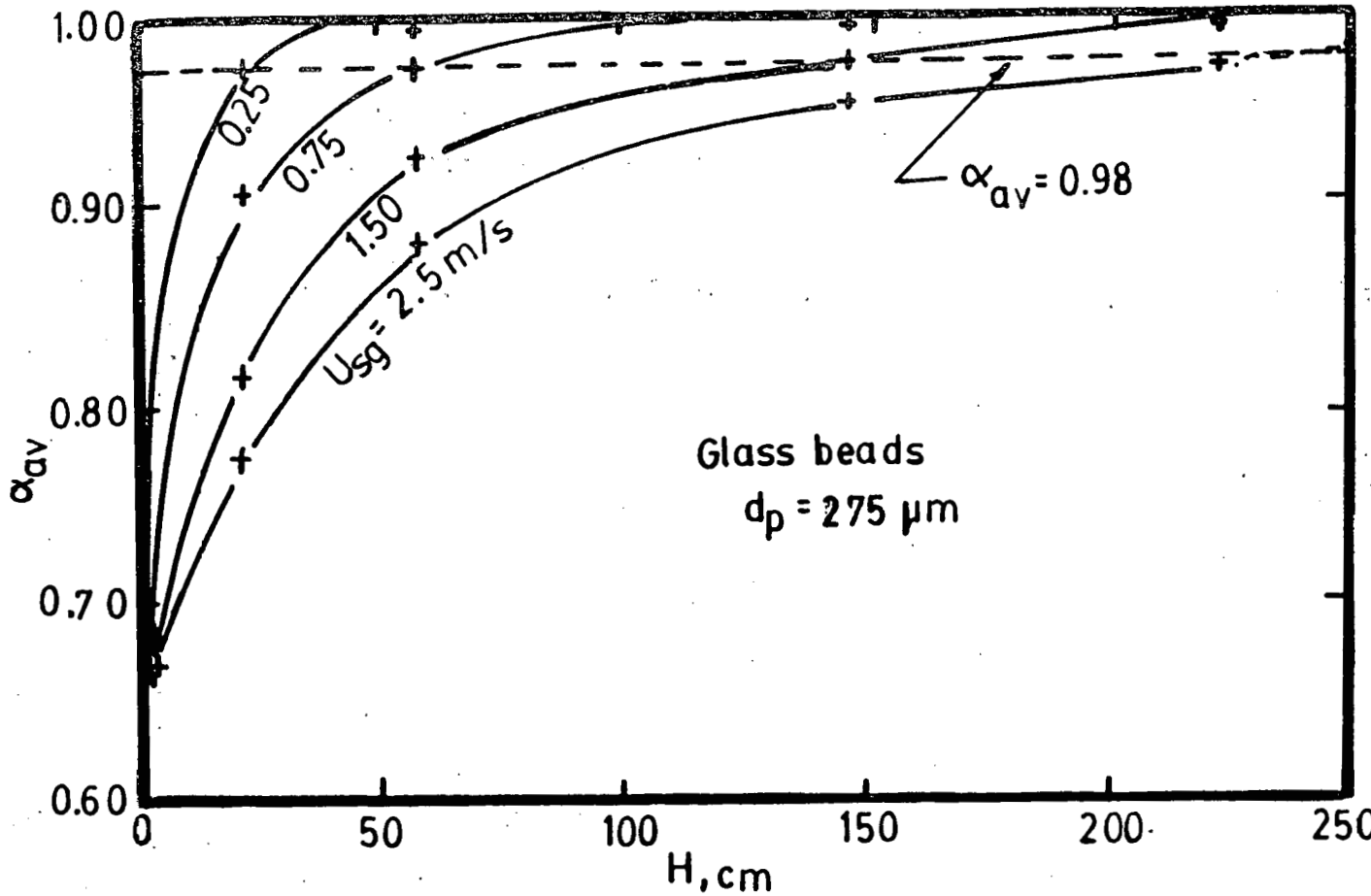

Fig. 44 Variation of average void fraction for glass beads with 275 µm mean diameter along the freeboard height

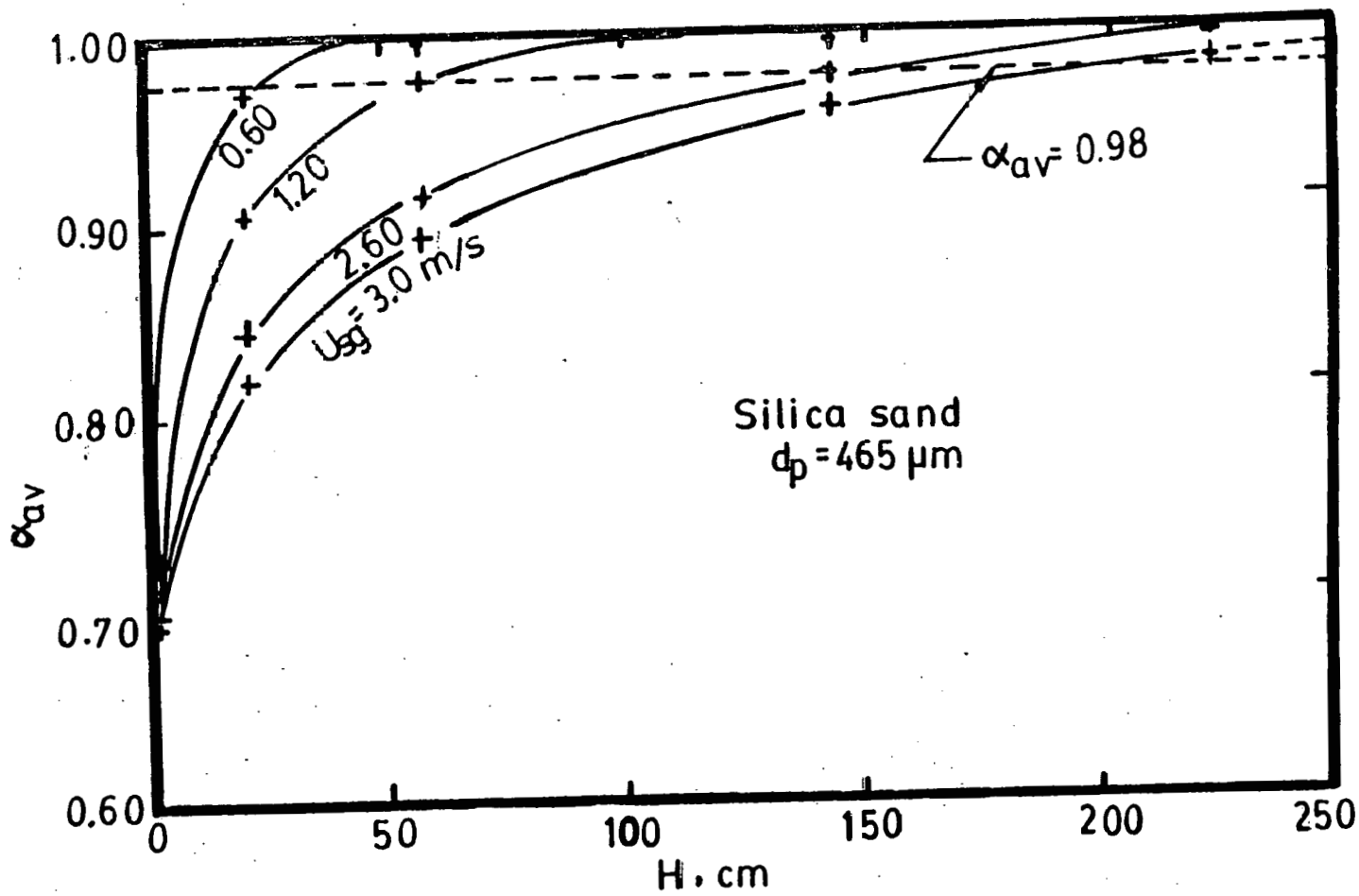

Fig. 45 Variation of average void fraction for silica sand with 465 μm mean diameter along the freeboard height

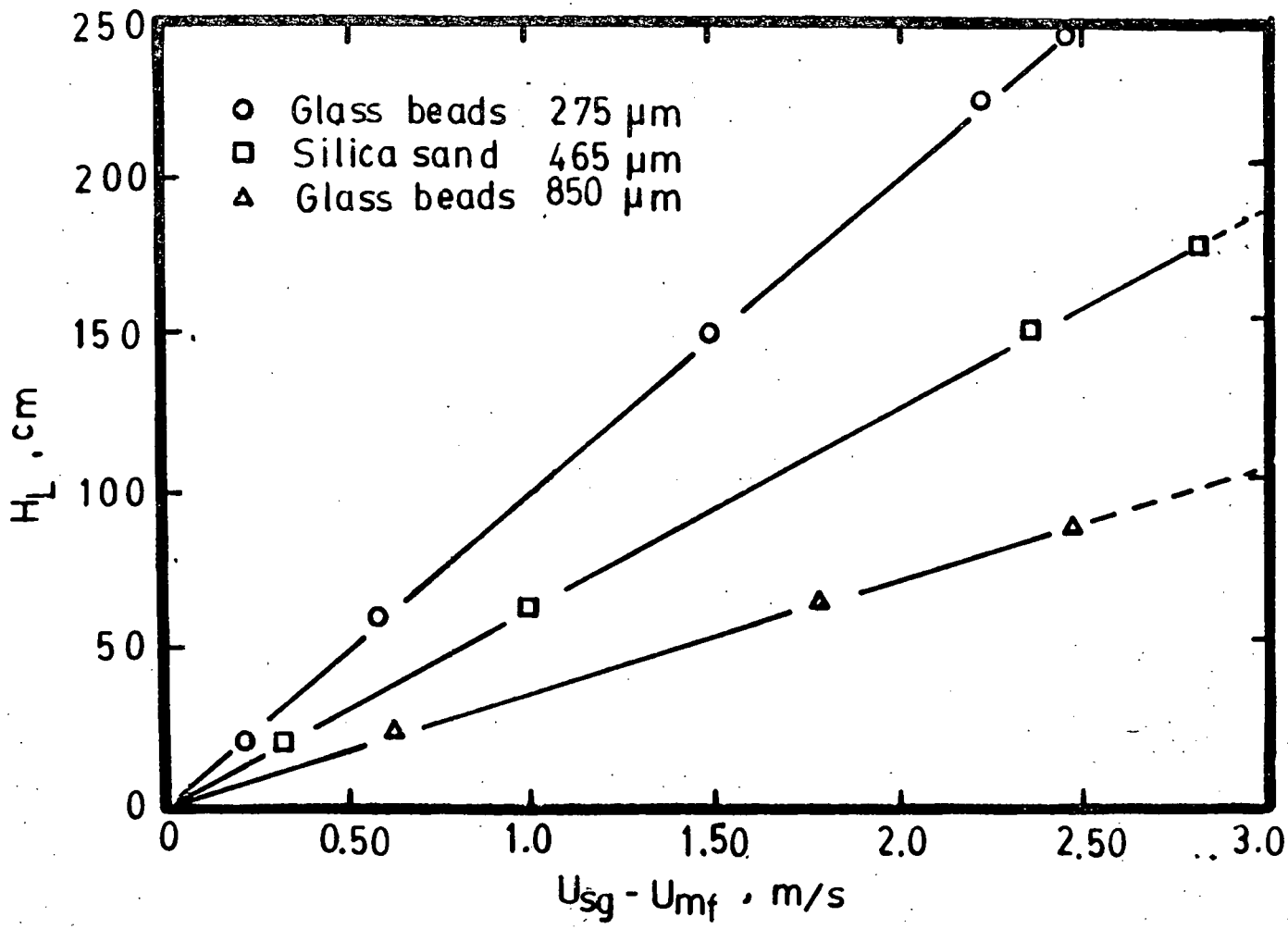

Fig. 46 Limiting entrainment height corresponding to 0.98 average void fraction around the tube for different test particles

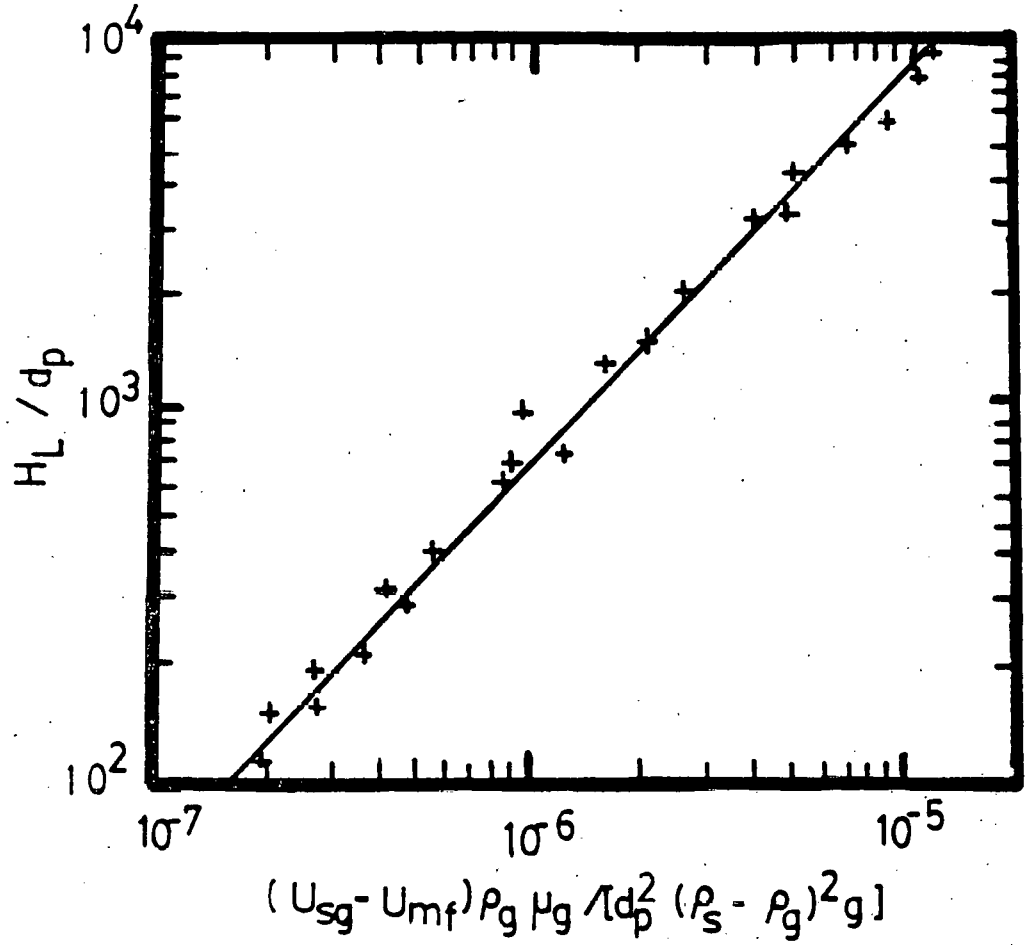

Fig. 47 Comparison of experimental data with limiting entrainment height correlation

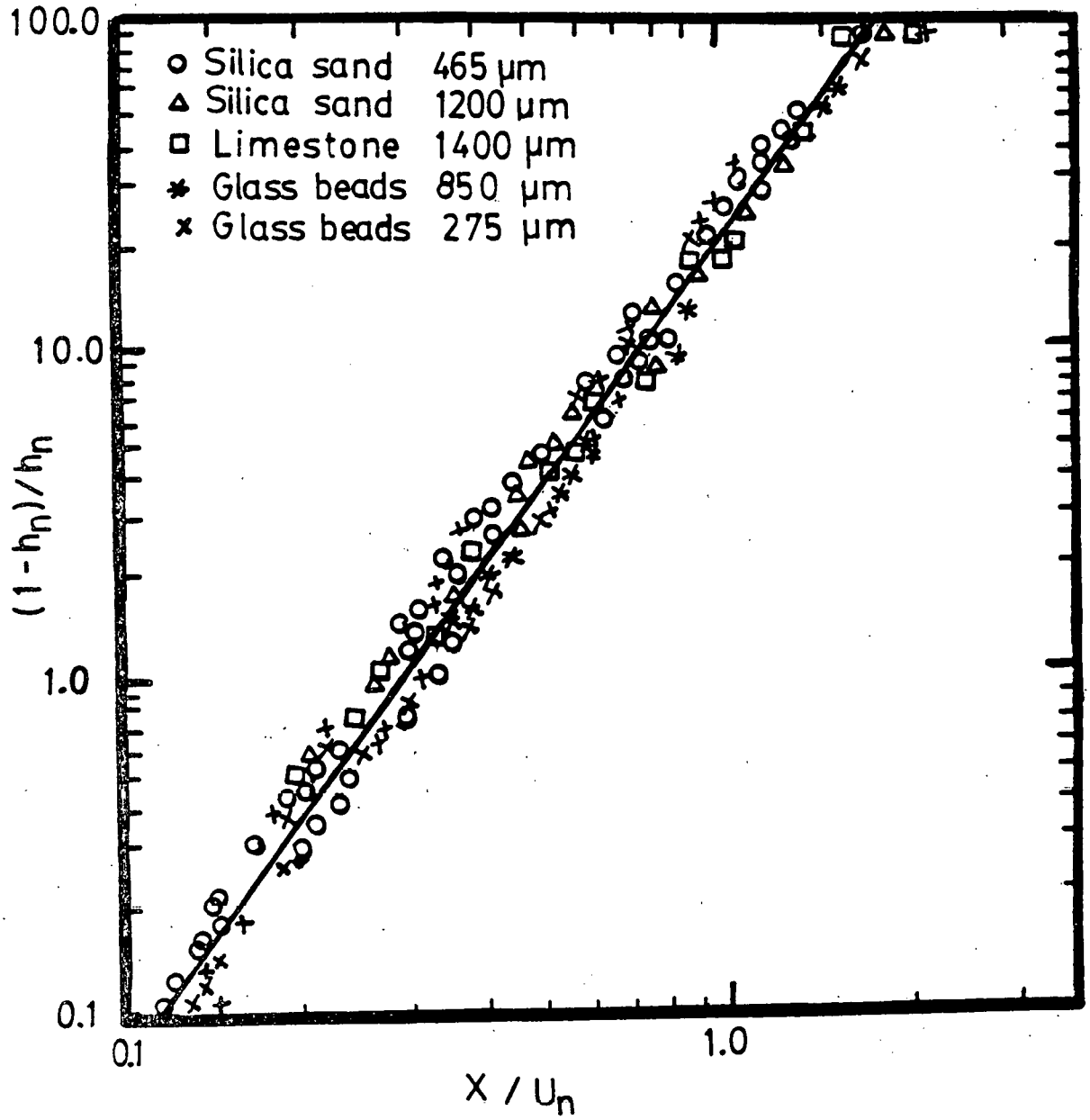

Fig. 48 Comparison of experimental data with the empirical heat transfer correlation

REFERENCES

1. Proceedings of the Fluidized Bed Combustion Technology Workshop, CONF-77042-P-42, Dept. of Energy, 1977.

2. Chen, J.C., Heat Transfer to Tubes in Fluidized Beds, ASME-AIChE Heat Transfer Conference, paper 76-HT-75, 1976.

3. Ainshtein, V.G., An Investigation of Heat Transfer Process Between Fluidized Beds and Single Tubes Submerged in the Bed, Hyrodynamics and Heat Transfer in Fluidized Beds, edited by Zabrodsky, S.S., MIT press, p. 270-272, 1966.

4. Andeen, B.R. and Glicksman, L.R., Heat Transfer to Horizontal Tube in Shallow Fluidized Beds, ASME-AIChE Heat Transfer Conf., paper no. 76-HT-67, Aug. 9-11, 1976.

5. Grewal, N.S. and Saxena, S.C., Heat Transfer Between a Horizontal Tube and Gas-Solid Fluidized Bed, Int. J. Heat Mass Transfer, vol. 23, p. 1505-1519, 1980.

6. Saxena, S. C., Grewal, N.S., Gabor, J.D., Zabrodsky, S.S. and Galershtein, D.M., Heat Transfer Between a Gas Fluidized Bed and Immersed Tube, Advances in Heat Transfer, Academic Press, vol. 14, p. 149-247, 1978.

7. Staub, F.W., Solids Circulation in Turbulent Fluidized Beds and Heat Transfer to Immersed Tube Banks, Journal of Heat Transfer,

vol.101,p. 391-396, 1979.

8. Vreedenberg, H.A., Heat Transfer Between a Fluidized Bed and a Horizontal Tube, Chemical Engineering Science, vol. 9, p. 52-60, 1958.

9. Biyikli, S. and Chen J.C., Effect of Mixed Particle Sizes on Local Heat Transfer Coefficients Around a Horizontal Tube in Fluidized Beds, 7th International Heat Transfer Conference, Germany,1982.

10. George, S.E. and Grace, J.R., Heat Transfer to Horizontal Tubes in Freeboard Region of Gas Fluidized Bed,AIChE Journal, vol. 28, no. 5, p. 759-765,1982.

11. Wood, R.T., Kuwata, M. and Staub,F.W., Heat Transfer to Horizontal Tube Banks in the Splash Zone of Fluidized Bed of Large Particles, Proceedings of the 1980 International Fluidization Conference,p. 235-242, 1980.

12. Byam, J., Pillai, K.K. and Roberts, A.G., Heat Transfer to Cooling Coils in the Splash Zone of a Pressurized Fluidized Bed Combustor, National Heat Transfer Conf., Milwaukee, 1981.

13. Chandran, R., Chen, J.C., Staub, F.W., Local Heat Transfer Coefficients Around Horizontal Tubes in Fluidized Beds, Journal of Heat Transfer, vol.102,p. 152-157, 1980.

14. Bunsal, R.K., Heat Transfer from Horizontal Tubes in Gas Fluidized Beds, National Heat Transfer Conference, Orlando, 1980.

15. Kunii, D. and Levenspiel, O., Fluidization Engineering, Krieger Publishing Company, New York, 1977.

16. Ozkaynak, T.F., Chen, J.C., Frankenfield, T.R., Heat Transfer in High Temperature Fluidized Beds, Institute of Thermo-Fluid Engineering &Science, TS-818, Lehigh University, PA 18015, 1981.

17. Industrial Application Fluidized Bed Combustion, Prepared by Exxon Research and Engineering Company for US Department of Energy Under Contract DE-AC21-76ET10379, 1980.

18. Ozkaynak, T.F. and Chen, J.C., Average Residence Times of Emulsion and Void Phases at the Surface of Heat Transfer Tubes in Fluidized Beds, AIChE Symp. Series, vol. 74,p. 334, 1978.

19. Nixon, T., Circuit Design for Capacitance Probes, Instrumentation Laboratory, Dept of ME and Mech., Lehigh University, 1978(unpublished).

20. Chandran, R., PhD. Thesis, Lehigh University, Bethlehem PA 18015, 1980.

21. Mickley,H.S. and Fairbanks,D.F., Mechanism of Heat Transfer to Fluidized Beds,AIChE Journal, vol.1,p. 374-384, 1955.

22. Ozkaynak, T.F. and Chen, J.C., Emulsion Phase Residence Time and Its Use in Heat Transfer Models in Fluidized Beds, AIChE Journal, vol. 26,no. 4, p. 544-550,1980.

23. Carslaw, H.S. and Jaeger, J.C., Conduction of Heat in Solids, Oxford Press, 1967.

24. Kubie, J. and Broughton, J., A Model of Heat Transfer in Gas Fluidized Beds, Int. J. Heat Mass Transfer, vol. 18, p. 289-299, 1975.

25. Mickley, H.S., Fairbanks, D.F. and Hawthorn, R.D., The Relation Between the Transfer Coefficient and Thermal Fluctuations in Fluidized Bed Heat Transfer, Chem. Eng. Prog. Symp. Series, vol.57, no. 32, p. 51-60, 1961.

26. Bauer, R and Schlunder, E.U., Effective Radial Thermal Conductivity of Packings in Gas Flow, Int. Chem. Eng., vol. 18, p. 189-203, 1978.

27. Hilbert, R., Warmeabge von Geheizen Drahten und Rohren, Forch. Gebiete Ingenieurw., vol. 4, p. 220-226, 1933.

28. Knudsen, J.D. and Katz, D.L., Fluid Dynamics and Heat Transfer, McGraw-Hill Book Company, New York, 1958.

29. Schugerl, K., Merz, M. and Fetting, F., Unregelmessiges Verhalten von Fliessbettsystemen bei Rheolcgischen Messungen, Chem. Eng. Science, vol. 15, p. 75-99, 1961.

30. Peters, K. and Schmidt, A., Investigations Concerning the Fluidized Bed Process, part I, Oesterr. Chemikerztg., vol. 54, p. 253-258, 1953.

31. Furukaw, J. and Ohmae, T., Liquidlike Properties of Fluidized Systems, Ind. Eng. Chem., vol. 50, no. 5, p. 821-828, 1958.

32. Matheson, G. L., Herbst, W.A. and Holt, P.H., Characteristics of Fluid-Solid Systems, Ind. Eng. Chem., vol. 41,p.1099-1104, 1949.

33. Siemens, W. and Helmer, L., Die Messungen der Wirbelschichtviskosität mit der Pneumatischen Rinne, Chem. Eng. Sci., vol. 17,p.555, 1962.

34. Touloukian, Y.S., Buyco, E.H., Thermophysical Properties of Matter, The TPRC Data Series, vol. 5, New York, 1970.

35. Pitts, D.R. and Sissom, L.E., Heat Transfer, McGraw-Hill Book Company, New York, 1977.

36. Siegel, R. and Howell, R.J., Thermal Radiation Heat Transfer, second edition, McGraw-Hill Book Company, New York, 1981.

37. Daskakov, A.P., The Mechanism of Heat Transfer Between a Fluidized Bed and a Surface, Int. Chem. Eng., vol. 4,no. 2, p. 320, 1964.

38. Yoshida, K., Kunii, D. and Levenspiel, D., Heat Transfer Mechanism between Wall Surface and Fluidized Bed,Int. J. Heat Mass Transfer, vol. 12,p. 529-536, 1969.

39. Toor, H.L. and Marchello, J.M., Film Penetration Model for

Mass and Heat Transfer Coefficients, AIChE J., vol. 4,p. 97-102, 1958.

40. Koppel, K.B., Pattel, R.D. and Holmes, J.T., Part 4: Wall to Fluidized Bed Heat Transfer Coefficients,AIChE J. vol. 16, no. 3, p. 464-471,1970.

41. Zenz, F.A. and Weil, N.A., A Theoritical Empirical Approach to Mechanism of Particle Entrainment from Fluidized Beds, AIChE J., vol. 4,no. 4, p. 472-479, 1958.

42. Zenz, F.A. and Othmer, D.F., Fluidization and Fluid Particle Systems, Reinhold, New York, 1960.

43. Fournal, A.B., Bergeogno, M.A. and Baker, C.G.J., Solids Entrainment in a Large Gas Fluidized Bed, Can. J. Chem. Eng., vol. 51,p. 401-404, 1973.

44. Lewis, W.K., Gilliland, E.R., and Lang, P.M., Entrainment From Fluidized Beds, Chem. Eng. Prog. Symp. Series, vol. 58,no.38, p. 65-78, 1962.

45. Roblee, L.H.S., Baird, R.M., and Tierney, J.W., Radial Porosity Variations in Packed Beds, AIChE J., vol. 4,no. 4, p. 460, 1958.

46. Gray, W.A., The Packing of Solid Particles, Powder Technology Series, Chapman and Hall,1968.

47. Korolev, V.N., Syrmyatnikov, N.Y., and Tolmachev, E.M.,The

Structure of Fixed and Fluidized Granular Beds Near Immersed Walls, J. Eng. Phys., vol. 21,no. 6, p. 973, 1971.

48. Gelperin, N.I. and Einstein, V.G., Heat Transfer in Fluidized Beds, in Fluidization, edited by Davidson, J.F. and Harrison, D., Academic Press, London, 1971.

49. Kunii, D. and Smith, J.M., Heat Transfer Characteristics of Porous Rocks, AIChE J., vol. 6, no.1, 1960.

50. Kunii, D. and Yagi, S., Studies on Heat Transfer Near Wall Surface in Packed Beds, AIChE J., vol. 6,no. 1, p. 71, 1960.

51. Kline, S.J. and McClintock, F.A., Describing Uncertainties in Single-Sample Experiments, Mech. Eng., p.3, 1953.

APPENDIX I - UNCERTAINTY ANALYSIS

The uncertainties in the calculated heat transfer coefficients were estimated on the basis of uncertainties in the primary measurements, using the method presented by Kline and McClintock [51]. The following instruments were used in the heat transfer experiments.

Data Logger: Esterline Angus, Model PD-2064. It has an accuracy of 0.1% of reading at room temperature.

Thermocouple: Premium grade Chromel-Alumel type. It has an accuracy of $\pm$ 1.1°C or $\pm$ 0.40% (whichever is greater).

Rotameters: Schutte & Koerting type. It has a calibrated accuracy of $\pm$ 1% in full scale.

The uncertainties in the heat transfer coefficients were calculated from the uncertainties in these instruments.

(a) Uncertainty in Low Temperature Heat Transfer Coefficients

Local heat transfer coefficients at room temperature were calculated by using Equation (1) in the text.

$$h = \frac{Q}{A_S (T_S - T_B)} \qquad (1)$$

or

$$h = \frac{I^2 R}{A_S (T_S - T_B)} \tag{1.1}$$

Where I and R are current flow and resistance in an Inconel foil strip. Applying the methods of Reference [51] yields the uncertainty in heat transfer coefficient (U_h) due to instrumentation precision as

$$U_h = \left[\left(\frac{\partial h}{\partial I} U_I\right)^2 + \left(\frac{\partial h}{\partial R} U_R\right)^2 + \left(\frac{\partial h}{\partial T_S} U_{T_S}\right)^2 + \left(\frac{\partial h}{\partial T_B} U_{T_B}\right)^2 + \left(\frac{\partial h}{\partial A_S} U_{A_S}\right)^2 \right]^{\frac{1}{2}} \tag{1.2}$$

where U_I, U_R, U_{T_S}, U_{T_B} and U_{A_S} are the uncertainties associated with the independent variables I, R, T_S, T_B and A_S. Substituting Equation (1.1) into Equation (1.2) and dividing the resultant by Equation (1.1) leads to Equation (1.3)

$$\frac{U_h}{h} = \left[4\left(\frac{U_I}{I}\right)^2 + \left(\frac{U_R}{R}\right)^2 + \left(\frac{U_{T_S}}{T_S - T_B}\right)^2 + \left(\frac{U_{T_B}}{T_S - T_B}\right)^2 + \left(\frac{U_{A_S}}{A_S}\right)^2 \right]^{\frac{1}{2}} \tag{1.3}$$

For a typical experimental run, values for various parameters in Equation (1.1) can be taken as follows

I = 3 amp

R = 0.81 ohm

T_S = 40°C

$T_B = 20°C$

$A_S = 15\ cm^2$

Surface area (A_S) and resistance (R) of a strip were measured by vernier meter (accuracy of $\mp$ 0.1 mm) and a Wheatstone bridge (accuracy Of 0.2% of reading) respectively. The current flow (I) was measured by the data logger using a shunt resistor. The uncertainties in the independent variables can be calculated as

$U_I = \mp 0.003$ amp

$U_R = \mp 0.00162$ ohm

$U_{T_S} = \mp 1.14°C$

$U_{T_B} = \mp 1.12°C$

$U_{A_S} = \mp 0.0001\ cm^2$

Where U_I, U_R, U_{T_S}, U_{T_B} and U_{A_S} are the uncertainties in the independent variables I, R, T_S, T_B and A_S. Substituting the above uncertainties and independent variables in Equation (1.3) gives the uncertainty in heat transfer coefficient as

$$\frac{U_h}{h} = \mp 7.8\%$$

(b) Uncertainty in High Temperature Heat Transfer Coefficient

Average heat transfer coefficients were calculated using Equation (3) in the text. The uncertainty due to instrumentation precision in heat transfer coefficient computations were calculated

using the method described in Reference [51]. Applying this method to Equation (3) results in the uncertainty in heat transfer coefficient ($U_{h_{av}}$) as

$$U_{h_{av}} = \left[\left(\frac{\partial h_{av}}{\partial \dot{m}} U_{\dot{m}}\right)^2 + \left(\frac{\partial h_{av}}{\partial T_o} U_{T_o}\right)^2 + \left(\frac{\partial h_{av}}{\partial T_i} U_{T_i}\right)^2 + \left(\frac{\partial h_{av}}{\partial T_B} U_{T_B}\right)^2 + \left(\frac{\partial h_{av}}{\partial T_{Sa}} U_{T_{Sa}}\right)^2 + \left(\frac{\partial h_{av}}{\partial C_{pw}} U_{C_{pw}}\right)^2 + \left(\frac{\partial h_{av}}{\partial A_p} U_{A_p}\right)^2 \right]^{\frac{1}{2}} \quad (1.4)$$

Where $U_{\dot{m}}$, U_{T_o}, U_{T_i}, U_{T_B}, $U_{T_{Sa}}$, $U_{C_{pw}}$, and U_{A_p} are the uncertainties in the independent variables $\dot{m}$, T_o, T_B, T_{Sa}, C_{pw} and A_p. Substituting Equation (3) into Equation (1.4) and dividing both sides by Equation (3) yields

$$\frac{U_{h_{av}}}{h_{av}} = \left[\left(\frac{U_{\dot{m}}}{\dot{m}}\right)^2 + \left(\frac{U_{T_o}}{T_o - T_i}\right)^2 + \left(\frac{U_{T_i}}{T_o - T_i}\right)^2 + \left(\frac{U_{T_B}}{T_B - T_{Sa}}\right)^2 + \left(\frac{U_{T_{Sa}}}{T_B - T_{Sa}}\right)^2 + \left(\frac{U_{C_{pw}}}{C_{pw}}\right)^2 + \left(\frac{U_{A_p}}{A_p}\right)^2 \right]^{\frac{1}{2}} \quad (1.5)$$

For a typical experimental run, values for the various parameters in Equation (3) can be as follows

$A_p = 288.43 \text{ cm}^2$

$\dot{m} = 47 \text{ gm/s}$

$T_o = 40°C$

$T_i = 15°C$

$T_B = 500°C$

$T_{Sa} = 130°C$

$C_{pw} = 4.184 \times 10^3$ J/kg°C

The uncertainty in specific heat of water can be $\mp$ 0.01% as given in Reference [34]. Other uncertainties in the independent variables can be computed as

$U_{A_p} = 0.00012$ cm^2

$U_{\dot{m}} = 0.8$ gm/s

$U_{T_o} = 1.14°C$

$U_{T_i} = 1.12°C$

$U_{T_B} = 2.50°C$

$U_{T_{Sa}} = 1.23°C$

$U_{C_{pw}} = 0.4184$ J/kg°C

Where $U_{\dot{m}}$, U_{T_o}, U_{T_i}, U_{T_B}, $U_{T_{Sa}}$ and $U_{C_{pw}}$ are the uncertainties in the independent variables $\dot{m}$, T_o, T_i, T_B, T_{Sa} and C_{pw}. Substitution of the above uncertainties and independent variables into Equation (1.5) gives the uncertainty in the heat transfer coefficient as

$$\frac{U_{h_{av}}}{h_{av}} = \mp 6.7\%$$

APPENDIX 2

LOW TEMPERATURE HEAT TRANSFER DATA

FREEBOARD HEAT TRANSFER COEFFICIENTS

Particle: Glass beads 275 μm
Tube elevation: 1.6 cm above the static bed
Static bed height: 36 cm

U_{sg} m/s	h, $W/m^2°K$								$\bar{h}$
	0°	45°	90°	135°	180°	225°	270°	315°	W/m^2K
0.166	560.8	369.0	206.1	171.0	186.1	181.3	209.8	357.4	280.2
0.219	464.7	311.8	191.5	187.2	226.2	185.5	193.5	321.0	260.2
0.284	423.0	276.5	190.7	242.4	301.7	215.3	165.7	294.3	263.7
0.355	436.2	260.2	182.1	254.9	313.8	217.7	142.0	275.4	260.3
0.467	451.5	240.1	155.3	259.7	314.0	218.9	129.0	267.0	254.5
0.571	472.5	243.4	155.9	255.0	304.7	210.4	124.4	268.9	254.4
0.672	504.5	236.6	147.5	281.1	343.3	212.4	113.7	263.6	262.8
0.830	529.0	231.4	140.4	278.5	344.9	205.2	110.4	264.9	263.0
0.961	472.4	225.6	141.7	293.3	419.0	248.5	122.4	269.8	274.1
1.053	444.8	223.8	144.6	293.9	432.9	240.7	118.6	250.7	268.8
1.245	419.0	205.9	130.2	342.3	578.9	268.0	110.5	221.6	284.5
1.425	487.5	226.0	120.0	288.9	602.8	301.1	115.4	245.7	298.4
1.607	463.4	214.2	122.6	324.8	450.3	237.2	94.7	232.9	367.5
1.763	450.3	198.5	115.1	302.8	411.6	244.4	96.0	224.0	255.3
1.898	469.5	211.7	119.0	302.9	418.5	233.5	97.7	236.3	261.1
2.06	459.8	209.1	114.8	300.5	414.0	243.0	95.5	235.0	259.0
2.212	463.0	225.4	115.0	325.6	475.4	252.8	100.9	254.3	276.9
2.406	470.9	276.9	123.0	309.5	460.6	240.7	119.3	304.3	288.1
3.101	426.1	266.1	102.5	192.5	288.2	153.9	105.7	305.4	330.2

FREEBOARD HEAT TRANSFER COEFFICIENTS

Particle: Glass beads 275 μm
Tube elevation: 19 cm above the static bed
Static bed height: 36 cm

U_{sg} m/s	h, W/m²°K								$\bar{h}$ W/m²K
	0°	45°	90°	135°	180°	225°	270°	315°	
0.140	10.34	8.52	8.19	9.82	11.41	9.78	8.14	8.46	9.58
0.173	10.57	8.56	8.10	9.55	12.82	9.62	8.12	8.56	9.49
0.229	13.62	10.11	9.47	11.14	14.75	11.07	9.40	10.07	11.20
0.175	35.40	8.04	9.77	11.75	17.78	11.16	9.46	7.95	13.92
0.330	38.32	9.00	10.85	14.27	21.96	12.56	10.13	8.32	15.80
0.405	161.20	23.23	16.61	35.08	61.59	31.55	15.00	21.64	45.74
0.485	213.22	32.58	19.74	42.40	77.80	38.12	17.30	28.89	58.77
0.579	256.02	48.29	26.60	62.67	106.90	50.04	22.27	42.68	76.94
0.704	353.95	146.90	32.25	74.16	136.60	66.43	31.15	150.79	124.03
0.828	369.69	182.70	52.46	122.63	212.79	104.35	52.25	190.65	160.94
1.037	367.30	191.33	57.24	123.14	259.74	118.84	56.99	208.88	173.00
1.169	445.09	226.98	115.35	158.58	342.63	155.43	107.20	235.55	223.35
1.331	509.02	233.39	114.70	150.30	405.29	171.60	114.11	269.53	245.99
1.495	464.66	227.79	102.73	173.74	426.88	177.27	114.83	274.70	245.32
1.652	422.87	256.09	110.17	182.94	355.63	164.41	114.90	281.82	236.10
1.729	407.03	250.43	110.45	179.94	406.73	193.29	115.46	246.91	241.03
1.824	500.69	266.78	110.97	192.54	402.30	209.62	141.16	304.09	265.89
1.962	450.01	262.72	119.49	200.26	405.13	203.14	129.60	298.30	258.78
2.06	424.38	273.85	127.31	233.22	397.43	182.14	137.45	308.99	260.60
2.320	473.44	292.97	129.18	222.35	424.03	204.82	138.63	337.05	277.81
2.878	333.03	262.85	126.73	212.58	383.44	202.01	127.5	283.72	241.73

FREEBOARD HEAT TRANSFER COEFFICIENTS

Particle: Glass beads 275 μm
Tube elevation: 58 cm above the static bed
Static bed height: 36 cm

U_{sg} m/s	h, $W/m^2°K$								$\bar{h}$
	0°	45°	90°	135°	180°	225°	270°	315°	W/m^2K
0.152	15.48	7.47	9.50	10.11	16.03	10.21	9.54	7.51	10.37
0.207	14.60	8.21	10.45	11.20	16.35	11.34	10.55	8.23	11.49
0.294	15.57	9.27	11.78	12.70	19.17	12.00	11.88	1.28	12.86
0.339	16.51	9.50	12.26	13.37	20.86	13.41	12.29	9.52	13.46
0.452	14.76	9.79	12.69	15.75	27.97	15.94	12.78	9.81	15.31
0.545	18.89	10.99	13.86	17.21	30.15	17.58	14.09	11.00	16.85
0.677	36.84	8.39	11.66	15.84	31.90	15.92	11.60	8.38	17.56
0.792	50.14	14.91	8.06	16.24	35.25	16.26	8.03	14.82	20.46
0.896	57.40	14.30	8.83	19.39	42.52	19.12	8.66	13.90	23.01
0.988	65.16	16.52	10.04	22.68	58.20	20.88	9.59	16.11	26.15
1.101	150.24	36.53	14.84	37.74	62.31	33.56	13.35	25.96	45.57
1.234	243.93	55.25	20.29	40.72	74.72	39.92	19.99	55.45	68.79
1.398	323.3	135.23	34.35	54.98	129.89	55.12	31.70	126.78	111.42
1.539	170.49	155.34	46.55	63.74	141.75	65.53	42.44	141.97	103.48
1.660	214.46	172.47	50.08	71.42	165.91	76.23	48.50	167.75	120.85
1.802	259.26	208.58	59.21	84.32	200.61	88.56	54.96	191.22	143.35
1.957	356.12	249.53	101.04	114.65	247.49	117.54	96.37	240.46	190.40
2.038	343.64	245.55	106.99	122.00	274.80	126.98	101.31	237.30	194.82
2.136	360.95	259.45	114.95	131.36	293.06	134.17	104.37	245.8	205.51
2.210	341.52	253.26	110.23	126.50	276.41	127.76	103.62	240.52	192.55
2.294	334.97	254.46	111.60	117.45	269.65	123.20	99.70	239.83	193.86
2.534	339.05	248.84	113.19	121.48	275.50	121.81	101.09	236.58	194.70

FREEBOARD HEAT TRANSFER COEFFICIENTS

Particle: Glass beads 275 μm
Tube elevation: 147 cm above the static bed
Static bed height: 36 cm

U_{sg} m/s	h, $W/m^2°K$								$\bar{h}$
	0°	45°	90°	135°	180°	225°	270°	315°	W/m^2K
0.169	18.41	5.63	4.40	8.60	18.69	8.69	4.47	5.39	9.29
0.254	20.60	6.54	5.66	11.74	26.00	11.82	5.74	6.30	11.80
0.341	19.67	5.39	7.56	18.41	29.80	18.53	7.56	5.26	14.03
0.452	23.54	6.30	8.58	21.82	35.64	21.88	8.56	6.22	16.56
0.633	34.20	6.50	9.18	23.66	38.70	23.56	8.92	6.38	18.88
0.734	20.40	6.64	9.24	24.42	40.06	24.22	9.10	6.56	20.14
0.873	42.36	6.92	9.75	26.14	43.10	26.02	9.56	6.80	21.32
1.120	44.86	7.32	10.20	27.64	45.90	27.52	10.02	7.20	22.58
1.243	49.15	8.12	11.26	30.91	52.16	31.31	11.07	7.94	25.23
1.481	52.73	8.38	11.62	31.90	52.89	32.90	11.44	8.32	26.09
1.572	53.58	8.67	11.92	33.37	54.82	32.91	11.73	8.60	26.95
1.776	58.98	9.11	12.28	34.85	57.57	34.67	12.03	9.00	28.56
1.853	77.70	9.10	16.28	42.34	77.14	48.84	16.02	8.60	35.34
2.013	85.98	10.58	17.34	48.00	69.90	27.64	16.94	9.50	39.48
2.101	79.08	29.73	18.06	39.71	64.88	40.88	17.71	27.47	39.95
2.215	97.58	31.28	18.60	42.32	71.29	43.07	18.30	27.75	43.78
2.325	129.64	27.91	12.11	37.06	78.52	42.56	12.71	28.30	45.47
2.403	150.52	27.91	11.08	38.51	83.27	44.59	11.96	22.29	48.78
2.594	173.26	30.73	11.65	43.14	74.86	37.93	10.88	25.70	51.02
2.623	202.30	34.37	13.56	47.78	71.02	37.95	11.62	30.07	56.08
2.975	245.25	31.94	12.83	45.79	69.27	36.98	11.32	27.00	60.05

FREEBOARD HEAT TRANSFER COEFFICIENTS

Particle: Glass beads 275 μm
Tube elevation: 225 cm above the static bed
Static bed height: 36 cm

U_{sg} m/s	h, $W/m^2°K$								$\bar{h}$ W/m^2K
	0°	45°	90°	135°	180°	225°	270°	315°	
0.152	10.96	9.84	5.98	10.64	15.38	10.74	5.00	9.70	9.66
0.234	10.06	9.04	5.36	12.14	17.74	12.20	5.36	8.94	10.10
0.289	7.78	9.08	5.52	12.98	19.18	13.20	5.58	9.06	10.54
0.336	10.98	9.99	6.07	14.51	21.55	14.70	6.09	10.02	11.74
0.419	14.00	12.23	7.43	18.10	22.89	18.55	7.58	12.33	14.68
0.531	16.04	13.85	8.42	20.80	31.35	21.14	8.40	13.83	16.71
0.665	17.62	14.96	8.97	22.71	34.51	22.81	9.10	14.74	17.98
0.732	19.33	16.08	9.70	25.32	37.97	25.32	9.68	16.03	19.93
0.838	20.49	16.63	8.11	26.34	39.93	26.48	8.00	10.58	20.32
0.933	21.80	17.30	6.79	27.85	42.15	28.05	6.82	17.46	21.04
1.160	26.04	20.76	8.07	33.24	49.50	33.33	8.04	20.55	24.96
1.309	47.81	10.11	10.56	31.64	64.29	31.71	10.58	10.10	27.09
1.539	59.99	12.04	12.40	37.62	75.88	34.96	12.66	12.16	32.34
1.896	60.18	11.94	12.20	37.44	65.06	37.74	12.32	11.98	32.36
2.052	66.80	13.41	10.64	37.62	81.28	35.34	10.56	12.16	33.47
2.199	67.90	15.92	10.90	41.14	90.98	37.92	10.85	14.48	36.26
2.335	75.30	16.20	11.19	39.51	93.88	38.23	11.07	13.98	37.43
2.618	69.56	19.28	21.94	33.95	98.14	36.57	21.48	16.29	39.56
2.714	76.94	22.13	26.73	40.54	77.39	44.92	23.50	19.15	41.41

IMMERSED TUBE HEAT TRANSFER COEFFICIENTS

Particle: Glass beads 850 μm
Tube elevation: 1.60 cm above the static bed
Static bed height: 36 cm

U_{sg} m/s	h, W/m²°K								$\bar{h}$ W/m²K
	0°	45°	90°	135°	180°	225°	270°	315°	
0.576	234.4	77.50	72.80	80.60	100.0	78.80	56.30	53.50	94.30
0.658	325.9	141.80	106.00	99.30	128.0	70.50	83.30	125.00	137.50
0.710	326.0	150.90	100.00	100.70	137.0	91.90	82.30	148.00	142.10
0.796	294.5	135.60	94.90	102.40	140.7	92.70	79.70	136.20	134.60
0.952	277.5	114.28	91.50	116.00	147.7	103.10	73.10	117.20	130.00
1.124	280.30	99.20	82.20	120.70	154.4	108.90	68.00	103.90	127.20
1.281	262.4	97.40	85.90	125.20	151.7	106.10	64.80	99.90	124.20
1.456	239.0	92.10	73.30	130.0	171.9	116.80	67.50	95.40	123.20
1.625	255.6	91.40	81.30	125.80	158.0	113.30	64.10	90.30	122.60
1.807	226.1	89.60	82.20	132.10	182.9	122.40	70.70	91.90	124.70
1.973	207.1	88.60	93.40	142.30	191.5	126.70	67.80	85.60	125.40
2.158	201.3	87.10	84.70	129.90	179.2	117.90	67.00	88.30	119.40
2.338	210.3	89.90	86.20	140.00	190.0	133.10	77.00	93.30	127.50
2.969	214.5	94.90	89.10	138.80	187.4	134.10	78.90	95.50	129.20
3.228	214.5	94.70	91.20	151.80	213.7	146.20	79.60	95.00	135.80
3.468	213.6	96.20	84.60	134.60	203.9	155.00	83.80	90.40	132.70
3.691	310.5	96.30	69.20	120.30	231.1	134.30	62.60	67.00	136.40

FREEBOARD HEAT TRANSFER COEFFICIENTS

Particle: Glass beads 850 μm
Tube elevation: 19 cm above the static bed
Static bed height: 36 cm

U_{sg} m/s	h, W/m²°K								$\bar{h}$ W/m²K
	0°	45°	90°	135°	180°	225°	270°	315°	
0.493	32.73	7.44	16.29	32.43	61.92	32.16	15.72	7.50	25.77
0.622	36.24	8.22	18.48	33.15	59.46	31.65	17.10	7.92	26.52
0.706	39.81	9.00	18.87	33.21	61.80	32.64	17.91	8.92	27.78
0.829	69.18	8.93	17.03	29.82	54.83	28.48	15.90	8.73	29.13
1.035	86.00	21.48	23.97	36.81	69.15	34.65	17.93	20.13	38.28
1.138	74.72	19.12	21.82	40.43	54.35	38.09	19.30	17.75	35.70
1.274	77.93	23.93	16.44	37.61	68.54	34.42	22.51	20.94	38.96
1.386	116.34	33.24	32.80	45.60	80.43	39.97	29.00	29.93	50.23
1.501	117.08	39.43	42.64	56.56	95.23	53.56	39.12	38.17	60.23
1.616	112.27	38.72	43.29	56.51	104.88	56.33	40.52	36.96	61.19
1.740	108.04	36.96	41.86	56.87	105.54	52.22	40.65	32.25	60.80
1.878	102.78	36.56	44.22	60.32	106.48	59.10	41.04	35.64	60.78
2.045	103.60	37.70	47.24	64.09	111.81	60.50	43.16	36.74	63.10
2.148	104.47	38.76	50.13	66.63	112.73	60.90	43.94	36.72	64.29
2.342	110.16	30.32	41.35	71.34	121.11	66.21	38.05	30.06	63.64
2.868	116.45	33.62	44.81	72.80	121.78	68.56	39.36	31.75	64.14
3.608	118.45	36.14	46.79	76.25	124.17	67.87	39.41	33.96	68.88
3.142	121.70	39.34	49.25	76.96	136.24	70.26	41.11	38.36	71.66

FREEBOARD HEAT TRANSFER COEFFICIENTS

Particle: Glass beads 850 μm
Tube elevation: 58 cm above the static bed
Static bed height: 36 cm

U_{sg} m/s	h, W/m²°K								$\bar{h}$ W/m²K
	0°	45°	90°	135°	180°	225°	270°	315°	
0.505	24.54	4.65	8.54	18.30	38.96	18.45	9.79	4.50	15.84
0.584	24.29	4.55	8.55	17.94	38.87	18.53	8.86	4.41	15.75
0.650	24.39	4.65	8.75	18.29	39.84	19.04	9.12	4.53	16.08
0.742	25.05	4.91	9.32	18.81	41.03	19.32	3.53	4.79	16.59
0.879	32.76	6.50	12.31	24.99	54.44	25.90	12.73	6.38	22.00
0.978	34.94	6.82	12.83	26.03	56.43	26.66	13.07	6.57	22.91
1.076	36.96	7.24	13.68	27.72	59.70	28.27	13.57	7.01	24.30
1.183	40.74	7.81	14.55	29.58	62.45	30.04	14.40	7.58	25.90
1.336	42.85	8.02	14.61	30.89	65.42	31.58	14.93	7.85	27.02
1.486	46.51	8.55	15.35	33.44	69.94	32.60	14.93	8.08	28.67
1.627	48.32	8.66	14.65	33.67	72.09	34.68	15.79	8.32	89.53
1.750	50.18	9.18	16.09	35.91	78.38	37.35	16.40	8.66	31.52
1.856	52.38	9.69	17.86	40.47	81.74	38.64	17.23	9.48	33.44
1.976	57.59	10.51	19.59	47.33	87.72	40.53	18.47	10.39	36.52
2.105	65.01	12.35	22.42	50.22	101.16	49.61	21.66	11.46	41.74
2.208	71.54	13.64	25.54	54.15	104.54	40.07	22.48	13.00	44.46
2.322	77.12	14.99	29.37	60.10	114.30	58.50	27.93	14.78	49.65
2.989	76.53	15.37	32.34	67.91	130.34	65.85	32.17	15.64	54.53
3.249	79.80	16.25	35.83	74.73	132.72	65.93	31.94	16.17	56.68

FREEBOARD HEAT TRANSFER COEFFICIENTS

Particle: Glass beads 850 μm
Tube elevation: 147 cm above the static bed
Static bed height: 36 cm

U_{sg} m/s	h, $W/m^2°K$								$\bar{h}$ W/m^2K
	0°	45°	90°	135°	180°	225°	270°	315°	
0.476	29.87	6.15	9.14	14.44	32.77	14.53	8.76	5.57	15.14
0.601	39.07	9.64	9.80	24.89	56.43	25.41	9.75	9.42	23.03
0.715	40.52	9.05	7.48	25.83	61.45	25.05	7.48	8.85	23.20
0.789	39.96	9.39	7.50	25.97	59.64	25.61	7.50	9.18	23.14
0.860	40.27	9.05	7.60	26.23	69.18	25.90	7.63	8.83	24.33
0.961	47.98	9.10	7.68	28.01	77.40	28.20	7.63	8.85	26.85
1.114	56.63	9.15	7.83	30.63	79.45	80.28	7.85	8.88	28.83
1.280	59.53	9.18	7.88	30.78	78.15	29.93	7.78	9.03	28.95
1.315	57.94	9.23	7.98	31.23	81.78	30.68	8.03	8.98	29.48
1.357	60.55	9.28	8.55	32.33	82.85	32.18	8.15	9.08	30.35
1.454	63.35	9.33	8.58	33.40	84.00	32.40	8.40	9.13	31.08
1.566	66.18	9.38	8.85	33.63	83.55	32.40	8.55	9.20	31.45
1.745	69.53	9.40	9.05	33.65	81.70	32.40	8.55	9.23	31.68
1.861	73.25	9.43	9.33	35.20	85.50	32.98	8.63	9.23	32.93
2.028	73.63	9.53	9.60	36.48	88.28	34.80	9.10	9.33	33.93
2.206	74.45	9.58	9.68	37.50	92.30	36.45	9.63	9.35	34.88
2.256	87.75	13.85	10.95	41.93	101.00	40.00	10.45	13.33	39.90
2.348	90.10	15.53	11.35	43.48	108.20	42.13	10.73	14.78	41.90
2.967	88.55	15.63	10.95	42.00	105.00	40.40	10.63	14.73	41.00
3.225	86.03	15.78	11.10	43.33	104.85	40.63	11.03	15.08	41.00

FREEBOARD HEAT TRANSFER COEFFICIENTS

Particle: Glass beads 850 μm
Tube elevation: 225 cm above the static bed
Static bed: 36 cm

U_{sg} m/s	h, $W/m^2°K$								$\bar{h}$ W/m^2K
	0°	45°	90°	135°	180°	225°	270°	315°	
0.512	21.84	5.70	5.42	23.34	42.04	23.52	5.52	5.44	16.60
0.618	32.10	5.78	4.62	21.94	44.60	22.12	4.74	5.52	16.41
0.678	22.20	5.82	4.72	22.60	46.26	23.00	4.86	5.62	16.88
0.753	23.40	6.88	4.92	23.34	27.46	23.50	5.00	7.70	17.64
0.811	30.13	6.80	4.98	23.98	48.70	24.18	5.06	6.64	18.80
0.974	31.02	6.92	5.08	24.88	50.42	25.06	5.22	6.80	10.46
1.105	43.10	8.07	6.03	31.17	59.43	31.37	6.07	7.92	24.15
1.194	45.47	8.07	6.08	39.70	62.10	40.04	6.31	7.85	26.14
1.282	46.33	8.16	5.96	38.37	60.39	39.09	6.09	8.05	26.53
1.315	48.53	8.45	6.09	39.38	62.02	40.28	6.29	8.32	27.41
1.395	50.97	8.73	6.27	40.33	63.16	40.61	6.31	8.69	28.14
1.480	53.06	9.13	6.47	41.82	65.85	42.79	6.73	9.15	29.37
1.562	57.79	9.92	7.04	44.48	69.37	45.17	7.15	9.94	31.94
1.708	60.21	10.34	7.33	46.20	70.99	46.20	7.50	10.30	34.43
1.879	63.84	10.92	7.70	47.78	73.55	48.51	7.63	10.82	33.84
1.934	67.01	11.40	7.88	49.63	76.21	50.36	8.03	11.42	35.24
2.099	69.50	11.95	8.21	51.68	80.10	51.99	8.27	12.10	36.81
2.178	71.70	12.21	8.32	52.27	80.56	52.67	8.45	12.14	37.29
2.997	72.45	12.45	8.49	53.88	81.20	52.77	8.54	12.50	37.77
3.130	74.16	12.96	8.93	55.84	86.53	57.46	8.93	13.00	39.73
3.258	78.39	13.40	8.98	57.57	88.10	57.57	9.28	13.68	40.38

IMMERSED TUBE HEAT TRANSFER

Particle: silica sand 285 μm
Tube elevation: 1.6 cm above the static bed height
Static bed height = 36 cm

U_{sg} m/s	h, $w/m^2°K$								$\bar{h}$ W/m^2K
	0°	45°	90°	135°	180°	225°	270°	315°	
0.171	173.6	217.4	181.6	146.0	161.7	147.4	164.7	240.3	179.1
0.194	141.6	159.3	171.8	144.7	169.9	143.0	155.0	145.0	153.7
0.233	147.4	173.9	199.2	141.7	172.3	136.6	177.0	166.3	164.0
0.284	151.2	173.4	193.6	144.8	177.6	136.0	186.2	169.8	166.6
0.337	198.6	191.8	189.5	154.8	185.3	142.7	176.4	205.6	180.6
0.407	313.2	203.8	181.3	167.4	209.0	165.8	172.2	229.1	205.5
0.550	356.9	201.6	191.0	183.7	216.6	166.1	153.0	215.0	210.5
0.652	405.9	194.2	155.5	173.4	213.6	167.3	139.2	225.0	209.3
0.794	394.6	181.5	148.9	212.0	255.6	201.6	126.9	205.6	215.9
0.962	399.2	183.4	150.0	239.4	285.4	207.0	119.7	204.0	223.5
1.119	397.0	182.5	125.3	235.5	292.6	200.0	101.3	190.5	215.7
1.248	389.2	182.4	141.7	280.5	358.6	231.0	109.9	192.6	235.7
1.388	368.7	169.7	131.6	297.6	373.4	243.2	106.1	191.5	235.2
1.591	359.2	165.5	130.0	294.6	364.0	237.2	103.6	178.8	229.4
1.619	383.0	163.2	121.0	275.3	357.2	235.6	102.0	182.3	227.5
1.769	435.0	176.5	122.6	295.8	391.8	247.3	108.4	198.8	247.0
1.902	423.7	172.9	125.2	297.2	378.9	235.0	103.7	195.9	242.0
2.117	386.1	175.2	132.8	321.3	400.3	264.3	100.0	188.0	246.0
2.201	355.0	167.8	123.3	314.5	383.0	246.3	98.8	189.6	234.8
2.373	364.1	176.6	111.3	282.2	381.8	240.4	49.4	202.4	232.3

FREEBOARD HEAT TRANSFER

Particle: silica sand 285 μm
Tube elevation: 19 cm above the static bed height
Static bed height = 36 cm

U_{sg} m/s	h, W/m²°K								$\bar{h}$ W/m²K
	0°	45°	90°	135°	180°	225°	270°	315°	
0.157	20.13	7.41	6.42	8.49	15.51	8.94	6.72	7.50	10.14
0.216	22.89	8.10	7.05	9.21	16.08	9.12	6.99	8.07	10.95
0.296	31.74	9.12	7.29	10.08	18.36	10.17	7.50	9.24	12.93
0.355	72.75	13.45	8.64	11.77	15.88	11.21	8.25	12.54	19.32
0.492	185.57	72.42	24.37	28.52	42.08	26.14	21.64	87.05	63.80
0.57	152.97	97.25	25.34	35.44	54.34	31.87	22.70	86.66	67.07
0.686	225.18	153.65	39.66	88.87	132.03	83.59	38.49	162.74	116.15
0.761	232.95	173.16	45.16	102.63	152.82	89.09	41.02	176.75	126.70
0.532	224.42	169.42	44.79	106.67	161.62	98.01	44.59	186.81	129.54
0.975	226.94	100.92	51.37	123.22	184.36	113.86	58.35	197.39	143.30
1.238	211.64	200.67	54.48	135.62	206.12	123.91	53.28	211.61	190.79
1.282	204.59	210.46	55.79	144.07	235.50	147.72	61.68	237.39	162.37
1.381	228.72	245.57	62.41	166.22	220.33	128.09	55.79	254.76	170.33
1.470	228.27	229.66	61.10	171.41	322.46	180.2	73.07	271.17	192.17
1.598	214.72	256.15	64.51	174.02	290.07	157.11	69.91	267.04	186.73
1.695	239.75	260.44	69.65	180.53	297.93	173.85	71.91	281.02	196.82
1.832	232.48	264.25	114.01	235.59	393.15	210.74	121.75	299.80	233.98
1.987	279.43	265.89	89.46	212.06	361.72	138.79	96.92	290.92	229.4
2.087	334.69	277.14	78.69	238.12	515.83	139.45	81.92	334.06	262.49
2.24	255.91	266.04	80.33	236.54	442.34	251.11	89.45	296.74	240.06
2.344	301.4	294.36	75.4	238.4	394.5	217.5	84.76	392.5	249.54
2.868	254.72	286.79	82.87	224.12	312.66	202.05	84.64	294.4	217.75

FREEBOARD HEAT TRANSFER

Particle: silica sand 285 μm
Tube elevation: 58 cm above the static bed height
Static bed height = 36 cm

U_{sg} m/s	h, $W/m^2°K$								$\bar{h}$ W/m^2K
	0°	45°	90°	135°	180°	225°	270°	315°	
0.162	20.92	4.78	6.70	11.22	25.66	11.54	6.94	4.08	11.56
0.227	18.64	4.44	6.76	11.74	26.66	12.04	7.04	4.34	11.56
0,286	18.62	4.52	7.22	12.64	28.78	12.90	7.40	4.44	12.06
0.331	19.50	5.82	7.96	13.42	30.70	13.72	7.82	4.72	12.80
0.427	22.38	5.42	8.44	15.10	39.60	15.50	8.68	5.24	14.42
0.530	13.99	6.12	9.42	17.52	40.30	17.94	9.72	5.92	16.86
0.688	52.04	7.54	10.88	20.42	47.10	20.92	10.84	7.08	22.10
0.782	101.38	4.44	6.34	12.75	49.46	12.27	6.18	4.22	22.13
0.994	135.56	5.84	7.42	16.40	40.48	15.83	7.13	5.06	29.22
1.160	173.61	37.18	22.76	40.49	84.60	40.87	22.19	32.82	56.82
1.336	170.32	77.37	25.66	63.30	143.02	61.19	22.86	64.43	78.52
1.496	165.74	106.28	29.62	66.67	146.04	70.52	27.51	96.52	88.61
1.648	168.21	133.46	40.88	80.23	153.14	78.15	39.01	134.54	103.45
1.737	154.17	145.56	44.78	92.45	188.59	94.31	42.30	146.63	113.60
1.842	156.24	158.75	49.75	97.29	214.18	100.27	51.36	166.84	124.34
1.901	148.31	161.74	52.36	99.79	209.09	93.43	45.67	168.34	122.34
1.98	157.29	178.33	63.66	103.24	205.20	99.13	56.23	200.99	132.66
2.065	151.57	185.72	64.70	112.44	222.95	106.87	60.42	228.02	141.59
2.153	155.53	251.54	116.05	165.74	316.90	184.60	109.55	298.31	199.79
2.989	160.59	263.52	120.08	181.13	310.22	199.95	112.09	290.03	203.34

FREEBOARD HEAT TRANSFER

Particle: silica sand 285 μm
Tube elevation: 147 cm above the static bed
Static bed height = 36 cm

U_{sg} m/s	h, W/m²°K								$\bar{h}$ W/m²K
	0°	45°	90°	135°	180°	225°	270°	315°	
0.244	20.60	6.20	8.0	12.0	25.0	12.02	8.06	3.82	12.20
0.363	17.20	5.60	7.60	11.60	23.80	11.54	7.80	3.40	11.40
0.473	24.18	5.735	8.68	15.593	36.58	15.81	8.99	5.425	15.19
0.551	24.99	5.456	9.083	16.895	39.99	17.771	9.083	5.115	15.934
0.680	28.74	7.63	10.50	20.30	48.30	19.775	10.50	7.34	19.145
0.778	43.20	7.20	9.45	18.81	46.20	18.48	9.48	7.04	19.98
0.960	52.26	8.10	10.53	21.66	50.4	21.30	10.29	7.53	22.74
1.133	49.59	8.16	10.86	22.14	52.54	21.60	10.29	8.04	22.80
1.298	58.59	9.30	11.58	24.21	58.20	24.0	11.28	8.94	25.74
1.503	22.32	10.08	12.33	35.61	69.0	34.95	12.0	9.75	31.35
1.565	67.83	10.95	12.03	44.28	75.81	43.50	11.52	10.71	34.56
1.607	70.38	11.94	11.79	44.70	77.40	44.40	11.64	11.28	35.43
1.732	153.75	10.075	10.525	40.75	71.65	39.925	10.40	9.90	43.375
1.785	205.4	9.44	9.12	35.80	60.80	34.60	8.84	8.96	47.24
1.856	228.9	18.90	9.68	38.0	70.46	36.80	9.24	14.96	53.50
1.961	246.20	31.40	11.02	30.32	44.84	32.48	10.56	29.56	59.60
2.087	272.5	30.95	33.6	46.3	133.70	55.02	35.20	27.6	66.73
2.169	279.87	39.45	35.50	59.88	175.48	62.20	34.20	34.50	77.63
2.208	209.5	38.40	35.4	60.01	175.5	57.04	33.0	35.46	80.53
2.373	309.5	42.3	36.80	65.20	182.10	66.30	38.3	43.30	98.0

FREEBPARD HEAT TRANSFER

Particle: silica sand 285 μm
Tube elevation: 225 cm above the static bed
Static bed height = 36 cm

U_{sg} m/s	h, W/m²°K								$\bar{h}$ W/m²K
	0°	45°	90°	135°	180°	225°	270°	315°	
0.168	21.08	5.84	7.12	15.04	26.12	15.12	7.28	5.28	12.82
0.227	19.96	5.12	6.98	15.26	26.58	15.28	7.16	4.92	12.66
0.295	16.48	4.64	6.90	15.64	27.74	15.76	7.00	4.52	12.34
0.372	18.26	6.72	8.88	18.16	30.64	18.26	9.04	6.56	14.56
0.459	18.92	6.96	9.24	19.50	33.30	19.70	9.36	6.84	15.48
0.560	19.80	4.22	9.68	20.78	35.64	20.96	10.76	8.08	16.36
0.640	23.00	6.80	9.78	24.45	43.55	24.58	9.98	16.63	18.60
0.724	24.80	7.33	10.45	26.62	47.58	26.73	10.66	7.15	20.18
0.963	26.74	7.82	11.26	29.10	51.89	29.55	11.61	7.66	21.94
1.044	29.51	8.60	12.40	31.95	57.01	32.51	12.60	8.46	24.14
1.131	31.50	9.02	12.88	13.68	60.25	34.27	13.30	8.88	25.48
1.220	33.80	9.58	13.78	36.12	64.10	36.06	13.80	9.41	27.08
1.342	35.70	10.71	15.24	37.52	66.30	38.14	14.59	9.85	28.28
1.478	37.49	10.47	14.64	38.84	69.50	39.87	15.06	10.36	29.54
1.593	39.06	10.92	15.46	40.37	71.96	40.85	15.34	10.81	30.60
1.697	43.93	11.70	16.07	42.34	75.49	42.62	15.94	11.56	32.45
1.829	50.99	12.94	16.57	45.53	80.64	45.61	16.88	12.35	35.20
1.941	59.23	13.92	17.50	58.44	87.05	49.59	18.06	13.22	38.42
2.052	65.21	14.48	17.42	48.98	89.10	59.66	18.10	15.55	39.52
2.192	79.67	16.77	19.40	52.70	100.00	55.67	19.94	14.79	44.88
2.858	84.89	20.67	26.57	65.36	135.77	75.32	27.25	15.78	56.45
2.997	88.01	21.16	34.53	84.73	145.52	99.06	39.12	19.68	66.85
3.130	86.80	22.33	35.45	86.70	158.63	107.53	39.25	19.05	69.40

IMMERSED TUBE HEAT TRANSFER COEFFICIENTS

Particle: silica sand 465 μm
Tube elevation: 1.6 cm above the static bed
Static bed height: 36 cm

U_{sg} m/s	h, W/m²°K								$\bar{h}$ W/m²K
	0°	45°	90°	135°	180°	225°	270°	315°	
0.256	195.5	182.9	141.2	112.3	100.9	113.5	135.0	218.8	150.0
0.307	200.4	200.0	138.0	119.3	117.3	115.6	135.2	196.7	153.0
0.354	239.1	202.5	143.7	127.1	128.9	119.2	132.3	204.0	162.1
0.407	260.4	198.4	144.2	126.7	135.1	122.3	130.9	218.1	167.0
0.484	443.2	214.3	135.2	150.6	192.2	143.9	135.0	245.6	207.5
0.570	384.3	183.9	135.0	155.0	193.3	142.2	125.2	221.3	192.5
0.685	379.2	167.8	120.8	154.0	193.3	149.9	120.6	213.1	187.3
0.808	441.9	159.10	113.8	153.4	188.4	138.6	102.5	187.1	185.6
0.890	470.2	165.51	116.3	151.6	197.5	141.9	97.9	187.9	191.1
0.966	412.0	155.0	108.8	156.4	193.7	141.7	102.5	178.5	181.0
1.164	416.3	154.3	108.0	163.1	204.3	144.7	87.3	161.7	199.9
1.188	406.8	149.0	112.6	178.0	225.7	147.8	92.3	163.8	184.5
1.351	379.1	138.8	109.6	170.7	239.6	156.5	94.8	148.6	179.7
1.542	362.7	134.3	107.9	176.4	246.2	155.4	95.3	145.4	176.7
1.588	331.2	118.3	104.8	175.0	226.3	146.5	90.3	141.7	166.8
1.724	326.4	117.8	105.0	176.0	243.9	149.8	94.93	144.3	169.8
1.883	333.9	118.9	110.4	197.4	264.5	167.6	92.8	139.9	178.2
2.057	322.4	120.3	105.4	204.9	294.9	189.1	99.1	133.3	183.7
2.288	289.0	111.0	104.2	219.0	299.0	189.5	93.2	133.7	179.8
2.369	310.0	114.5	102.4	202.4	280.3	177.0	91.6	136.1	176.8
3.101	307.7	118.4	112.4	216.0	297.9	176.5	90.7	132.3	181.5

FREEBOARD HEAT TRANSFER COEFFICIENTS

Particle: silica sand 465 μm
Tube elevation: 19 cm above the static bed
Static bed height: 36 cm

U_{sg} m/s	h, $W/m^2°K$								$\bar{h}$ W/m^2K
	0°	45°	90°	135°	180°	225°	270°	315°	
0.235	16.26	4.98	5.52	12.14	27.22	12.52	5.64	4.96	11.18
0.330	17.92	5.56	5.98	13.04	27.94	12.64	5.98	5.44	11.78
0.396	27.18	6.30	6.24	13.94	28.94	12.88	6.06	6.24	13.58
0.435	46.44	7.98	7.42	15.34	29.60	17.18	6.50	7.40	16.74
0.489	72.78	9.62	7.58	15.74	33.32	14.90	7.40	9.54	21.36
0.570	248.98	51.81	16.23	19.75	31.95	18.54	15.70	50.12	56.63
0.628	262.18	59.11	17.99	22.46	35.62	19.80	15.53	51.12	60.48
0.736	290.52	70.58	21.23	30.41	51.43	27.15	18.68	66.08	71.98
0.917	328.81	107.91	37.36	58.00	101.15	48.27	32.87	102.05	102.2
1.100	326.81	112.39	40.21	77.60	127.1	60.84	34.33	110.41	112.34
1.234	268.09	95.46	38.09	70.23	132.64	73.82	36.71	97.95	102.75
1.329	273.63	101.80	40.27	83.67	134.28	74.24	38.88	103.16	106.23
1.464	278.14	109.58	42.44	105.46	186.39	88.05	41.76	104.95	119.60
1.625	266.11	116.19	43.48	97.38	181.32	82.27	43.00	121.90	118.96
1.801	254.15	128.08	53.11	122.15	202.59	87.67	47.56	130.43	128.21
1.957	248.34	135.89	51.07	99.82	160.48	83.61	57.23	138.30	120.6
2.031	272.8	152.51	59.08	129.42	221.06	108.23	55.40	155.0	114.14
2.111	256.3	136.82	57.50	117.73	210.53	114.75	56.14	146.54	137.03
2.338	281.36	146.95	63.52	138.64	253.0	119.71	60.73	154.86	152.31
2.868	274.34	144.12	63.41	128.49	228.78	120.79	63.39	160.35	147.95
3.008	317.50	172.35	68.70	149.23	244.54	109.46	52.46	163.50	159.68

FREEBOARD HEAT TRANSFER COEFFICIENTS

Particle: silica sand 465 μm
Tube elevation: 58 cm above the static bed
Static bed height = 36 cm

U_{sg} m/s	h, W/m²°K								$\bar{h}$ W/m²K
	0°	45°	90°	135°	180°	225°	270°	315°	
0.205	20.04	5.10	5.92	15.0	32.28	15.36	10.14	5.00	14.10
0.264	18.88	4.94	5.70	14.88	32.20	15.18	9.98	4.90	13.84
0.324	17.86	4.84	9.98	15.40	33.52	15.82	11.16	4.80	14.04
0.446	18.16	5.02	10.24	15.98	35.02	16.46	10.52	4.94	14.54
0.539	18.74	5.28	10.68	16.90	37.06	17.26	10.94	5.12	15.24
0.631	21.28	5.96	11.72	18.36	40.58	19.12	11.98	5.76	16.84
0.691	22.38	6.26	12.28	19.34	42.64	21.22	12.58	6.06	17.72
0.783	25.08	6.62	12.88	20.64	45.18	21.32	12.96	6.36	18.58
0.884	27.92	7.04	13.24	21.40	46.80	21.78	13.36	6.60	19.76
0.984	29.72	7.42	13.68	23.08	59.88	23.20	13.82	7.02	20.98
1.172	26.48	8.20	14.44	24.86	55.68	25.76	14.20	7.28	23.36
1.302	91.78	16.66	22.33	34.10	81.94	33.86	21.80	14.39	39.62
1.468	188.22	19.00	19.20	32.11	72.56	32.45	18.85	17.04	49.93
1.557	202.43	20.52	19.83	34.14	79.79	34.22	20.45	17.94	53.67
1.696	211.26	21.50	22.95	38.95	90.18	36.33	21.55	19.91	57.83
1.944	251.43	27.91	27.43	43.66	98.80	38.93	23.93	24.13	67.03
1.878	232.75	30.55	30.90	47.94	106.80	43.27	26.32	28.23	68.34
2.083	221.58	34.68	36.51	56.71	117.52	45.44	30.08	29.96	71.56
2.270	217.84	34.24	40.10	65.69	133.94	49.49	34.19	34.65	76.26
2.989	218.73	44.30	46.21	87.95	184.33	77.67	41.18	44.49	93.09
3.122	241.50	87.22	69.79	104.36	221.16	93.53	60.83	92.29	121.46
3.249	192.03	93.21	31.16	95.76	216.06	96.24	68.67	89.43	116.57

FREEBOARD HEAT TRANSFER COEFFICIENTS

Particle: silica sand 465 μm
Tube elevation: 147 cm above the static bed
Static bed height = 36 cm

U_{sg} m/s	h, $W/m^2°K$								$\bar{h}$ W/m^2K
	0°	45°	90°	135°	180°	225°	270°	315°	
0.244	14.34	6.34	3.71	10.49	19.02	10.47	3.71	5.95	9.25
0.363	12.93	7.38	3.29	9.33	17.11	9.48	3.29	7.50	8.79
0.473	20.52	10.95	4.88	13.70	25.14	13.74	4.74	11.09	13.10
0.551	26.54	14.04	6.02	17.96	32.84	17.90	6.04	14.32	16.94
0.680	27.56	14.50	5.96	18.40	33.70	18.40	6.04	14.86	16.42
0.778	28.30	14.84	6.18	18.56	35.96	19.42	6.12	15.16	18.20
0.960	31.84	16.14	6.66	21.02	38.94	20.80	6.38	16.30	19.76
1.133	36.58	18.20	7.26	22.76	41.46	22.42	7.00	18.84	21.82
1.298	39.12	19.46	7.38	24.10	43.26	28.02	7.24	19.84	22.96
1.503	41.16	19.98	7.76	25.50	45.06	24.84	7.70	20.22	24.02
1.535	65.13	19.54	10.94	36.54	52.70	36.54	10.58	20.04	31.52
1.607	70.36	20.20	11.30	36.58	53.28	37.44	11.10	20.92	32.48
1.732	73.96	20.78	11.50	38.40	53.28	37.62	10.90	20.34	32.94
1.772	76.72	22.48	11.72	39.14	55.90	33.30	11.26	22.58	34.80
1.856	72.22	21.98	11.90	40.92	57.40	39.96	11.56	22.30	34.88
1.961	77.60	22.56	10.82	41.52	58.26	40.78	12.00	23.56	36.02
2.087	76.70	22.90	12.30	42.72	58.88	42.12	12.06	23.58	36.41
2.169	82.56	23.96	12.48	43.40	61.72	43.60	12.52	24.86	38.14
2.208	82.42	24.88	12.74	44.46	72.08	44.46	12.58	25.40	39.84
2.373	87.04	25.54	13.38	46.14	82.48	46.84	13.16	25.68	42.54
3.033	103.46	27.98	14.64	48.38	87.20	48.38	13.58	26.56	46.88
3.225	133.00	33.80	16.92	52.76	97.92	56.60	15.58	29.44	54.52

FREEBOARD HEAT TRANSFER COEFFICIENTS

Particle: silica sand 465 μm
Tube elevation: 225 cm above the static bed
Static bed height = 36 cm

U_{sg} m/s	h, W/m²°K								$\bar{h}$ W/m²K
	0°	45°	90°	135°	180°	225°	270°	315°	
0.228	26.76	5.26	7.44	19.42	30.62	19.66	7.66	5.14	15.24
0.299	24.54	5.01	7.30	19.80	31.02	19.66	7.40	4.92	14.94
0.379	23.38	4.96	7.28	20.24	32.04	20.32	7.42	4.86	15.06
0.474	23.12	5.00	7.38	21.12	33.98	21.32	7.48	4.88	15.52
0.547	23.94	5.08	7.56	21.94	35.30	22.06	7.66	4.96	16.06
0.699	24.30	5.22	7.76	13.06	37.22	23.32	7.88	5.08	17.72
0.877	25.78	5.48	8.12	24.80	39.86	25.04	8.32	5.36	17.80
1.032	27.84	5.88	4.60	26.46	42.68	26.70	8.84	5.74	19.10
1.143	29.22	6.20	8.94	27.94	45.22	28.80	9.22	6.10	20.14
1.245	46.44	6.62	9.64	30.02	48.22	30.22	8.74	6.48	22.42
1.363	58.66	6.76	9.95	31.06	50.38	30.34	10.0	6.68	25.60
1.476	59.04	6.94	10.22	32.24	51.42	32.36	10.40	7.02	26.26
1.219	60.92	6.72	10.54	33.74	54.24	33.84	10.80	7.12	27.30
1.633	62.86	6.48	10.94	34.72	55.54	34.54	10.98	7.38	28.06
1.752	65.80	7.86	11.40	36.20	57.74	36.20	11.50	7.74	29.30
1.843	67.84	8.12	11.60	37.38	60.50	37.90	11.82	8.01	30.40
1.970	71.84	8.64	12.30	39.38	63.18	40.06	12.54	8.60	32.08
2.159	75.88	9.00	12.36	40.64	64.74	40.64	12.76	9.08	33.14
2.858	78.24	9.24	13.00	41.80	67.32	42.32	13.30	9.26	34.30
2.997	69.76	9.42	12.86	42.90	68.10	43.20	13.42	9.62	34.92
3.130	86.26	11.04	13.30	44.84	73.44	45.52	13.60	9.62	37.10

APPENDIX 3

HIGH TEMPERATURE HEAT TRANSFER DATA

IMMERSED TUBE HEAT TRANSFER COEFFICIENTS
Particle: Limestone 1400 μm
Tube elevation: 15 cm above distributor
Static bed height: 36 cm

T_B = 300°C		T_B = 500°C		T_B = 750°C	
U_{sg},m/s	h_{av},W/m²°C	U_{sg},m/s	h_{av},W/m²°C	U_{sg},m/s	h_{av},W/m²°C
0.75	77.20	0.82	125.71	1.12	206.71
1.12	94.57	1.07	163.62	2.04	209.68
1.32	116.82	1.21	158.47	2.25	211.73
1.58	121.30	1.87	153.21	2.87	208.12
1.94	118.61	2.25	155.62	3.51	207.48
2.46	106.32	2.87	148.70	4.02	203.13
2.61	105.83	3.28	152.41	4.52	204.25
3.04	102.21	3.87	148.72	4.62	202.81
3.11	100.64	4.57	146.13	5.04	201.25

SINGLE PHASE HEAT TRANSFER COEFFICIENTS
FOR GAS ALONE

0.98	33.30	0.89	50.20	1.50	91.50
1.12	34.50	1.50	55.70	1.87	94.70
1.42	36.70	1.86	57.20	2.11	96.00
1.98	40.20	2.12	59.00	2.64	99.50
2.45	42.60	2.73	61.70	3.11	102.80
2.56	43.10	3.41	64.50	3.52	105.50
2.87	44.60	3.86	66.60	3.84	106.70
3.35	46.50	4.12	66.90	4.22	109.90
3.42	47.20	4.38	68.20	4.86	112.90

FREEBOARD HEAT TRANSFER COEFFICIENTS
Particle: Limestone 1400 μm
Tube elevation: 19 cm above static bed
Static bed height: 36 cm

T_B = 300°C		T_B = 500°C		T_B = 750°C	
U_{sg},m/s	h_{av},W/m²°C	U_{sg},m/s	h_{av},W/m²°C	U_{sg},m/s	h_{av},W/m²°C
0.93	36.43	1.13	63.16	1.59	98.18
1.22	40.47	1.68	68.25	2.25	106.48
1.95	41.53	2.03	74.66	2.87	109.18
2.22	42.49	2.47	83.75	3.47	116.72
2.57	67.30	2.86	84.81	3.92	121.13
2.85	72.75	3.12	98.71	4.11	125.82
2.99	73.45	3.72	119.63	4.32	128.31
3.04	73.15	4.31	138.60	4.43	135.26
3.25	75.19	4.56	129.21	4.61	144.15
3.31	75.20	4.61	132.13	4.83	168.12
3.38	78.12	4.82	133.45	5.46	179.45

IMMERSED TUBE HEAT TRANSFER COEFFICIENTS
Particle: Silica sand 1200 μm
Tube elevation: 15 cm above the distributor
Static bed height: 36 cm

0.61	110.40	1.03	206.80	1.12	285.90
0.72	132.70	1.25	205.40	1.32	287.30
0.82	155.70	1.53	206.50	1.94	293.40
1.22	163.40	1.87	202.50	2.29	282.30
1.58	176.60	2.21	206.80	3.06	298.75
2.07	188.10	2.83	209.70	3.38	285.90
2.25	188.30	3.07	204.50	3.63	287.50
2.49	189.80	3.48	205.40	4.05	276.58
3.01	188.00	3.77	211.80	4.29	281.20
3.10	192.30	3.98	210.40	4.76	284.60
3.15	193.20	4.23	210.00	5.07	288.00

FREEBOARD HEAT TRANSFER COEFFICIENTS
Particle: Silica sand 1200 μm
Tube elevation: 19 cm above static bed
Static bed height: 36 cm

T_B = 300°C		T_B = 500°C		T_B = 750°C	
U_{sg},m/s	h_{av},W/m²°C	U_{sg},m/s	h_{av},W/m²°C	U_{sg},m/s	h_{av},W/m²°C
1.62	38.10	1.02	82.10	1.15	125.80
1.94	63.50	1.25	86.60	1.83	128.60
2.01	68.40	1.60	89.70	2.40	136.80
2.34	76.30	1.97	107.70	2.67	153.50
2.48	75.40	2.01	119.60	3.15	181.80
2.64	76.40	2.32	135.00	3.53	193.70
2.75	77.80	2.64	143.40	3.96	208.90
2.87	88.10	3.04	151.30	4.25	207.10
2.93	91.80	3.28	154.20	4.87	199.30
3.01	94.70	3.63	159.10	4.93	200.10
3.12	108.20	4.09	173.00	5.01	213.50

FREEBOARD HEAT TRANSFER COEFFICIENTS
Particle: Silica sand 1200 μm
Tube elevation: 58 cm above static bed
Static bed height: 36 cm

0.74	40.20	1.12	56.60	1.29	91.80
0.93	40.70	1.53	58.70	1.47	92.70
1.21	39.40	1.85	61.20	1.98	96.30
1.56	39.60	2.10	61.30	2.15	107.20
1.97	39.40	2.46	62.30	2.56	111.00
2.15	43.70	2.97	65.70	2.88	117.30
2.47	45.90	3.22	66.20	3.42	128.60
2.96	50.30	3.49	66.80	3.78	129.10
3.01	50.70	3.52	74.70	4.22	134.90
3.08	51.80	3.87	78.80	5.01	145.60
3.14	52.20	4.17	89.30	5.53	152.00

FREEBOARD HEAT TRANSFER COEFFICIENTS
Particle: Limestone 1400 μm
Tube elevation: 58 cm above static bed
Static bed height: 36 cm

T_B = 300°C		T_B = 500°C		T_B = 750°C	
U_{sg},m/s	h_{av},W/m²°C	U_{sg},m/s	h_{av},W/m²°C	U_{sg},m/s	h_{av},W/m²°C
0.87	39.70	0.93	52.73	1.12	91.50
1.12	41.21	1.15	54.87	1.93	101.75
1.42	42.31	1.57	58.71	2.25	109.65
1.87	43.61	1.83	59.68	2.63	113.41
2.35	44.82	2.15	64.48	3.08	118.25
2.68	46.13	2.88	68.12	3.51	123.83
2.83	47.21	3.13	74.56	3.87	129.33
2.96	58.11	3.79	79.82	4.19	131.75
3.11	49.87	4.01	83.15	4.58	136.13
3.21	50.15	4.21	88.66	4.87	139.75
3.38	50.10	4.48	89.75	5.09	144.18

IMMERSED TUBE HEAT TRANSFER COEFFICIENTS
Particle: Silica sand 465 μm
Tube elevation: 15 cm above the distributor
Static bed height: 36 cm

0.65	255.70	1.06	350.80	0.89	407.70
0.88	303.60	1.27	372.30	1.51	439.30
1.02	321.90	1.42	401.40	2.03	424.90
1.25	307.80	1.95	412.10	2.48	428.60
1.56	298.70	2.21	407.30	2.97	431.30
1.71	283.50	2.59	403.90	3.28	436.60
2.10	300.60	3.29	401.80	3.81	440.20
2.53	295.20	3.68	408.50	4.43	459.40
3.04	305.70	4.12	416.40	5.02	556.50

FREEBOARD HEAT TRANSFER COEFFICIENTS
Particle: Silica sand 465 μm
Tube elevation: 19 cm above static bed
Static bed height: 36 cm

T_B = 300°C		T_B = 500°C		T_B = 750°C	
U_{sg},m/s	h_{av},W/m²°C	U_{sg},m/s	h_{av},W/m²°C	U_{sg},m/s	h_{av},W/m²°C
0.97	115.00	1.52	178.50	1.32	207.40
1.25	119.70	1.97	242.20	1.56	221.80
1.49	128.70	2.45	278.60	1.87	234.10
1.79	163.70	2.83	305.30	2.02	248.50
2.08	194.80	3.06	312.70	2.14	256.50
2.52	257.20	3.26	329.60	2.43	273.80
2.88	267.60	3.38	357.13	2.69	305.10
3.07	273.70	3.49	364.20	3.16	388.50
3.41	303.40	3.67	376.90	3.45	427.70

FREEBOARD HEAT TRANSFER COEFFICIENTS
Particle: Silica sand 465 μm
Tube elevation: 58 cm above static bed
Static bed height: 36 cm

0.62	45.20	1.21	84.90	1.55	140.60
0.86	53.70	1.43	96.50	1.83	148.30
1.10	62.60	1.86	113.40	2.15	156.30
1.48	78.30	2.11	137.20	2.38	167.90
1.65	91.20	2.47	166.60	2.59	189.50
1.89	108.00	2.75	172.80	2.78	202.80
2.49	156.40	3.07	175.90	2.96	233.60
3.10	170.70	3.21	186.70	3.08	241.30
3.32	179.60	3.41	208.30	3.28	247.40

FREEBOARD HEAT TRANSFER COEFFICIENTS
Particle: Silica sand 465 μm
Tube elevation: 147 cm above static bed
Static bed height: 36 cm

T_B = 300°C		T_B = 500°C		T_B = 750°C	
U_{sg},m/s	h_{av},W/m²°C	U_{sg},m/s	h_{av},W/m²°C	U_{sg},m/s	h_{av},W/m²°C
0.48	44.20	0.69	71.20	1.28	101.50
0.93	48.50	0.87	72.80	1.47	100.80
1.23	53.70	1.42	74.30	1.83	102.90
1.56	59.20	1.82	78.20	2.13	141.40
1.84	60.70	2.05	82.20	2.52	152.70
2.11	63.70	2.46	94.50	2.94	161.20
2.56	73.20	2.98	107.60	3.07	162.10
2.98	95.30	3.02	120.80	3.11	167.30
3.47	114.00	3.38	134.70	3.38	172.70

APPENDIX 4

TRANSIENT BED-SURFACE CONTACT DATA

TRANSIENT BED-SURFACE CONTACT BEHAVIOR
Particle: Glass bead 275 μm
Tube elevation: 1.60 cm above the static bed
Static bed height: 36 cm

U_{sg}	α_L @ Angle β			α_D @ Angle β			f_L @ Angle β			$\theta_{n,s}$ @ Angle β			$\theta_{p,s}$ @ Angle β		
m/s	0°	90°	180°	0°	90°	180°	0°	90°	180°	0°	90°	180°	0°	90°	180°
0.182	0.910	0.943	0.934	0.585	0.682	0.623	0.312	0.582	0.372	0.652	0.211	0.382	0.549	0.194	0.351
0.250	0.885	0.931	0.923	0.521	0.649	0.546	0.249	0.561	0.296	0.757	0.182	0.314	0.830	0.212	0.343
0.495	0.877	0.902	0.892	0.515	0.623	0.538	0.223	0.524	0.268	0.687	0.163	0.281	0.762	0.208	0.344
0.746	0.851	0.888	0.884	0.512	0.627	0.532	0.178	0.512	0.257	0.601	0.157	0.253	0.610	0.183	0.302
1.015	0.854	0.890	0.872	0.510	0.619	0.533	0.158	0.581	0.249	0.581	0.136	0.221	0.611	0.157	0.295
1.312	0.859	0.894	0.873	0.495	0.616	0.541	0.148	0.523	0.251	0.532	0.110	0.211	0.582	0.123	0.309
1.603	0.864	0.892	0.871	0.505	0.623	0.547	0.157	0.528	0.259	0.501	0.109	0.208	0.581	0.118	0.301
2.02	0.868	0.894	0.881	0.517	0.631	0.551	0.172	0.529	0.258	0.482	0.090	0.207	0.578	0.105	0.292
2.504	0.872	0.902	0.892	0.528	0.639	0.550	0.203	0.535	0.264	0.468	0.090	0.206	0.583	0.093	0.281
2.812	0.871	0.904	0.898	0.531	0.642	0.562	0.227	0.547	0.272	0.431	0.082	0.198	0.503	0.087	0.278

TRANSIENT BED-SURFACE CONTACT BEHAVIOR
Particle: Glass beads 275 μm
Tube elevation: 19 cm above the static bed
Static bed height: 36 cm

0.345	0.987	0.992	0.988	0.762	0.788	0.779	0.9138	0.995	0.974	0.039	0.020	0.071	0.052	0.030	0.091
0.505	0.963	0.988	0.971	0.723	0.770	0.768	0.853	0.910	0.868	0.105	0.054	0.088	0.138	0.027	0.139
0.745	0.931	0.978	0.963	0.682	0.744	0.730	0.678	0.903	0.823	0.217	0.073	0.097	0.325	0.067	0.165
1.040	0.921	0.961	0.950	0.663	0.710	0.694	0.561	0.823	0.780	0.284	0.074	0.123	0.378	0.066	0.173
1.295	0.892	0.958	0.921	0.621	0.702	0.681	0.410	0.804	0.714	0.312	0.076	0.142	0.432	0.073	0.182
1.610	0.887	0.942	0.915	0.601	0.691	0.660	0.332	0.761	0.664	0.387	0.076	0.169	0.439	0.081	0.203
2.081	0.881	0.930	0.903	0.582	0.675	0.671	0.281	0.701	0.572	0.411	0.079	0.180	0.427	0.085	0.242
2.485	0.878	0.915	0.890	0.542	0.641	0.609	0.241	0.620	0.480	0.420	0.081	0.193	0.435	0.084	0.238
2.610	0.874	0.910	0.890	0.538	0.630	0.561	0.234	0.563	0.33	0.417	0.080	1.195	0.447	0.095	0.245
2.807	0.875	0.908	0.894	0.532	0.633	0.557	0.228	0.541	0.28	0.423	0.080	0.192	0.485	0.087	0.252

TRANSIENT BED-SURFACE CONTACT BEHAVIOR
Particle: Glass beads 275 μm
Tube elevation: 55 cm above the static bed
Static bed height: 36 cm

U_{sg}	α_L @ Angle β			α_D @ Angle β			f_L @ Angle β			$\theta_{n,s}$ @ Angle β			$\theta_{p,s}$ @ Angle β		
m/s	0°	90°	180°	0°	90°	180°	0°	90°	180°	0°	90°	180°	0°	90°	180°
0.762	0.991	1.00	0.997	0.789	0.80	0.793	0.992	1.00	0.998	0.055	0.00	0.003	0.081	0.016	0.08
1.037	0.987	0.997	0.984	0.776	0.786	0.781	0.973	0.987	0.980	0.115	0.009	0.019	0.060	0.018	0.071
1.301	0.964	0.991	0.972	0.768	0.771	0.760	0.954	0.976	0.953	0.123	0.011	0.031	0.171	0.020	0.084
1.501	0.920	0.987	0.963	0.753	0.761	0.753	0.870	0.953	0.912	0.143	0.017	0.058	0.182	0.028	0.088
2.09	0.921	0.979	0.954	0.722	0.757	0.741	0.882	0.930	0.904	0.137	0.026	0.078	0.189	0.036	0.102
2.485	0.920	0.965	0.957	0.703	0.758	0.720	0.881	0.910	0.861	0.139	0.029	0.081	0.188	0.032	0.113
2.550	0.918	0.971	0.955	0.704	0.751	0.701	0.776	0.887	0.825	0.144	0.031	0.094	0.201	0.031	0.129
2.820	0.921	0.963	0.954	0.694	0.743	0.687	0.762	0.874	0.793	0.142	0.039	0.096	0.203	0.037	0.131

TRANSIENT BED-SURFACE CONTACT BEHAVIOR
Particle: Glass beads 275 μm
Tube elevation: 147 cm above the static bed
Static bed height: 36 cm

2.00	0.991	1.00	0.998	0.798	0.80	0.80	0.995	1.00	0.999	0.001	0.00	0.00	0.002	0.00	0.00
2.350	0.987	1.00	0.991	0.791	0.80	0.798	0.998	1.00	0.994	0.005	0.00	0.004	0.008	0.00	0.005
2.500	0.977	1.00	0.993	0.783	0.80	0.796	0.999	1.00	0.999	0.011	0.00	0.007	0.013	0.00	0.006
2.650	0.979	1.00	0.987	0.781	0.80	0.798	0.997	1.00	1.00	0.014	0.00	0.008	0.017	0.00	0.009
2.800	0.981	0.998	0.990	0.786	0.797	0.793	0.995	1.00	0.993	0.023	0.00	0.016	0.024	0.00	0.011

TRANSIENT BED-SURFACE CONTACT BEHAVIOR
Particle: Glass beads 275 μm
Tube elevation: 225 cm above the static bed
Static bed height: 36 cm

2.501	1.00	1.00	1.00	0.80	0.80	0.80	1.00	1.00	1.00	0.001	0.00	0.00	0.00	0.00	0.00
2.800	0.993	0.998	0.994	0.794	0.80	0.80	1.00	1.00	1.00	0.001	0.00	0.00	0.00	0.00	0.00

TRANSIENT BED-SURFACE CONTACT BEHAVIOR
Particle: silica sand 465 μm
Tube elevation: 1.6 cm above the static bed
Static bed height: 36 cm

U_{sg}	α_L			α_D			f_L			$\theta_{n,s}$			$\theta_{p,s}$		
	@ Angle β			@ Angle β			@ Angle β			@ Angle β			@ Angle β		
m/s	0°	90°	180°	0°	90°	180°	0°	90°	180°	0°	90°	180°	0°	90°	180°
0.275	0.925	0.942	0.924	0.578	0.703	0.683	0.432	0.771	0.492	0.669	0.051	0.112	0.696	0.029	0.103
0.450	0.915	0.938	0.921	0.572	0.643	0.646	0.381	0.742	0.476	0.715	0.110	0.169	0.682	0.090	0.202
0.750	0.906	0.924	0.920	0.569	0.665	0.625	0.330	0.739	0.454	0.705	0.090	0.170	0.625	0.110	0.200
0.850	0.900	0.921	0.921	0.561	0.681	0.634	0.304	0.743	0.451	0.684	0.077	0.140	0.615	0.109	0.198
1.06	0.893	0.920	0.918	0.564	0.656	0.638	0.278	0.747	0.462	0.656	0.063	0.135	0.605	0.106	0.188
1.300	0.881	0.917	0.917	0.568	0.649	0.640	0.242	0.746	0.471	0.573	0.061	0.130	0.587	0.192	0.178
1.500	0.872	0.911	0.908	0.573	0.651	0.642	0.251	0.745	0.470	0.541	0.057	0.128	0.543	0.084	0.181
2.00	0.864	0.909	0.900	0.531	0.649	0.653	0.258	0.751	0.474	0.511	0.052	0.119	0.522	0.086	0.173
2.500	0.863	0.909	0.894	0.536	0.657	0.651	0.261	0.750	0.478	0.485	0.048	0.120	0.501	0.083	0.144
2.800	0.868	0.900	0.878	0.538	0.661	0.652	0.273	0.754	0.471	0.462	0.044	0.119	0.491	0.081	0.132

TRANSIENT BED-SURFACE CONTACT BEHAVIOR
Particle: Silica sand 465 μm
Tube elevation: 19 cm above the static bed
Static bed height: 36 cm

0.455	0.981	0.993	0.981	0.763	0.789	0.773	0.983	0.987	0.991	0.023	0.009	0.031	0.080	0.008	0.025
0.750	0.961	0.981	0.954	0.746	0.781	0.752	0.786	0.952	0.843	0.110	0.016	0.044	0.150	0.039	0.081
0.850	0.943	0.976	0.944	0.731	0.776	0.741	0.623	0.930	0.817	0.187	0.108	0.052	0.202	0.042	0.097
1.08	0.920	0.961	0.932	0.719	0.763	0.734	0.560	0.917	0.774	0.230	0.021	0.063	0.395	0.044	0.102
1.500	0.903	0.954	0.930	0.701	0.750	0.715	0.512	0.887	0.729	0.257	0.026	0.075	0.377	0.041	0.113
2.06	0.887	0.943	0.921	0.683	0.741	0.699	0.483	0.853	0.683	0.293	0.028	0.082	0.381	0.052	0.116
2.500	0.871	0.931	0.910	0.651	0.732	0.681	0.412	0.802	0.641	0.311	0.031	0.088	0.384	0.058	0.117
2.800	0.870	0.915	0.905	0.628	0.712	0.682	0.324	0.774	0.604	0.369	0.033	0.096	0.405	0.057	0.121

TRANSIENT BED-SURFACE CONTACT BEHAVIOR
Particle: Silica sand 465 μm
Tube elevation: 58 cm above the static bed
Static bed height: 36 cm

U_{sg}	α_L @ Angle β			α_D @ Angle β			f_L @ Angle β			$\theta_{n,s}$ @ Angle β			$\theta_{p,s}$ @ Angle β		
m/s	0°	90°	180°	0°	90°	180°	0°	90°	180°	0°	90°	180°	0°	90°	180°
1.500	0.989	0.993	0.991	0.791	0.80	0.792	0.941	0.998	0.988	0.011	0.09	0.007	0.013	0.010	0.017
1.750	0.977	0.979	0.981	0.773	0.783	0.781	0.901	0.963	0.952	0.012	0.08	0.021	0.017	0.012	0.024
2.00	0.954	0.971	0.963	0.751	0.761	0.760	0.868	0.940	0.928	0.014	0.011	0.029	0.016	0.019	0.026
2.500	0.943	0.964	0.958	0.733	0.734	0.748	0.792	0.925	0.877	0.019	0.014	0.036	0.024	0.023	0.039
2.800	0.938	0.952	0.941	0.721	0.724	0.741	0.778	0.904	0.849	0.023	0.020	0.049	0.028	0.028	0.053

TRANSIENT BED-SURFACE CONTACT BEHAVIOR
Particle: Silica sand 465 μm
Tube elevation: 147 cm above the static bed
Static bed height: 36 cm

2.00	0.989	1.00	0.991	0.782	0.80	0.789	1.00	1.00	1.00	0.00	0.00	0.001	0.00	0.00	0.004
2.500	0.991	1.00	0.989	0.791	0.80	0.799	0.998	1.00	1.00	0.003	0.00	0.00	0.005	0.00	0.001
2.800	0.976	1.00	0.991	0.783	0.80	0.791	0.993	1.00	0.997	0.007	0.00	0.009	0.011	0.00	0.017

TRANSIENT BED-SURFACE CONTACT BEHAVIOR
Particle: Glass beads 850 μm
Tube elevation: 1.60 cm above the static bed
Static bed height: 36 cm

U_{sg}	α_L @ Angle β			α_D @ Angle β			f_L @ Angle β			$\theta_{n,s}$ @ Angle β			$\theta_{p,s}$ @ Angle β		
m/s	0°	90°	180°	0°	90°	180°	0°	90°	180°	0°	90°	180°	0°	90°	180°
0.520	0.956	0.978	0.963	0.716	0.754	0.747	0.757	0.935	0.830	0.254	0.031	0.046	0.317	0.043	0.262
0.720	0.951	0.971	0.961	0.708	0.743	0.739	0.624	0.916	0.803	0.427	0.049	0.182	0.419	0.087	0.256
0.805	0.935	0.963	0.956	0.693	0.734	0.733	0.681	0.897	0.750	0.348	0.036	0.201	0.399	0.071	0.234
0.108	0.920	0.956	0.947	0.681	0.730	0.720	0.642	0.853	0.713	0.328	0.024	0.173	0.388	0.060	0.224
1.485	0.912	0.948	0.933	0.676	0.718	0.703	0.593	0.827	0.641	0.226	0.023	0.180	0.372	0.055	0.215
1.755	0.904	0.939	0.929	0.661	0.693	0.685	0.514	0.806	0.603	0.200	0.024	0.178	0.366	0.056	0.220
2.00	0.906	0.931	0.930	0.650	0.691	0.677	0.487	0.781	0.581	0.202	0.021	0.146	0.326	0.051	0.146
2.504	0.897	0.927	0.925	0.656	0.684	0.665	0.483	0.762	0.542	0.186	0.023	0.117	0.314	0.048	0.152
2.800	0.896	0.923	0.916	0.651	0.670	0.661	0.451	0.748	0.534	0.187	0.021	0.087	0.315	0.043	0.173

TRANSIENT BED-SURFACE CONTACT BEHAVIOR
Particle: Glass beads 850 μm
Tube elevation: 19 cm above the static bed
Static bed height: 36 cm

0.735	0.991	1.00	0.993	0.789	0.80	0.792	0.969	1.00	0.987	0.081	0.001	0.016	0.132	0.012	0.018
0.815	0.978	0.993	0.987	0.773	0.793	0.783	0.951	0.994	0.973	0.085	0.010	0.023	0.152	0.014	0.047
1.083	0.963	0.987	0.973	0.764	0.786	0.779	0.925	0.987	0.954	0.103	0.09	0.031	0.137	0.028	0.060
1.406	0.957	0.984	0.971	0.751	0.778	0.771	0.868	0.963	0.904	0.120	0.012	0.038	0.148	0.032	0.073
1.760	0.951	0.978	0.968	0.732	0.765	0.760	0.804	0.947	0.851	0.728	0.017	0.041	0.168	0.035	0.075
2.01	0.949	0.971	0.959	0.739	0.753	0.752	0.781	0.912	0.807	0.131	0.016	0.043	0.187	0.036	0.091
2.527	0.948	0.963	0.951	0.701	0.731	0.730	0.754	0.874	0.781	0.143	0.015	0.048	0.187	0.032	0.081
2.810	0.940	0.965	0.952	0.693	0.720	0.718	0.740	0.870	0.776	0.150	0.015	0.056	0.191	0.031	0.096

TRANSIENT BED-SURFACE CONTACT BEHAVIOR
Particle: Glass beads 850 μm
Tube elevation: 58 cm above the static bed
Static bed height: 36 cm

2.00	1.00	1.00	1.00	0.80	0.80	0.80	1.00	1.00	1.00	0.00	0.00	0.00	0.00	0.00	0.00
2.510	0.996	1.00	0.997	0.796	0.80	0.793	0.993	1.00	1.00	0.00	0.00	0.00	0.002	0.00	0.003
2.798	0.994	0.993	0.991	0.789	0.791	0.790	0.992	1.00	0.991	0.001	0.00	0.003	0.006	0.00	0.003

* U.S. GOVERNMENT PRINTING OFFICE: 1984—746-081/2513